Entropy-Stable Positivity-Preserving Schemes for Multiphase Flows

by

Benjamin Jacob Simpson

A thesis
presented to the University of Waterloo
in fulfillment of the
thesis requirement for the degree of
Master of Mathematics
in
Applied Mathematics

Waterloo, Ontario, Canada, 2024

Author's Declaration

I hereby declare that I am the sole author of this thesis. This is a true copy of the thesis, including any required final revisions, as accepted by my examiners.

I understand that my thesis may be made electronically available to the public.

Abstract

High-intensity focused ultrasound is a promising non-invasive medical technology that has been successfully used to ablate tumors, as well as in the treatment of other conditions. Researchers believe high-intensity focused ultrasound could see clinical application in other areas such as disruption of the blood brain barrier and sonoporation. However, such advances in medical technology requires fundamental insight into the physics associated with high-intensity focused ultrasound, such as the phenomena known as acoustic cavitation and the collapse of the ensuing bubble cavity. The multiphase description of flow phenomena is an attractive option for modelling such problems as all fluids in the domain are modelled using a single set of governing equations, as opposed to separate systems of equations for each phase and therefore, separate meshes for each fluid. In this thesis, we are interested in studying the bubble collapse problem numerically, to elucidate the physics behind the collapse of acoustically driven bubbles.

We seek to develop high-order numerical methods to solve this problem, due to their potential to increase computational efficiency. However, high-order methods typically have stability issues, especially when considering complex physics. For this reason, high-order entropy-stable summation-by-parts schemes are a popular method used to simulate compressible flow equations. These methods offer provable stability through satisfying a discrete entropy inequality, which is used to prove discrete L_2 stability. Such stability proofs rely on the fundamental assumption that the densities and volume (or void) fractions of both phases remain positive. However, we seek numerical schemes that can simulate flows where the densities and volume fractions get arbitrarily close to zero and, as such, could become negative as the simulation progresses. To address this problem, we present a novel high-order entropy-stable positivity-preserving scheme to solve the 1-D isentropic Baer-Nunziato model. The key to our proposed scheme is a novel artificial dissipation operator, which has tuneable dissipation coefficients that allow the scheme to have provable nodewise positivity of the densities and volume fractions. This new scheme is constructed by mixing a high-order entropy-conservative scheme with a first-order entropy-stable positivity-preserving scheme to create a high-order entropy-stable positivity-preserving scheme. Numerical results which demonstrate the convergence, positivity, and shock capturing capabilities of the scheme are presented.

Acknowledgements

First, I would like to thank Professor Del Rey Fernández for the patience and guidance he has given me throughout my thesis project. His advice and instruction has helped me grow as a professional and as a researcher, and has greatly improved my work. Furthermore, he has developed many exceptional opportunities for me to not only present my research at international conferences, but also to travel to collaborate with researchers in Germany. These opportunities have greatly enhanced my experience as a graduate student and I will always be grateful for them. I would also like to thank Professor Sivaloganathan for his advice and direction throughout my degree, my presentations and writing have benefited from his expertise. I want to also thank the other members of my examining committee for the feedback they have provided, it has improved the quality of this thesis immensely.

Thank you to all of my peers in my research group for the help and support along the way. Our coffee times have been a bright point in the day when research is particularly challenging. I wish you all the best in your academic and professional careers and I look forward to seeing what you all accomplish.

Thank you to my mother, father, and brother for your support throughout my academic career. It is safe to say that I would not have come this far without you all in my corner. Thank you for believing in me and providing me with the support I needed, I am so grateful to have a family like you. So many times throughout my thesis project I have listened to the wisdom from my parents "if you get stuck on a problem and are frustrated... walk away and come back to it with fresh eyes." This is some of the best advice I have ever gotten and helped tremendously throughout my thesis project.

Finally, I want to thank my best friend and beloved partner, Elizabeth Silva. You have been my guiding light since we met back in high school. Thank you for your support, encouragement, and patience with me throughout my master's degree. I always knew I could come to you when I had a particularly challenging day and you would be a source of inspiration, comfort, happiness, and understanding. I look forward to seeing where our future takes us.

"Don't complain that the rose bush has thorns - be happy that the thorn bush has roses" - German proverb

Table of Contents

List of Figures

List of Abbreviations

CFD Computational Fluid Dynamics

HIFU High-Intensity Focused Ultrasound

IBP Integration By Parts

IBVP Initial-Boundary-Value Problem

PDE Partial Differential Equation

RK Runge-Kutta

SAT Simultaneous Approximation Term

SBP Summation-By-Parts

SSP Strong Stability Preserving

List of Symbols

Ω Denotes the set of admissible states for the isentropic Baer-Nunziato model.

$\boldsymbol{u}$ Denotes the vector of conserved variables for the isentropic Baer-Nunziato model.

$\boldsymbol{u}_{j,i}$ Denotes the vector of conserved variables for the isentropic Baer-Nunziato model on element j, and node i.

$u^{(a)}$ Denotes the a^{th} conserved variables for the isentropic Baer-Nunziato model.

$\circ$ Denotes the Hadamard product – entry-wise multiplication between two matrices of the same size.

$\boldsymbol{v}$ Denotes the vector of primitive variables for the isentropic Baer-Nunziato model.

$\otimes$ Denotes the tensor product.

Chapter 1

Introduction

1.1 High-Intensity Focused Ultrasound

High-intensity focused ultrasound (HIFU) is a noninvasive medical technology that uses specific transducer geometry to focus the ultrasound beam and its associated energy onto millimeter-sized targets [36]. Ultrasound waves provide several benefits, such as, precise control over the location that energy is deposited into the medium, enabling deep tissue treatment, and improved focus onto the target due to its small wavelengths [39]. During World War Two, submarines observed that high intensity ultrasound waves resulted in the death of nearby fish through heating [36], thus, using focused ultrasound for locally heating tissues was one of its early clinical applications. Today, HIFU is used clinically as a non-invasive treatment to ablate solid malignant tumors, including those in the liver, pancreas, kidney, bone, breast, and prostate [36]. Furthermore, clinicians can use imaging techniques such as magnetic resonance imaging as well ultrasound imaging to monitor the HIFU treatment process in real time [36]. HIFU has seen clinical success in treating other conditions such as brain disorders, essential tremors, Parkinson's disease, chronic pain, and non-malignant pain [36].

There are several new areas that researchers believe HIFU could see clinical application in [36], such as vessel blockage, disruption of the blood brain barrier, and sonoporation [36, 69]. However, such advances require fundamental insight into the physics associated with HIFU. The two main mechanisms associated with HIFU are local tissue heating, which has been put into clinical practice for ablating tumors, and acoustic cavitation [15]. The ultrasound field that is generated by the HIFU transducer causes a drop in fluid pressure in localised regions, resulting in a phase change, causing cavitation [7]. This cavity appears

as a bubble in the fluid, and will expand in time as more air from the surrounding fluid diffuses into the bubble [7]. When the bubble is large enough and the amplitude of the acoustic field is sufficient in magnitude, the bubble will grow to at least twice the initial size [68]. As the bubble grows in size, the fluid pressure increases, which slows the rate of growth until the bubble reaches a maximum radius, at which point, the bubble collapses [68]. When this collapse occurs near a wall, a fluid jet will develop through the center of the bubble, towards the wall [7]. This fluid jet can lead to large pressures on the surface of the wall and even cause damage such as cell pitting [7]. The collapse of the bubble is something that, if controlled, has many practical applications since the collapse can puncture soft tissue, and the bubbles can be used to disrupt flow through blood vessels [69, 65]. However, such control requires a detailed understanding of the underlying physics, which is currently poorly understood [44].

In this thesis, we are interested in studying the bubble collapse problem as many of the new areas of HIFU research involve the process of acoustic cavitation and either utilizing or mitigating the bubble collapse [36, 69]. We wish to study this problem numerically to elucidate the physics behind the collapse of an acoustically driven bubble. In this thesis, we will develop numerical schemes which solve a set of one-dimensional multiphase flow equations. This work can be extended to multiple dimensions and will be applicable to simulating a bubble collapse problem. In the literature, there are two main numerical approaches that are taken to study the dynamics of a bubble; a sharp interface approach [67] and a multiphase approach[4, 11, 50]. In the sharp interface approach, the two phases, being liquid and gas, are meshed separately, leading to a very well defined interface. However, since we are looking to study the collapse of the bubble, we will not be using the sharp interface approach because the collapse is such a violent process that meshing is difficult, if not impossible in this scenario. Instead, we will use the multiphase approach, which represents an attractive alternative for simulating the bubble collapse problem as both phases are modelled using the same set of governing equations, thus, there is no need for separate meshing. In the next section, we review the current literature for simulating multiphase flows.

1.2 The Numerical Simulation of Multiphase Flows

Computational fluid dynamics (CFD) is used in many applications such as within the aerospace, automotive, and maritime industries [66]. In the last 50 years, CFD has evolved into an essential tool for both fundamental science as well as for engineering analysis, design, and optimization. CFD is attractive because it enables recovering the full solution

and can be used in scenarios where experiments are too costly or impossible. High-order numerical methods have the potential to improve the efficiency of numerical simulations given their faster error convergence. For sufficiently fine error tolerances, high-order methods require significantly coarser meshes, as compared to first-order methods [28]. This has the potential to drastically speed up simulation times, since fewer computational resources are needed to run simulations on a coarse mesh. While high-order methods have the potential to improve computational efficiency, they are also prone to Gibbs oscillations around large-magnitude features such as shocks, which can destroy the accuracy of the numerical solution [23]. Furthermore, even for smooth solutions, high-order methods can have stability problems for non-linear problems, and therefore, provable stability is key to maturing these methods to production level capable of routinely solving practical problems in industry.

There is an extensive body of research that focuses on stabilizing high-order methods in the presence of large magnitude features. A common approach taken to stabilize high-order schemes is called shock capturing [64]. There are several methods which are used to determine regions containing sharp features that include inspecting the smoothness of the numerical solution [63, 62, 25, 54], developing a physics-based sensor that searches for strong compression (such as shock waves) or other features that produce a large gradient, such as shear layers [47, 45, 5]. Then, once a region with a sharp feature has been detected, schemes will use one or more of the following techniques to stabilize around the feature: limiters [51, 55], filtering [31], and artificial viscosity [63, 62, 50, 13]. A method constructed to stabilize the numerical scheme should have provable mathematical properties that are consistent with the properties of the continuous problem.

In this thesis, we will use the isentropic Baer-Nunziato equations to study the bubble collapse problem (more details on the isentropic Baer-Nunziato model is provided in section 2.2). Numerical schemes have been developed to simulate multiphase flows that discretely mimic the non-linear entropy stability property, (2.7), (i.e., the second law of thermodynamics) of the continuous equation [50, 11, 13, 12, 14]. Such a scheme that, at least semi-discretely, satisfies this entropy inequality is called entropy-stable. It can be shown that, by satisfying the non-linear entropy inequality, one can find a bound on the L_2 norm of the solution itself (see section 2.2 for the continuous case and section 5.1 for the discrete analog). In addition to entropy stability, one must guarantee that the thermodynamic variables, such as density, remain positive even when arbitrarily close to zero. In fact, a fundamental assumption used in the entropy stability proofs is that the thermodynamic variables are positive over the entire domain. There are several approaches that have been pursued to preserve positivity for multiphase flows including: Coquel *et al.* [13], who use an HLL approximate Riemann solver, Trojak and Dzanic [61] developed a

positivity-preserving parameter-free numerical stabilization approach, which uses adaptive entropy filtering, and Renac [50] has developed a scheme which preserves the positivity of the cell averages and then uses a limiting approach to ensure positivity at the node level.

1.3 Thesis Organization and Summary of Results

In this thesis, we develop a new, high-order entropy-stable scheme for the isentropic Baer-Nunziato equations, (2.3), which preserves the node-wise positivity of the densities of the two phases as well as the positivity and boundedness of the void fractions. We take inspiration from the work of Upperman and Yamaleev [63], who developed an entropy-stable node-wise positivity-preserving scheme for the Navier-Stokes equations. In their work, they utilize the Brenner regularization of the Navier-Stokes equations to add artificial viscosity to their scheme and through the use of tuneable dissipation coefficients and time step restriction, they are able to maintain positivity of density and temperature. To the best of this author's knowledge, the Baer-Nunziato equations have no viscous regularization that would lead to the creation of an appropriate dissipation operator that would allow for positivity to be maintained. **A major contribution** of this thesis, is the development of a novel artificial dissipation operator that ensures both entropy-stability as well as preserving the positivity of the densities and void fractions, importantly, node-wise.

The key idea of the methodology applied in this thesis is to construct a first-order entropy-stable positivity-preserving scheme using the novel artificial dissipation operator. The artificial dissipation operator has tuneable dissipation coefficients that can be used, along with suitable time step restriction, to preserve the node-wise positivity of the void fractions and densities as well as the boundedness of the void fractions. Then, this scheme can be mixed with a high-order scheme, which has no positivity preserving properties, to create a scheme that is high-order, entropy-stable, and positivity-preserving.

In chapter 2, we will review what it means for a partial differential equation (PDE) to be well-posed. In this discussion, we detail an energy expression which is a necessary condition for a non-linear PDE to be considered well-posed. Then, we introduce the isentropic Baer-Nunziato equations and detail the entropy stability, as well as L_2 stability, of the equations at the continuous level. In particular, we detail how the entropy inequality leads to a bound on the L_2 norm of the solution itself.

In chapter 3, we introduce high-order diagonal-norm summation-by-parts (SBP) operators as well as their key properties that allow them to discretely mimic integration by parts (IBP). Furthermore, we showcase the simultaneous approximation term (SAT) technique in relation to the toy problem of the linear advection equation to demonstrate how

SAT terms weakly impose boundary conditions and inter-element coupling. We also show how the SBP-SAT technique can be used to develop stability statements for an equation by performing an example on the linear advection equation. We then show numerical results that demonstrate the convergence properties of SBP operators as well as the stability properties. Finally, we demonstrate a special first-order derivative operator that will be used in the first-order entropy-stable positivity-preserving scheme. We demonstrate how schemes that are discretized with this operator have a truncation error that is first-order theoretically, and present numerical results that confirm schemes constructed with this operator converge at first-order.

In chapter 4, we develop a high-order entropy-conservative scheme for the isentropic Baer-Nunziato equations. This scheme can handle smooth, periodic solutions to the isentropic Baer-Nunziato equations, but has no positivity-preserving properties. Furthermore, the scheme developed in chapter 4 has no entropy-dissipative terms, and as such, cannot handle problems with shocks. Since we are looking to study the bubble collapse problem, which introduces a shock into the system, we use this scheme as a base to which we add entropy-dissipative terms to render the resulting scheme both entropy-stable and positivity-preserving.

We begin chapter 5 by developing a first-order entropy-stable positivity-preserving scheme for the isentropic Baer-Nunziato model; this scheme is a **major contribution** of this work. We add element interface dissipation as well as the novel artificial dissipation operator to the entropy-conservative scheme developed in chapter 4, except, here we use the special first derivative operator detailed in chapter 3, instead of a high-order derivative operator. Then, we take inspiration from the work of Upperman [62] to mix the first-order entropy-stable positivity-preserving scheme and the high-order entropy-conservative scheme detailed in chapter 4, to create a high-order entropy-stable positivity-preserving scheme; this mixed scheme is another **major contribution** of this work.

In chapter 6, we present numerical results obtained from simulations using the schemes developed in the previous chapters. We show results for the entropy-conservative scheme detailed in chapter (4) and the first- and high-order entropy-stable positivity-preserving schemes detailed in chapter 5. Specifically for the high-order entropy-stable positivity-preserving scheme, we show the numerical results obtained for two different Riemann problems to demonstrate both the positivity-preserving qualities and the shock capturing capabilities of the numerical scheme. Finally, in chapter 7, we summarize the contributions of this thesis as well as present future research directions.

Chapter 2

Isentropic Baer-Nunziato Model

In this chapter, we briefly review the concept of well-posedness and demonstrate a method to construct stability statements. In the remainder of the thesis, the objective will be to construct numerical methods that are provably stable, mimicking the continuous stability proofs step by step. Finally, we introduce the isentropic Baer-Nunziato equations; the multiphase equations that will be considered in this thesis and can be used to model the bubble collapse problem. We demonstrate how to construct an L_2 bound on the continuous form of the equations, starting from an entropy inequality that the Baer-Nunziato equations must satisfy.

2.1 Well-Posedness of a Continuous Problem

In mathematics, for a problem to be considered well-posed, it must satisfy 3 properties [29]:

1. A solution exists.
2. The solution is unique.
3. The solution depends continuously on the data.

Requirements 1) and 2) are self-explanatory, however, we require a mathematical means of determining 3). In this thesis, we look to construct L_2 bounds on the solution, which, for linear problems, is sufficient to demonstrate continuous dependence on the data. For

non-linear problems, such a bound is a necessary condition. To expand further, consider the following initial-boundary-value problem (IBVP) in one spatial dimension:

$$\begin{aligned} \frac{\partial u}{\partial t} + R(u) &= S(x,t), \quad x \in [x_L, x_R], \quad t > 0, \\ BC(u) &= G(t), \\ u(x,0) &= F(x), \end{aligned} \tag{2.1}$$

where u is a function of space and time, $R(u)$ is a differential operator, S is a source term, $BC(u)$ is a boundary operator that encodes the boundary conditions, $G(t)$, of the problem, and $F(x)$ denotes the initial conditions. For this IBVP to be considered well-posed, one of the conditions that must be met, is that the norm of the solution is bounded by the data of the problem, which includes $S(x,t)$, $G(t)$, and $F(x)$ [29]. Generically, this bound has the following form:

$$\|u\|_u^2 \leq \gamma(\|S\|_S^2 + \|G\|_G^2 + \|F\|_F^2), \tag{2.2}$$

where γ is a positive quantity that can depend on time, but, is independent of the data. Notice that each norm has a different subscript; this is to indicate that the same norm does not need to be used for each term. Note that (2.2) bounds the norm of the solution by the data of the problem, and for nonlinear equations, such as the Baer-Nunizato model, this is a necessary condition for well-posedness. Furthermore, for linear problems, it can be shown that the stability statement (2.2), leads to a statement that the solution depends continuously on the data of the problem and further, can lead to a statement on uniqueness.

Throughout this thesis, for any problem that is studied, we will develop a stability statement in the form of (2.2) at the continuous level, to ensure that this necessary condition for well-posedness is met. Then, we will construct numerical schemes which mimic the stability statement at the discrete level. This means that our schemes will have stability, which is of practical importance in the simulation of PDEs, as we want to ensure the solution remains bounded as the scheme is marched in time.

2.2 Isentropic Baer-Nunziato Model

Compressible two-phase flow models find extensive applications throughout physics and engineering. For example, in aerospace propulsion systems, kerosene is stored in a compressed form and is injected into the combustion chamber via small droplets [46]. A model that is commonly used to study such two-phase flow systems is the Baer-Nunziato model [4, 3]. This model was originally developed by Baer and Nunziato to describe the behaviour

of a reacting two-phase mixture of solid grains and a gaseous combustion product. The model was later adapted to study the mixture of liquid and gas phases in [52, 11, 21, 27]. This makes the Baer-Nunziato model appealing for studying acoustic cavitation in relation to HIFU, since the bubble collapse problem is composed of a gaseous bubble surrounded by liquid. The equations describes a two-temperature, two-velocity, two-pressure system. It is a seven equation model with two momentum, continuity, and energy equations along with one equation which describes the evolution of the void fractions, also known as volume fractions. However, in this thesis, we will study the isentropic Baer-Nunziato model, which is a five equation system and does not contain energy equations for each phase.

The isentropic Baer-Nunziato model is a system of first-order, nonlinear PDEs, which contain a nonconservative term. The Baer-Nunziato equations are strictly hyperbolic under certain restrictions on the solution, that will be defined later in this chapter. We assume that our solution lies within the set of admissible states such that the system of equations is hyperbolic. Hyperbolic PDEs can generate discontinuous solutions as they evolve in time even for smooth initial data. Furthermore, the evolution of the two phases are coupled through the use of a nonconservative term in the form $\mathsf{c}(\boldsymbol{u})\frac{\partial \boldsymbol{u}}{\partial x}$, which is dependent upon the gradient of the phase fractions. This nonconservative product is not unique at discontinuities and this leads to uncertainty in the value of the nonconservative term, which must then be defined at the discontinuity. Possible choices for this definition can either be based on the choice of Lipschitz paths which connect different states around discontinuities [17], or the kinetic relations derived from the physical entropy [6]. Furthermore, since we are interested in studying the bubble collapse problem, we are interested in studying discontinuous solutions to the Baer-Nunziato model, as the collapse of the bubble introduces a shock into the system. To study discontinuous solutions, we need to study the weak form of the PDE. This means that the solution will not be unique, thus, we need a way to ensure that the scheme will converge to a reasonable solution. To this end, we seek solutions that satisfy a nonlinear stability condition, called the entropy condition [40]. This entropy condition is based off of a given convex entropy function for the system of equations. By satisfying this entropy condition, we are ensuring that if the scheme converges, then it will converge to a physically relevant solution. In the case of a system of PDEs, satisfying this entropy condition is a necessary, but not sufficient condition for well-posedness. Schemes which satisfy this entropy condition are known as entropy-conservative or entropy-stable depending on whether the scheme is designed to conserve entropy, or dissipate it. Thus, in later chapters, to solve the isentropic Baer-Nunziato model numerically, we will create entropy-conservative schemes to solve problems in which entropy is conserved, e.g., smooth solutions with periodic boundary conditions. Furthermore, we will create entropy-stable schemes to handle problems that produce entropy. For example, the mathematical entropy

of a system must decrease across a shock according to the second law of thermodynamics. Tadmor, [60] developed a framework to create entropy-conservative and entropy-stable numerical fluxes in the context of hyperbolic conservation laws. These fluxes will either conserve or dissipate the mathematical entropy of the system. This work has since been extended to nonconservative systems through the use of fluctuation fluxes [48]. In this thesis, we will use the fluctuation fluxes of Renac [50] to solve the isentropic Baer-Nunziato model.

Here, we consider the two-velocity two-pressure isentropic Baer-Nunziato model [4, 3] with void fractions α_i, densities ρ_i, and velocities v_i for phases $i = 1, 2$. Associated with each phase are the pressure $p_i = p_i(\rho_i)$, specific internal energy, e_i, and enthalpy, h_i, which are governed by the equations $\frac{de_i}{d\rho_i} = \frac{p_i}{\rho_i^2}$ and $h_i = e_i + \frac{p_i}{\rho_i}$, respectively. Moreover, the speed of sound is defined as $c_i = \sqrt{dp_i/d\rho_i}$. Here, we will be considering polytropic ideal gas with equations of state $p_i(\rho_i) = k\rho_i^{\gamma_i}$, for $k > 0$ and $\gamma_i > 1$. The governing equations for the Cauchy problem have the form,

$$\frac{\partial \boldsymbol{u}}{\partial t} + \frac{\partial \boldsymbol{f}(\boldsymbol{u})}{\partial x} + \mathsf{c}(\boldsymbol{u})\frac{\partial \boldsymbol{u}}{\partial x} = 0, x \in \mathbb{R}, t > 0, \tag{2.3a}$$

$$\boldsymbol{u}(x, 0) = \boldsymbol{u}_0, x \in \mathbb{R}, \tag{2.3b}$$

where $\boldsymbol{u}_0(x)$ is a known initial condition and

$$\boldsymbol{u} = \begin{pmatrix} \alpha_1 \\ \alpha_1\rho_1 \\ \alpha_1\rho_1 v_1 \\ \alpha_2\rho_2 \\ \alpha_2\rho_2 v_2 \end{pmatrix}, \boldsymbol{f}(\boldsymbol{u}) = \begin{pmatrix} 0 \\ \alpha_1\rho_1 v_1 \\ \alpha_1(\rho_1 v_1^2 + p_1) \\ \alpha_2\rho_2 v_2 \\ \alpha_2(\rho_2 v_2^2 + p_2) \end{pmatrix}, \mathsf{c}(\boldsymbol{u})\frac{\partial \boldsymbol{u}}{\partial x} = \begin{pmatrix} v_I \\ 0 \\ -p_I \\ 0 \\ p_I \end{pmatrix} \frac{\partial \alpha_1}{\partial x}.$$

The terms v_I and p_I denote the interface velocity and pressure, where, in this thesis $v_I = v_2$ and $p_I = p_1$ have been chosen as closure laws for the interface velocity and pressure as used in [50]. Note that a large body of work is focused on deriving different closures for the interface velocity and pressure, aimed at various applications. For example, in the original paper of Baer and Nunizato [4], the closures $v_I = v_1$ and $p_I = p_2$ were proposed for the case where one of the phases is nearly incompressible. Furthermore, the void fractions, α_i, must satisfy the saturation condition

$$\alpha_1 + \alpha_2 = 1. \tag{2.4}$$

The Baer-Nunziato model is only weakly hyperbolic since the system has the following real eigenvalues $\Gamma_i,\ i = 1, 2, \ldots, 5$ [13]:

$$\Gamma_1 = v_2,\ \Gamma_2 = v_1 - c_1,\ \Gamma_3 = u_1 + c_1,\ \Gamma_4 = v_2 - c_2,\ \Gamma_5 = u_2 + c_2,$$

where, the right eigenvectors are linearly independent if, and only if [13],

$$\alpha_1 \neq 0, \quad \alpha_2 \neq 0, \quad |v_1 - v_2| \neq c_1. \tag{2.5}$$

Thus, the system is strictly hyperbolic if the conditions in (2.5) are satisfied. Furthermore, define the set of admissible states as

$$\Omega = \{\boldsymbol{u} \in \mathbb{R}^5 \mid 0 < \alpha_i < 1, \rho_i > 0, i = 1, 2\}. \tag{2.6}$$

The conservative portion of (2.3a), $\frac{\partial \boldsymbol{f}(\boldsymbol{u})}{\partial x}$, describes the variations in the physical quantities and the nonconservative term, $\mathsf{c}(\boldsymbol{u})\frac{\partial \boldsymbol{u}}{\partial x}$, couples the phases. Furthermore, if the void fractions, α_i's, are constant in space, the two phases decouple into two systems of compressible Euler equations [14]. Additionally, smooth solutions to the system (2.3) satisfy the following equation [13],

$$\frac{\partial \eta(\boldsymbol{u})}{\partial t} + \frac{\partial q(\boldsymbol{u})}{\partial x} = 0.$$

Furthermore, for non-smooth, weak solutions to (2.3), one adds the entropy criterion in order to select a physically relevant solution. Therefore, a weak solution to the Baer-Nunziato equations is one that satisfies the following nonlinear stability (or entropy) condition

$$\frac{\partial \eta(\boldsymbol{u})}{\partial t} + \frac{\partial q(\boldsymbol{u})}{\partial x} \leq 0, \tag{2.7}$$

in a weak sense [30]. Equation (2.7) holds for the (mathematical) entropy-entropy flux pair, η and q, respectively

$$\eta(\boldsymbol{u}) = \sum_{i=1}^{2} \alpha_i \rho_i \left(\frac{v_i^2}{2} + e_i(\rho_i) \right),\ q(\boldsymbol{u}) = \sum_{i=1}^{2} \alpha_i \rho_i \left(\frac{v_i^2}{2} + h_i(\rho_i) \right) v_i, \tag{2.8}$$

where η is a strictly convex function when $\boldsymbol{u} \in \Omega$ [50]. Then, define the entropy variables as $\boldsymbol{w}^{\mathrm{T}} = \frac{\partial \eta}{\partial \boldsymbol{u}}$. Then, for $\boldsymbol{u} \in \Omega$, the entropy pair satisfies

$$\frac{d\eta}{d\boldsymbol{u}} \left(\frac{\partial f(\boldsymbol{u})}{\partial x} + \mathsf{c}(\boldsymbol{u}) \frac{\partial \boldsymbol{u}}{\partial x} \right) = \boldsymbol{w}^{\mathrm{T}} \left(\frac{\partial f(\boldsymbol{u})}{\partial x} + \mathsf{c}(\boldsymbol{u}) \frac{\partial \boldsymbol{u}}{\partial x} \right) = \frac{\partial q(\boldsymbol{u})}{\partial x}. \tag{2.9}$$

When the solution contains a discontinuity, the inequality in (2.7) becomes a strict inequality to account for the decreasing entropy across a shock. The system (2.3) can also be written in quasi-linear form

$$\frac{\partial \boldsymbol{u}}{\partial t} + \mathsf{A}\left(\boldsymbol{u}\right)\frac{\partial \boldsymbol{u}}{\partial x} = 0, \quad x \in \mathbb{R},\ t > 0, \tag{2.10}$$

where $\mathsf{A} : \Omega \ni \boldsymbol{u} \mapsto \mathsf{A}\left(\boldsymbol{u}\right) = \frac{\partial \boldsymbol{f}}{\partial \boldsymbol{u}} + \mathsf{c}\left(\boldsymbol{u}\right) \in \mathbb{R}^{5\times 5}$ is a matrix-valued function for smooth solutions of (2.3).

As stated previously, our solution must satisfy the entropy condition (2.7). We will now show how to construct this entropy inequality at the continuous level. Furthermore, when developing numerical schemes to solve the Baer-Nunziato equations, we will construct schemes that mimic this analysis step-by-step at the discrete level. Another motivation to constructing schemes which satisfy the entropy inequality, (2.7), is based on the work of Dafermos [16], who proved that this inequality leads to an L_2 bound on the solution.

Remark 2.2.1. Next, we will show the continuous entropy-stability analysis and the how this results in an L_2 bound on the solution. In this thesis, our aim is to develop schemes that enable stability proofs that follow the continuous stability proofs in a one-to-one fashion and this will be the focus of later chapters.

To derive the bound on the entropy of the solution, we multiply the PDE (2.3) by the entropy variables and integrate over the spatial domain, $x \in [x_L, x_R]$. First, we will show this in the case of a smooth, periodic problem,

$$\int_{x_L}^{x_R} \boldsymbol{w}^{\mathrm{T}} \frac{\partial \boldsymbol{u}}{\partial t} dx + \int_{x_L}^{x_R} \boldsymbol{w}^{\mathrm{T}} \left(\frac{\partial f(\boldsymbol{u})}{\partial x} + \mathsf{c}(\boldsymbol{u}) \frac{\partial \boldsymbol{u}}{\partial x} \right) dx = 0.$$

Then, use (2.9) on the second term on the left hand side and rewrite the entropy variables in the first term on the left hand side as $\boldsymbol{w}^{\mathrm{T}} = \frac{\partial \eta}{\partial \boldsymbol{u}}$ to find that

$$\int_{x_L}^{x_R} \frac{\partial \eta}{\partial \boldsymbol{u}} \frac{\partial \boldsymbol{u}}{\partial t} dx + \int_{x_L}^{x_R} \frac{\partial q(\boldsymbol{u})}{\partial x} dx = 0.$$

Next, the first term on the left hand side can be simplified using chain rule to obtain

$$\int_{x_L}^{x_R} \frac{\partial \eta}{\partial t} dx + \int_{x_L}^{x_R} \frac{\partial q(\boldsymbol{u})}{\partial x} dx = 0.$$

We have the same form as (2.7), but, in the case of smooth, periodic solutions, we keep the equality, i.e.,

$$\int_{x_L}^{x_R} \frac{\partial \eta}{\partial t} dx + \int_{x_L}^{x_R} \frac{\partial q(\boldsymbol{u})}{\partial x} dx = 0.$$

Using the Leibniz integration rule on the first term on the left hand side and evaluating the second integral on the left hand side results in

$$\frac{d}{dt} \int_{x_L}^{x_R} \eta dx = q(x_L) - q(x_R),$$

where, since we are considering a periodic problem, $q(x_L) = q(x_R)$, thus,

$$\frac{d}{dt} \int_{x_L}^{x_R} \eta dx = 0.$$

Therefore, in the case of smooth, periodic solutions to (2.3), the integral of the entropy of the solution over the domain is constant. Now, consider non-smooth, periodic solutions to (2.3). In this case, to account for the entropy loss across a shock, we use a strict inequality [13], to find that

$$\frac{d}{dt} \int_{x_L}^{x_R} \eta dx < 0.$$

Therefore, in general, periodic solutions to (2.3) satisfy the following bound on the entropy of the solution

$$\frac{d}{dt} \int_{x_L}^{x_R} \eta dx \leq 0. \tag{2.11}$$

Now, we will show that the entropy inequality of the system implies a bound on the norm of the solution. We follow the derivation of Svärd [57], who has proved this result for the Navier-Stokes equations, but, adapt the proof to the Baer-Nunziato equations. We will study a periodic problem. To begin, we define a new entropy

$$\overline{\eta} = \eta - \eta(\boldsymbol{u}_0) - \eta'(\boldsymbol{u}_0)^{\mathrm{T}}(\boldsymbol{u} - \boldsymbol{u}_0),$$

where $\eta' = \frac{\partial \eta}{\partial \boldsymbol{u}}$ and $\boldsymbol{u}_0$ is a constant, non-zero state. For the state $\boldsymbol{u}_0$ we choose $\alpha_i = (\alpha_i)_0 > 0$ and $\rho_i = (\rho_i)_0 > 0$, $i = 1, 2$. Similarly define $\frac{\partial \overline{q}}{\partial x} = \frac{\partial \overline{\eta}}{\partial \boldsymbol{u}}(\frac{\partial \boldsymbol{f}}{\partial x} + \mathsf{c}\frac{\partial \boldsymbol{u}}{\partial x})$. This new entropy $\overline{\eta}$, satisfies an entropy inequality as long as the original entropy function, η, does.

We also define the new entropy variables as $\overline{\boldsymbol{w}}^{\mathrm{T}} = \frac{\partial \overline{\eta}}{\partial \boldsymbol{u}} = \eta' - \eta'(\boldsymbol{u}_0)$, where, $\frac{\partial \overline{\boldsymbol{w}}}{\partial x} = \frac{\partial \boldsymbol{w}}{\partial x}$. Now, left multiply (2.3a) by $\overline{\boldsymbol{w}}^{\mathrm{T}}$ and integrate over the spatial domain to find that

$$\int_{x_L}^{x_R} \overline{\boldsymbol{w}}^{\mathrm{T}} \frac{\partial \boldsymbol{u}}{\partial t} dx + \int_{x_L}^{x_R} \overline{\boldsymbol{w}}^{\mathrm{T}} \left(\frac{\partial \boldsymbol{f}}{\partial x} + \mathsf{c} \frac{\partial \boldsymbol{u}}{\partial x} \right) dx = 0.$$

Note that $\overline{\boldsymbol{w}}^{\mathrm{T}} \boldsymbol{u}_t = \frac{\partial \overline{\eta}}{\partial \boldsymbol{u}} \frac{\partial \boldsymbol{u}}{\partial t} = \frac{\partial \overline{\eta}}{\partial t}$ and $\overline{\boldsymbol{w}} \left(\frac{\partial \boldsymbol{f}}{\partial x} + \mathsf{c} \frac{\partial \boldsymbol{u}}{\partial x} \right) = \frac{\partial \overline{q}}{\partial x}$. Thus,

$$\int_{x_L}^{x_R} \frac{\partial \overline{\eta}}{\partial t} dx + \int_{x_L}^{x_R} \frac{\partial \overline{q}}{\partial x} dx = 0.$$

We are now in the form of the entropy inequality (2.7), thus, since we are considering both smooth and discontinuous solutions, we replace the equality with an inequality as follows

$$\int_{x_L}^{x_R} \frac{\partial \overline{\eta}}{\partial t} dx + \int_{x_L}^{x_R} \frac{\partial \overline{q}}{\partial x} dx \leq 0.$$

The second term on the left hand side vanishes since we are considering periodic problems, therefore,

$$\int_{x_L}^{x_R} \frac{\partial \overline{\eta}}{\partial t} dx \leq 0. \tag{2.12}$$

Then, we Taylor expand η around $\boldsymbol{u}_0$ to find that

$$\eta(\boldsymbol{u}) = \eta(\boldsymbol{u}_0) + \eta'(\boldsymbol{u}_0)^{\mathrm{T}}(\boldsymbol{u} - \boldsymbol{u}_0) + \frac{1}{2}(\boldsymbol{u} - \boldsymbol{u}_0)^{\mathrm{T}} \eta''(\boldsymbol{u}(\theta))(\boldsymbol{u} - \boldsymbol{u}_0), \tag{2.13}$$

where $\eta'' = \frac{\partial^2 \eta}{\partial \boldsymbol{u}^2}$. By Taylor's Formula, there exists some $\theta \in [0, 1]$ such that $\boldsymbol{u}(\theta) = \boldsymbol{u}_0(1 - \theta) + \boldsymbol{u}\theta$ and (2.13) holds. By assumption, the solution $\boldsymbol{u} \in \Omega$, where Ω is the space of admissible states as defined in (2.6). Thus, we have that $\alpha_i > 0$ and $\rho_i > 0$ for $i = 1, 2$. Furthermore, we have picked our constant state, $\boldsymbol{u}_0$ such that $(\alpha_i)_0 > 0$ and $(\rho_i)_0 > 0$ for $i = 1, 2$. Thus, we have that $\alpha_i(\theta) > 0$ and $\rho_i(\theta) > 0$. Therefore, $\boldsymbol{u}(\theta) \in \Omega$ and $\eta(\boldsymbol{u}(\theta))$ is a strictly convex function. Then, since $\eta(\boldsymbol{u}(\theta))$ is strictly convex, its Hessian, $\eta''(\boldsymbol{u}(\theta))$, is positive definite, which means its eigenvalues are all real and positive. Thus, $\eta''_{min}(t) > 0$, where $\eta''_{min}(t)$ is the minimum eigenvalue of $\eta''(\boldsymbol{u}(\theta), t)$ in space and time. Notice that $\overline{\eta}$ has been defined such that

$$\overline{\eta} = \eta - \eta(\boldsymbol{u}_0) - \eta'(\boldsymbol{u}_0)^{\mathrm{T}}(\boldsymbol{u} - \boldsymbol{u}_0) = \frac{1}{2}(\boldsymbol{u} - \boldsymbol{u}_0)^{\mathrm{T}} \eta''(\boldsymbol{u}(\theta))(\boldsymbol{u} - \boldsymbol{u}_0). \tag{2.14}$$

Integrate equation (2.12) in time from $t = 0$ to $t = T$ to find that

$$\int_{x_L}^{x_R} \overline{\eta}(\boldsymbol{u}(x, T)) dx \leq \int_{x_L}^{x_R} \overline{\eta}(\boldsymbol{u}(x, 0)) dx,$$

where, substituting (2.14) into the left hand side of the above equation results in

$$\frac{1}{2}\int_{x_L}^{x_R}(\boldsymbol{u}-\boldsymbol{u}_0)^{\mathrm{T}}\eta''(\boldsymbol{u}(\theta(T)))(\boldsymbol{u}-\boldsymbol{u}_0)dx \leq \int_{x_L}^{x_R}\overline{\eta}(\boldsymbol{u}(x,0))dx.$$

Therefore, we can say that $\int_{x_L}^{x_R}(\boldsymbol{u}-\boldsymbol{u}_0)^{\mathrm{T}}\eta''(\boldsymbol{u}(\theta(T)))(\boldsymbol{u}-\boldsymbol{u}_0)dx \leq C$. From this, we can deduce that

$$\int_{x_L}^{x_R}(\boldsymbol{u}-\boldsymbol{u}_0)^{\mathrm{T}}\eta''_{min}(\boldsymbol{u}-\boldsymbol{u}_0)dx = \eta''_{min}\int_{x_L}^{x_R}(\boldsymbol{u}-\boldsymbol{u}_0)^{\mathrm{T}}(\boldsymbol{u}-\boldsymbol{u}_0)dx \leq C. \tag{2.15}$$

Now, rewrite the integrand $(\boldsymbol{u}-\boldsymbol{u}_0)^{\mathrm{T}}(\boldsymbol{u}-\boldsymbol{u}_0)$ as follows

$$\begin{aligned}\boldsymbol{u}^{\mathrm{T}}\boldsymbol{u} &= (\boldsymbol{u}-\boldsymbol{u}_0+\boldsymbol{u}_0)^{\mathrm{T}}(\boldsymbol{u}-\boldsymbol{u}_0+\boldsymbol{u}_0),\\ &= (\boldsymbol{u}-\boldsymbol{u}_0)^{\mathrm{T}}(\boldsymbol{u}-\boldsymbol{u}_0)+2(\boldsymbol{u}-\boldsymbol{u}_0)^{\mathrm{T}}\boldsymbol{u}_0+\boldsymbol{u}_0^{\mathrm{T}}\boldsymbol{u}_0,\\ &\leq 2(\boldsymbol{u}-\boldsymbol{u}_0)^{\mathrm{T}}(\boldsymbol{u}-\boldsymbol{u}_0)+2\boldsymbol{u}_0^{\mathrm{T}}\boldsymbol{u}_0.\end{aligned} \tag{2.16}$$

To see why the inequality in the last line holds, first, change the notation so that it is easier to read. Let $x=(\boldsymbol{u}-\boldsymbol{u}_0)$ and $y=\boldsymbol{u}_0$. Then, start from

$$\begin{aligned}0 &\leq (x-y)^2,\\ 0 &\leq x^2-2xy+y^2.\end{aligned}$$

Adding $x^2+2xy+y^2$ to both sides of the above equation gives

$$x^2+2xy+y^2 \leq 2x^2+2y^2,$$

which is the exact inequality obtained in (2.16). Now, integrate (2.16) over the spatial domain to find that

$$\int_{x_L}^{x_R}\boldsymbol{u}^{\mathrm{T}}\boldsymbol{u}dx \leq 2\int_{x_L}^{x_R}(\boldsymbol{u}-\boldsymbol{u}_0)^{\mathrm{T}}(\boldsymbol{u}-\boldsymbol{u}_0)dx+2\int_{x_L}^{x_R}\boldsymbol{u}_0^{\mathrm{T}}\boldsymbol{u}_0dx.$$

Then, from (2.15) we have that $\int_{x_L}^{x_R}(\boldsymbol{u}-\boldsymbol{u}_0)^{\mathrm{T}}(\boldsymbol{u}-\boldsymbol{u}_0)dx \leq \frac{C}{\eta''_{min}}$. Thus, we find that

$$\int_{x_L}^{x_R}\boldsymbol{u}^{\mathrm{T}}\boldsymbol{u}dx \leq 2\frac{C}{\eta''_{min}}+2\int_{x_L}^{x_R}\boldsymbol{u}_0^{\mathrm{T}}\boldsymbol{u}_0dx.$$

Defining $\|\boldsymbol{u}\|^2=\int_{x_L}^{x_R}\boldsymbol{u}^{\mathrm{T}}\boldsymbol{u}dx$ results in

$$\|\boldsymbol{u}\|^2 \leq 2\frac{C}{\eta''_{min}}+2\|\boldsymbol{u}_0\|^2.$$

Therefore, by bounding the entropy of the solution, it is possible to obtain a bound on the norm of the solution itself. Thus, entropy stability implies that the problem is stable.

Remark 2.2.2. Here, we have used the entropy analysis to prove stability. In chapter 3, we will use an energy method; there exist many other methods to prove stability, and more broadly, well-posedness such as the compactness method and the theory of semigroups [22].

In this thesis, we will be creating numerical schemes to solve the isentropic Baer-Nunizato model that have provable properties such as entropy stability, i.e., a numerical scheme which satisfies the entropy condition (2.7). To discretize the spacial derivatives in the isentropic Baer-Nunziato equations, (2.3), we will use SBP operators [56, 43, 20], combined with the SAT technique [18], to weakly enforce the boundary conditions. The SBP-SAT technique is detailed in the next chapter.

Chapter 3

Summation By Parts Operators

3.1 Motivation

In the numerical simulation of PDEs, the potential enhancements in efficiency offered by higher-order methods has been known for some time [38, 59]. As the computational error tolerance of the numerical solution becomes more stringent, the benefit that high-order methods can provide becomes more pronounced. In CFD, higher-order methods can be advantageous when applied to time-dependent problems that require high-resolution. Developing high-order numerical schemes for the solution of non-linear PDEs that are efficient and stable is a particular challenge even for smooth problems. One approach to address this challenge is through the use of SBP operators (matrix difference operators for approximating derivatives at nodes in a mesh) [56, 43, 20], with boundary conditions and inter-element coupling weakly enforced by SATs [26, 9, 18]. Another difficulty in the use of high-order methods is that practical problems can contain singularities and discontinuities such as shock waves. The theory behind high-order methods assumes a sufficiently smooth solution and as such, high-order methods are prone to spurious oscillations around discontinuities. Thus, significant research effort has been spent on developing schemes that damp these spurious oscillations [53].

The SBP-SAT technique is desirable because, as we will show in this chapter and throughout the remainder of this thesis, it can be used to create discretizations with provable properties. For example, given a PDE, we can generate a stability statement at the continuous level as part of the process of proving a problem is well-posed. We can then mimic this statement at the semi-discrete level using the SBP-SAT technique, to prove that our scheme will be stable at the semi-discrete level. Thus, throughout this thesis, we

will create discretizations using the SBP-SAT technique that have provable properties such as stability.

3.2 High-Order Summation By Parts Operators

In one dimension and in this thesis, the physical domain, $x \in [x_L, x_R]$, is discretized into n equally sized elements, with N uniformly distributed points per element such that, on some element, k, we have the set of nodes

$$[x_{k,1}, x_{k,2}, \ldots, x_{k,N}],$$

where, $x_{(k-1),N} = x_{k,1}$. Here, we have introduced the notation that will be used for the remainder of the thesis: to describe a quantity "b" located on element j, and node i, we use the notation $b_{j,i}$. These points are referred to as solution points as they are where the value of the solution is approximated, i.e., the solution on the k^{th} element is approximated as $\boldsymbol{u}_k(t) = [\boldsymbol{u}(x_{k,1}, t), \ldots, \boldsymbol{u}(x_{k,N}, t)]^{\mathrm{T}} = [\boldsymbol{u}_{k,1}, \ldots, \boldsymbol{u}_{k,N}]^{\mathrm{T}}$.

The spatial derivatives in (2.3) are discretized using finite-difference operators that satisfy the SBP property [58, 8]. SBP operators are mimetic of IBP (3.1) at the discrete level,

$$\int_{x_L}^{x_R} v \frac{\partial u}{\partial x}\, dx = vu\Big|_{x_L}^{x_R} - \int_{x_L}^{x_R} u \frac{\partial v}{\partial x}\, dx, \tag{3.1}$$

and are defined as [18, 58]

Definition 3.2.1 (Summation-by-parts operator)**.** A degree p matrix difference operator, $\mathsf{D} \in \mathbb{R}^{N \times N}$, is an approximation to the first derivative $\left(\frac{\partial}{\partial x}\right)$ on the domain $x \in [x_L, x_R]$, at the nodes $[x_1, x_2, \ldots, x_N]$, where $x_1 = x_L$ and $x_N = x_R$, with the SBP property if

1. $\mathsf{D}\boldsymbol{x}^k = \mathsf{P}^{-1}\mathsf{Q}\boldsymbol{x}^k = k\boldsymbol{x}^{k-1},\ k = 0, 1, \ldots, p,$
2. $\mathsf{P} = \mathsf{P}^{\mathrm{T}}, \quad \boldsymbol{x}^{\mathrm{T}}\mathsf{P}\boldsymbol{x} > 0,\ \forall \boldsymbol{x} \neq 0,$
3. $\mathsf{Q} + \mathsf{Q}^{\mathrm{T}} = \mathsf{E}, \quad \mathsf{E} = \mathrm{diag}(-1, 0, \ldots, 0, 1).$

With $p = 2$, the following matrices satisfy the SBP conditions

$$\mathsf{D} = \frac{1}{h}\begin{bmatrix}
-24/17 & 59/34 & -4/17 & -3/34 & & & & & & & \\
-1/2 & 0 & 1/2 & 0 & 0 & & & & & & \\
4/43 & -59/86 & 0 & 59/86 & -4/43 & 0 & & & & & \\
3/98 & 0 & -59/98 & 0 & 32/49 & -4/49 & & & & & \\
0 & 0 & 1/12 & -8/12 & 0 & 8/12 & -1/12 & & & & \\
 & & & \ddots & \ddots & \ddots & \ddots & \ddots & & & \\
 & & & 1/12 & -8/12 & 0 & 8/12 & -1/12 & 0 & 0 \\
 & & & & 4/49 & -32/49 & 0 & 59/98 & 0 & -3/98 \\
 & & & & & 4/43 & -59/86 & 0 & 59/86 & -4/43 \\
 & & & & & & 0 & -1/2 & 0 & 1/2 \\
 & & & & & & 3/4 & 4/17 & -59/34 & 24/17
\end{bmatrix},$$

$$\mathsf{P} = h\,\mathrm{diag}(17/48, 59/48, 43/48, 49/48, 1, \ldots, 1, 49/48, 43/48, 59/48, 17/48),$$

$$\mathsf{Q} = \begin{bmatrix}
-1/2 & 59/96 & -1/12 & -1/32 & & & & & & & \\
-59/96 & 0 & 59/96 & 0 & & & & & & & \\
1/12 & -59/96 & 0 & 59/96 & -1/12 & & & & & & \\
1/32 & 0 & -59/96 & 0 & 8/12 & -1/12 & & & & & \\
0 & 0 & 1/12 & -8/12 & 0 & 8/12 & -1/12 & & & & \\
 & & & \ddots & \ddots & \ddots & \ddots & \ddots & & & \\
 & & & 1/12 & -8/12 & 0 & 8/12 & -1/12 & 0 & 0 \\
 & & & & 1/12 & -8/12 & 0 & 59/96 & 0 & -1/32 \\
 & & & & & 1/12 & -59/96 & 0 & 59/96 & -1/12 \\
 & & & & & & 0 & -59/96 & 0 & 59/96 \\
 & & & & & & 1/32 & 1/12 & -59/96 & 1/2
\end{bmatrix},$$

where h denotes the mesh spacing. From Definition (3.2.1), the derivative operator approximates a first derivative with a truncation error of order p, i.e.,

$$\frac{\partial g}{\partial x}(\boldsymbol{x}, t) = \mathsf{D}\boldsymbol{g} + \boldsymbol{T}_p, \tag{3.2}$$

where $\frac{\partial g}{\partial x}(\boldsymbol{x}, t)$ is a vector of the derivative of g evaluated at the solution points $\boldsymbol{x}$, at time t, and $\max(|\boldsymbol{T}_p|) = \mathcal{O}(h^p)$. Furthermore, P defines an inner product and norm as follows

$$\begin{aligned}
(\boldsymbol{u}, \boldsymbol{v})_P &= \boldsymbol{u}^{\mathrm{T}}\mathsf{P}\boldsymbol{v}, \\
\|\boldsymbol{u}\|_P^2 &= \boldsymbol{u}^{\mathrm{T}}\mathsf{P}\boldsymbol{u}, \\
\int_{x_L}^{x_R} uv dx &\approx \boldsymbol{u}^{\mathrm{T}}\mathsf{P}\boldsymbol{v},
\end{aligned}$$

where $\boldsymbol{u}$ and $\boldsymbol{v}$ are vectors constructed by evaluating the functions u and v, respectively, at $\boldsymbol{x}$. In this thesis, we use diagonal-norm finite difference SBP operators and will alternatively write $\mathsf{E} = \boldsymbol{t_R}\boldsymbol{t_R}^{\mathrm{T}} - \boldsymbol{t_L}\boldsymbol{t_L}^{\mathrm{T}}$ where

$$\begin{aligned} \boldsymbol{t_L} &= [1, 0, \ldots, 0]^{\mathrm{T}}, \\ \boldsymbol{t_R} &= [0, \ldots, 0, 1]^{\mathrm{T}}. \end{aligned} \tag{3.3}$$

Using Definition (3.2.1) the SBP property can be demonstrated as follows,

$$\begin{aligned} \boldsymbol{v}^{\mathrm{T}}\mathsf{PD}\boldsymbol{u} &= \boldsymbol{v}^{\mathrm{T}}\mathsf{P}\left(\mathsf{P}^{-1}\mathsf{Q}\right)\boldsymbol{u}, \\ &= \boldsymbol{v}^{\mathrm{T}}\mathsf{Q}\boldsymbol{u}, \\ &= \boldsymbol{v}^{\mathrm{T}}\left(\mathsf{E} - \mathsf{Q}^{\mathrm{T}}\right)\boldsymbol{u}, \\ &= \boldsymbol{v}^{\mathrm{T}}\mathsf{E}\boldsymbol{u} - \boldsymbol{v}^{\mathrm{T}}\mathsf{Q}^{\mathrm{T}}\boldsymbol{u}, \\ &= \boldsymbol{v}^{\mathrm{T}}\mathsf{E}\boldsymbol{u} - \boldsymbol{v}^{\mathrm{T}}\mathsf{Q}^{\mathrm{T}}\mathsf{P}^{-1}\mathsf{P}\boldsymbol{u}, \\ \underbrace{\boldsymbol{v}^{\mathrm{T}}\mathsf{PD}\boldsymbol{u}}_{\approx \int_{x_L}^{x_R} v u_x \, dx} &= \underbrace{v_N u_N - v_1 u_1}_{= vu\Big|_{x_L}^{x_R}} - \underbrace{\boldsymbol{v}^{\mathrm{T}}\mathsf{D}^{\mathrm{T}}\mathsf{P}\boldsymbol{u}}_{\approx \int_{x_L}^{x_R} u v_x \, dx}, \end{aligned}$$

which demonstrates that SBP operators are mimetic of IBP.

3.3 Simultaneous Approximation Terms

In this thesis, enforcing boundary conditions as well as inter-element coupling is accomplished using the SAT technique [18]. SATs are penalty terms which enforce boundary conditions in a weak sense. Meaning that, instead of setting the solution at boundary nodes to exactly equal the boundary conditions, we penalize deviations from the boundary conditions.

3.3.1 Linear Advection Equation

To motivate the use of SBP operators and SATs, consider the linear advection equation with a positive unit wave speed:

$$\begin{aligned} \frac{\partial u}{\partial t} + \frac{\partial u}{\partial x} &= 0, x \in [x_L, x_R], t > 0, \\ u(x_L, t) &= G(t), \\ u(x, 0) &= F(x). \end{aligned} \tag{3.4}$$

We can demonstrate the stability of the equation at the continuous level by using the energy method [18]. We multiply (3.4) by u and integrate over the spatial domain to find that

$$\int_{x_L}^{x_R} u\frac{\partial u}{\partial t}dx + \int_{x_L}^{x_R} u\frac{\partial u}{\partial x}dx = 0.$$

The term $u\frac{\partial u}{\partial t}$ can be rewritten using chain rule as

$$u\frac{\partial u}{\partial t} = \frac{1}{2}\frac{\partial u^2}{\partial t},$$

and applying IBP to the second term of the left hand side results in

$$\int_{x_L}^{x_R} u\frac{\partial u}{\partial x}dx = \frac{1}{2}u^2\Big|_{x_L}^{x_R}.$$

Furthermore, we can use Leibniz integration rule on the temporal term, thus,

$$\begin{aligned}\frac{d}{dt}\int_{x_L}^{x_R} u^2dx + \boldsymbol{u}^2\Big|_{x_L}^{x_R} &= 0,\\ \frac{d}{dt}\int_{x_L}^{x_R} u^2dx &= -\left(u(x_R)^2 - u(x_L)^2\right).\end{aligned}$$

Defining $\|u\|^2 = \int_{x_L}^{x_R} u^2dx$, the above equation can be written as

$$\frac{d}{dt}\|u\|^2 = u(x_L)^2 - u(x_R)^2.$$

We can integrate in time from $t = 0$ to $t = T$ to find that

$$\begin{aligned}\int_0^T \frac{d}{dt}\|u\|^2\,dt &= \int_0^T u(x_L)^2 - u(x_R)^2\,dt,\\ &= \int_0^T u(x_L)^2\,dt - \int_0^T u(x_R)^2\,dt.\end{aligned}$$

The second term on the right hand side is less than or equal to zero since the integrand is positive for all $u(x_R)$, thus

$$\int_0^T \frac{d}{dt}\|u\|^2\,dt \leq \int_0^T u(x_L)^2\,dt.$$

Integrating the left hand side and substituting the boundary condition $u(x_L) = G(t)$ results in

$$\|u(\cdot, T)\|^2 - \|u(\cdot, 0)\|^2 \leq \int_0^T G(t)^2 \, dt.$$

Finally, substitute the initial condition, $u(x, 0) = F(x)$, to obtain

$$\|u(\cdot, T)\|^2 \leq \|F(\cdot)\|^2 + \int_0^T G(t)^2 \, dt.$$

Thus, we have bounded the norm of the solution by the data of the problem, and since the PDE is linear, this bound can then be used to show continuous dependence on the data of the problem, as required for well-posedness.

We can mimic this continuous stability analysis at the semi-discrete level using the SBP-SAT technique as follows. We discretize the spatial domain in (3.4) using a single element with N nodes for convenience – we will perform the same analysis in the next section using multiple elements. The numerical solution reads $\boldsymbol{u} = [u_1, \ldots, u_N]^{\mathrm{T}}$. Then, using the SBP derivative operator to approximate the spatial derivative and adding the SAT term $\boldsymbol{SATs} = -\gamma \mathsf{P}^{-1} \boldsymbol{t_L} \left(u_1 - G(t)\right)$, to weakly enforce the boundary condition, the semi-discrete scheme reads

$$\begin{aligned} \boldsymbol{u}_t + \mathsf{D}\boldsymbol{u} &= \boldsymbol{SATs}, \\ \boldsymbol{u}_t + \mathsf{D}\boldsymbol{u} &= -\gamma \mathsf{P}^{-1} \boldsymbol{t_L} \left(u_1 - G(t)\right). \end{aligned} \tag{3.5}$$

At first glance, it is not clear why the added SAT term enforces the boundary condition and what its effect on the solution is. Shortly, we will derive the SATs from a discontinuous Galerkin point of view, but here we point out that in (3.5), inside of the brackets on the right hand side is a rearrangement of the boundary condition. Thus, we are approximating the PDE as well as the boundary conditions simultaneously. Now, we mimic the continuous analysis at the semi-discrete level by left multiplying the semi-discrete scheme by $\boldsymbol{u}^{\mathrm{T}}\mathsf{P}$, which is the discrete equivalent of multiplying by the solution and integrating over the domain, to find that

$$\frac{1}{2}\frac{d\boldsymbol{u}^{\mathrm{T}}\mathsf{P}\boldsymbol{u}}{dt} + \boldsymbol{u}^{\mathrm{T}}\mathsf{Q}\boldsymbol{u} = -\gamma \boldsymbol{u}^{\mathrm{T}} \boldsymbol{t_L} (u_1 - G(t)), \tag{3.6}$$

where, $\boldsymbol{u}^{\mathrm{T}}\mathsf{P}\frac{\partial \boldsymbol{u}}{\partial t} = \frac{1}{2}\frac{d\boldsymbol{u}^{\mathrm{T}}\mathsf{P}\boldsymbol{u}}{dt}$, is the discrete analog to, $\int u \frac{\partial u}{\partial t} \, dx = \frac{1}{2}\frac{d}{dt}\int u^2 \, dx$. Then, the

second term on the left hand side can be written as follows,

$$\begin{aligned}
\boldsymbol{u}^{\mathrm{T}}\mathsf{Q}\boldsymbol{u} &= \boldsymbol{u}^{\mathrm{T}}\left(\mathsf{E}-\mathsf{Q}^{\mathrm{T}}\right)\boldsymbol{u}, \\
&= \boldsymbol{u}^{\mathrm{T}}\mathsf{E}\boldsymbol{u} - \boldsymbol{u}^{\mathrm{T}}\mathsf{Q}^{\mathrm{T}}\boldsymbol{u}, \\
\boldsymbol{u}^{\mathrm{T}}\mathsf{Q}\boldsymbol{u} &= \boldsymbol{u}^{\mathrm{T}}\mathsf{E}\boldsymbol{u} - \boldsymbol{u}^{\mathrm{T}}\mathsf{Q}\boldsymbol{u}, \\
\boldsymbol{u}^{\mathrm{T}}\mathsf{Q}\boldsymbol{u} &= \frac{1}{2}\boldsymbol{u}^{\mathrm{T}}\mathsf{E}\boldsymbol{u}.
\end{aligned}$$

Plugging the above result into (3.6) results in

$$\begin{aligned}
\frac{1}{2}\frac{d\boldsymbol{u}^{\mathrm{T}}\mathsf{P}\boldsymbol{u}}{dt} + \frac{1}{2}\boldsymbol{u}^{\mathrm{T}}\mathsf{E}\boldsymbol{u} &= -\gamma\boldsymbol{u}^{\mathrm{T}}\boldsymbol{t}_{\boldsymbol{L}}(u_1 - G(t)), \\
\frac{1}{2}\frac{d}{dt}\|\boldsymbol{u}\|_P^2 &= -\frac{1}{2}\boldsymbol{u}^{\mathrm{T}}\mathsf{E}\boldsymbol{u} - \gamma\boldsymbol{u}^{\mathrm{T}}\boldsymbol{t}_{\boldsymbol{L}}(u_1 - G(t)).
\end{aligned}$$

Now, substituting the form of E, one finds that

$$\begin{aligned}
\frac{1}{2}\frac{d}{dt}\|\boldsymbol{u}\|_P^2 &= -\frac{1}{2}u_N^2 + \frac{1}{2}u_1^2 - \gamma u_1^2 + \gamma u_1 G(t), \\
&= -\frac{1}{2}u_N^2 - (\gamma - \frac{1}{2})u_1^2 + \gamma u_1 G(t).
\end{aligned}$$

Now, complete the square on the last two terms to obtain

$$\frac{1}{2}\frac{d}{dt}\|\boldsymbol{u}\|_P^2 = -\frac{1}{2}u_N^2 - (\gamma - \frac{1}{2})\left(u_1 - \frac{\gamma}{2(\gamma - \frac{1}{2})}G(t)\right)^2 + \frac{\gamma^2}{4|\gamma - \frac{1}{2}|}G^2(t).$$

The first two terms on the right hand side are less than or equal to zero for all values of u_1, u_N, and $G(t)$ when $\gamma > \frac{1}{2}$. Therefore, by choosing $\gamma > \frac{1}{2}$ and defining,

$$\Gamma = \frac{\gamma^2}{4\left(\gamma - \frac{1}{2}\right)},$$

we have,

$$\frac{1}{2}\frac{d}{dt}\|\boldsymbol{u}\|_P^2 \leq \Gamma G^2(t).$$

Then, integrate in time to find that

$$\begin{aligned}
\int_0^T \frac{d}{dt}\|\boldsymbol{u}\|_P^2 \, dt &\leq 2\int_0^T \Gamma G^2(t) \, dt, \\
\|\boldsymbol{u}(T)\|_P^2 - \|\boldsymbol{u}(0)\|_P^2 &\leq 2\int_0^T \Gamma G^2(t) \, dt.
\end{aligned}$$

Moving the initial condition to the right hand side results in

$$\|\boldsymbol{u}(T)\|_P^2 \leq \|F(x)\|_P^2 + 2\Gamma \int_0^T G^2(t)\, dt.$$

Therefore, we have bounded the norm of the numerical solution by the data of the problem as in the continuous case. This analysis also gives us a restriction on the value of γ that scales the SAT term, i.e., $\gamma > \frac{1}{2}$. With the choice of $\gamma = 1$, the scheme can be shown to be conservative, which is an important property to satisfy via the Lax-Wendroff [40] theorem for discretizations of conservation laws.

As demonstrated, one of the main purposes of the SBP-SAT technique is to enable the design of arbitrary-order accurate spatial discretizations, that are provably stable [18]. Here we have shown stability using the energy method, but, for the isentropic Baer-Nunizato model, we will prove stability of the problem using the entropy of the system. Furthermore, approximating the derivative in an element is completely determined by the solution within that element. This means that, in the multi-element case, the only information that is passed between elements is when computing the SAT terms to enforce the element coupling, as will be shown in the next section. Additionally, the SBP-SAT technique allows for solutions that are discontinuous across element interfaces [18], as we do not strongly enforce solution continuity at element interfaces. Meaning that, for some element, j, we do not adjust the solution so that the last node on the j^{th} element is equal to the first node on the $(j+1)^{th}$ element. Instead, to couple adjacent elements, we use SAT terms which weakly couples the numerical solution across the interface. In the next section we will demonstrate the use of SAT terms which are used to both enforce periodic boundary conditions as well as coupling element interfaces.

3.3.2 Inter-element Coupling SATs

Now that we have motivated the use of SATs, we demonstrate the use of symmetric and upwind SATs, which will be used throughout this thesis to enforce periodic boundary conditions and couple adjacent elements since we will study periodic solutions to the isentropic Baer-Nunziato model. To demonstrate how symmetric and upwind SATs enforce these conditions, we once again consider the linear advection equation from the previous section. In this section, we study periodic problems on the domain $[x_L, x_R]$, to study periodic boundary conditions.

As in the last chapter, we can show stability of the equation with periodic boundary conditions at the continuous level. We begin by adding the periodic boundary term to

(3.4).

$$\begin{aligned} \frac{\partial u}{\partial t} + \frac{\partial u}{\partial x} &= 0, x \in [x_L, x_R], t > 0, \\ u(x_L, t) &= u(x_R, t), \\ u(x, 0) &= F(x). \end{aligned} \tag{3.7}$$

Once again, multiplying the equation by u and integrating over the spatial domain one finds that

$$\frac{d}{dt}\int_{x_L}^{x_R} u^2 dx = -\left(u(x_R)^2 - u(x_L)^2\right) = 0.$$

From here, integrate in time from $t = 0$ to $t = T$ to obtain

$$\|u(T)\|^2 = \|F\|^2.$$

Thus, we have bounded the norm of the solution by the data of the problem. We mimic this continuous stability at the discrete level by discretizing the domain into n equally sized elements, with N nodes per element. Our discrete scheme will have the following generic form,

$$\frac{d\boldsymbol{u}_k}{dt} + \mathsf{D}\boldsymbol{u}_k = \boldsymbol{SATs}, \quad k = 1, 2, \ldots, n. \tag{3.8}$$

We now justify the SATs that will be used by considering the discretization of (3.4) using a discontinuous Galerkin type of approach (the presentation here is not meant to be rigorous, for more detail see the following book [31]). The first step is to construct the weak form of (3.4) by multiplying the linear advection equation by a test function, v, from an appropriate function space, and integrating over a given element k. Then, we will discretize the results using arbitrary-order SBP operators. This will give us a general form of the SATs. Suppose we are studying an element k such that on this element, $x \in [x_l, x_r]$. Then, multiplying (3.4) by a test function, v, and integrating over the element leads to

$$\int_{x_l}^{x_r} v\frac{\partial u}{\partial t}dx + \int_{x_l}^{x_r} v\frac{\partial u}{\partial x}dx = 0.$$

Then, using IBP on the second term on the left hand side results in

$$\int_{x_l}^{x_r} v\frac{\partial u}{\partial t}dx - \int_{x_l}^{x_r} \frac{\partial v}{\partial x}udx + vu\Big|_{x_l}^{x_r} = 0.$$

The next step in the discontinuous Galerkin approach is to replace u with some numerical flux, u^*, which will approximate u at the element interfaces resulting in

$$\int_{x_l}^{x_r} v\frac{\partial u}{\partial t}dx - \int_{x_l}^{x_r} \frac{\partial v}{\partial x}udx + vu^*\Big|_{x_l}^{x_r} = 0.$$

Apply IBP to the second term on the left hand side of the equation to find that

$$\int_{x_l}^{x_r} v\frac{\partial u}{\partial t}dx + \int_{x_l}^{x_r} v\frac{\partial u}{\partial x}dx = v(u-u^*)\Big|_{x_l}^{x_r}.$$

We can now discretize the equation using arbitrary-order SBP operators. As follows,

$$\boldsymbol{v}^{\mathrm{T}}\mathsf{P}\frac{d\boldsymbol{u}_k}{dt} + \boldsymbol{v}^{\mathrm{T}}\mathsf{P}\mathsf{D}\boldsymbol{u}_k = v_{k,N}(u_{k,N} - u_R^*) - v_{k,1}(u_{k,1} - u_L^*).$$

We can use (3.3) to re-write the right hand side of the above equation using $v_{k,N} = \boldsymbol{t}_{\boldsymbol{R}}^{\mathrm{T}}\boldsymbol{v}$ and $v_{k,1} = \boldsymbol{t}_{\boldsymbol{L}}^{\mathrm{T}}\boldsymbol{v}$, with similar definitions for u:

$$\begin{aligned}
\boldsymbol{v}^{\mathrm{T}}\mathsf{P}\frac{d\boldsymbol{u}_k}{dt} + \boldsymbol{v}^{\mathrm{T}}\mathsf{P}\mathsf{D}\boldsymbol{u}_k &= \boldsymbol{v}^{\mathrm{T}}\boldsymbol{t}_{\boldsymbol{R}}(\boldsymbol{t}_{\boldsymbol{R}}^{\mathrm{T}}\boldsymbol{u}_k - u_R^*) - \boldsymbol{v}^{\mathrm{T}}\boldsymbol{t}_{\boldsymbol{L}}(\boldsymbol{t}_{\boldsymbol{L}}^{\mathrm{T}}\boldsymbol{u}_k - u_L^*),\\
\boldsymbol{v}^{\mathrm{T}}\left[\mathsf{P}\frac{d\boldsymbol{u}_k}{dt} + \mathsf{P}\mathsf{D}\boldsymbol{u}_k\right] &= \boldsymbol{v}^{\mathrm{T}}\left[\boldsymbol{t}_{\boldsymbol{R}}(\boldsymbol{t}_{\boldsymbol{R}}^{\mathrm{T}}\boldsymbol{u}_k - u_R^*) - \boldsymbol{t}_{\boldsymbol{L}}(\boldsymbol{t}_{\boldsymbol{L}}^{\mathrm{T}}\boldsymbol{u}_k - u_L^*)\right].
\end{aligned}$$

Since this must hold for arbitrary v, we have that the terms inside the square brackets must be equal, therefore,

$$\mathsf{P}\frac{d\boldsymbol{u}_k}{dt} + \mathsf{P}\mathsf{D}\boldsymbol{u}_k = \boldsymbol{t}_{\boldsymbol{R}}(\boldsymbol{t}_{\boldsymbol{R}}^{\mathrm{T}}\boldsymbol{u}_k - u_R^*) - \boldsymbol{t}_{\boldsymbol{L}}(\boldsymbol{t}_{\boldsymbol{L}}^{\mathrm{T}}\boldsymbol{u}_k - u_L^*),$$

where u_R^* is the numerical flux evaluated at the right boundary and u_L^* is the numerical flux evaluated at the left boundary. Multiplying the above equation by P^{-1} gives

$$\frac{d\boldsymbol{u}_k}{dt} + \mathsf{D}\boldsymbol{u}_k = \mathsf{P}^{-1}\boldsymbol{t}_{\boldsymbol{R}}(\boldsymbol{t}_{\boldsymbol{R}}^{\mathrm{T}}\boldsymbol{u}_k - u_R^*) - \mathsf{P}^{-1}\boldsymbol{t}_{\boldsymbol{L}}(\boldsymbol{t}_{\boldsymbol{L}}^{\mathrm{T}}\boldsymbol{u}_k - u_L^*),$$

which is in the exact form of (3.8) with

$$\boldsymbol{SAT}\boldsymbol{s} = \mathsf{P}^{-1}\boldsymbol{t}_{\boldsymbol{R}}(\boldsymbol{t}_{\boldsymbol{R}}^{\mathrm{T}}\boldsymbol{u}_k - u_R^*) - \mathsf{P}^{-1}\boldsymbol{t}_{\boldsymbol{L}}(\boldsymbol{t}_{\boldsymbol{L}}^{\mathrm{T}}\boldsymbol{u}_k - u_L^*). \tag{3.9}$$

All that remains is to choose a suitable numerical flux u^*. Recall that the numerical flux needs to be designed so that it approximates u at the element interfaces. Here, we will show

two suitable numerical fluxes that can be chosen for the linear advection equation, namely, the upwind numerical flux and a central numerical flux. Since (3.4) advects information from left to right, it is logical that we would use an upwind numerical flux since we want to take information from the upwind direction. In fact, this is the numerical flux we will use to study the convergence rates of the multi-element scheme in the next section. However, we still show the symmetric SATs that are obtained with a central flux, as these SATs mimic the SATs we use in the Baer-Nunziato equations to couple adjacent elements and weakly enforce periodic boundary conditions.

We begin by examining the upwind SATs. The upwind numerical flux for (3.4) is given by $u_L^* = u_{(k-1),N} = \boldsymbol{t}_R^{\mathrm{T}} \boldsymbol{u}_{k-1}$ and $u_R^* = u_{k,N} = \boldsymbol{t}_R^{\mathrm{T}} \boldsymbol{u}_k$. Plugging this choice of u^* into (3.9) results in

$$\boldsymbol{SATs} = \mathsf{P}^{-1} \boldsymbol{t_R} (\cancel{\boldsymbol{t}_{\boldsymbol{R}}^{\mathrm{T}} \boldsymbol{u}_k - \boldsymbol{t}_{\boldsymbol{R}}^{\mathrm{T}} \boldsymbol{u}_k}) - \mathsf{P}^{-1} \boldsymbol{t_L} (\boldsymbol{t}_{\boldsymbol{L}}^{\mathrm{T}} \boldsymbol{u}_k - \boldsymbol{t}_{\boldsymbol{R}}^{\mathrm{T}} \boldsymbol{u}_{(k-1)}),$$

therefore, using an upwind numerical flux in (3.9), we find the upwind SATs,

$$\boldsymbol{SATs} = -\mathsf{P}^{-1} \boldsymbol{t_L} (\boldsymbol{t}_{\boldsymbol{L}}^{\mathrm{T}} \boldsymbol{u}_k - \boldsymbol{t}_{\boldsymbol{R}}^{\mathrm{T}} \boldsymbol{u}_{(k-1)}). \tag{3.10}$$

Now that we have found the upwind SATs that come from using the upwind flux in (3.9), we will show the use of the central flux to create symmetric SATs. The central flux takes the average of the numerical solution on either side of the element interface, i.e., $u_R^* = 0.5(u_{k,N} + u_{(k+1),1}) = 0.5(\boldsymbol{t}_{\boldsymbol{R}}^{\mathrm{T}} \boldsymbol{u}_k + \boldsymbol{t}_{\boldsymbol{L}}^{\mathrm{T}} \boldsymbol{u}_{(k+1)})$, and $u_L^* = 0.5(u_{k,1} + u_{(k-1),N}) = 0.5(\boldsymbol{t}_{\boldsymbol{L}}^{\mathrm{T}} \boldsymbol{u}_k + \boldsymbol{t}_{\boldsymbol{R}}^{\mathrm{T}} \boldsymbol{u}_{(k-1)})$. Plugging these choices of the numerical flux function into (3.9) results in

$$\boldsymbol{SATs} = \frac{1}{2} \mathsf{P}^{-1} \boldsymbol{t_R} (\boldsymbol{t}_{\boldsymbol{R}}^{\mathrm{T}} \boldsymbol{u}_k - \boldsymbol{t}_{\boldsymbol{L}}^{\mathrm{T}} \boldsymbol{u}_{(k+1)}) - \frac{1}{2} \mathsf{P}^{-1} \boldsymbol{t_L} (\boldsymbol{t}_{\boldsymbol{L}}^{\mathrm{T}} \boldsymbol{u}_k - \boldsymbol{t}_{\boldsymbol{R}}^{\mathrm{T}} \boldsymbol{u}_{(k-1)}). \tag{3.11}$$

In our study of the multi-element semi-discrete scheme we will use the upwind SATs (3.10) to weakly enforce the boundary condition as well as the inter-element coupling. Using these SATs, the semi-discrete scheme for the multi-element linear advection equation can be written as

$$\frac{d\boldsymbol{u}_k}{dt} = -\mathsf{D} \boldsymbol{u}_k - \mathsf{P}^{-1} \boldsymbol{t_L} (\boldsymbol{t}_{\boldsymbol{L}}^{\mathrm{T}} \boldsymbol{u}_k - \boldsymbol{t}_{\boldsymbol{R}}^{\mathrm{T}} \boldsymbol{u}_{(k-1)}), \quad k = 1, 2, \ldots, n. \tag{3.12}$$

Note that since we are considering periodic problems, when $k = 1$, $k - 1 = n$. We would like to show that (3.12) mimics the stability analysis that was performed at the continuous

level. We left multiply (3.12) by $\boldsymbol{u}_k^{\mathrm{T}}\mathsf{P}$ resulting in

$$\begin{aligned}
&\frac{1}{2}\frac{d}{dt}\boldsymbol{u}_k^{\mathrm{T}}\mathsf{P}\boldsymbol{u}_k + \boldsymbol{u}_k^{\mathrm{T}}\mathsf{P}\mathsf{D}\boldsymbol{u}_k = -\boldsymbol{u}_k^{\mathrm{T}}\mathsf{P}\mathsf{P}^{-1}\boldsymbol{t}_{\boldsymbol{L}}(\boldsymbol{t}_{\boldsymbol{L}}^{\mathrm{T}}\boldsymbol{u}_k - \boldsymbol{t}_{\boldsymbol{R}}^{\mathrm{T}}\boldsymbol{u}_{(k-1)}),\\
&\underbrace{\frac{1}{2}\frac{d}{dt}\boldsymbol{u}_k^{\mathrm{T}}\mathsf{P}\boldsymbol{u}_k}_{(1)} + \underbrace{\boldsymbol{u}_k^{\mathrm{T}}\mathsf{Q}\boldsymbol{u}_k}_{(2)} = \underbrace{-\boldsymbol{u}_k^{\mathrm{T}}\boldsymbol{t}_{\boldsymbol{L}}(\boldsymbol{t}_{\boldsymbol{L}}^{\mathrm{T}}\boldsymbol{u}_k - \boldsymbol{t}_{\boldsymbol{R}}^{\mathrm{T}}\boldsymbol{u}_{(k-1)})}_{(3)}.
\end{aligned} \tag{3.13}$$

First, term (1) can be rewritten as $\frac{1}{2}\frac{d}{dt}\|\boldsymbol{u}_k\|_P^2$. Then, term (2) can be re-written using the SBP property $\mathsf{Q} = \mathsf{E} - \mathsf{Q}^{\mathrm{T}}$ as

$$\begin{aligned}
\boldsymbol{u}_k^{\mathrm{T}}\mathsf{Q}\boldsymbol{u}_k &= \boldsymbol{u}_k^{\mathrm{T}}(\mathsf{E} - \mathsf{Q}^{\mathrm{T}})\boldsymbol{u}_k,\\
\boldsymbol{u}_k^{\mathrm{T}}\mathsf{Q}\boldsymbol{u}_k &= \boldsymbol{u}_k^{\mathrm{T}}\mathsf{E}\boldsymbol{u}_k - \boldsymbol{u}_k^{\mathrm{T}}\mathsf{Q}^{\mathrm{T}}\boldsymbol{u}_k.
\end{aligned}$$

We can take the transpose of the second term on the right hand side since it is a scalar value to find that

$$\begin{aligned}
\boldsymbol{u}_k^{\mathrm{T}}\mathsf{Q}\boldsymbol{u}_k &= \boldsymbol{u}_k^{\mathrm{T}}\mathsf{E}\boldsymbol{u}_k - \boldsymbol{u}_k^{\mathrm{T}}\mathsf{Q}\boldsymbol{u}_k,\\
\boldsymbol{u}_k^{\mathrm{T}}\mathsf{Q}\boldsymbol{u}_k &= \frac{1}{2}\boldsymbol{u}_k^{\mathrm{T}}\mathsf{E}\boldsymbol{u}_k.
\end{aligned}$$

Then, substituting the form of the E matrix results in

$$\boldsymbol{u}_k^{\mathrm{T}}\mathsf{Q}\boldsymbol{u}_k = \frac{1}{2}(u_{k,N}^2 - u_{k,1}^2).$$

Finally, we expand term (3) as

$$-\boldsymbol{u}_k^{\mathrm{T}}\boldsymbol{t}_{\boldsymbol{L}}(\boldsymbol{t}_{\boldsymbol{L}}^{\mathrm{T}}\boldsymbol{u}_k - \boldsymbol{t}_{\boldsymbol{R}}^{\mathrm{T}}\boldsymbol{u}_{(k-1)}) = u_{k,1}u_{(k-1),N} - u_{k,1}^2.$$

Plugging this back into (3.13) we find that for an element k,

$$\frac{1}{2}\frac{d}{dt}\|\boldsymbol{u}_k\|_P^2 = -\frac{1}{2}u_{k,N}^2 - \frac{1}{2}u_{k,1}^2 + u_{k,1}u_{(k-1),N}.$$

Now, sum over all n elements

$$\frac{1}{2}\sum_{k=1}^{n}\left(\frac{d}{dt}\|\boldsymbol{u}_k\|_P^2\right) = \sum_{k=1}^{n}\left(-\frac{1}{2}u_{k,N}^2 - \frac{1}{2}u_{k,1}^2 + u_{k,1}u_{(k-1),N}\right).$$

Expanding the sum on the right hand side and gathering like terms gives

$$\begin{aligned}\frac{1}{2}\sum_{k=1}^{n}\left(\frac{d}{dt}\|\boldsymbol{u}_k\|_P^2\right) &= \sum_{k=1}^{n}\left(-\frac{1}{2}u_{k,1}^2 + u_{k,1}u_{(k-1),N} - \frac{1}{2}u_{(k-1),N}^2\right), \\ &= -\frac{1}{2}\sum_{k=1}^{n}\left(u_{k,1}^2 - 2u_{k,1}u_{(k-1),N} + u_{(k-1),N}^2\right), \\ \frac{1}{2}\sum_{k=1}^{n}\left(\frac{d}{dt}\|\boldsymbol{u}_k\|_P^2\right) &= -\frac{1}{2}\sum_{k=1}^{n}(u_{k,1} - u_{(k-1),N})^2,\end{aligned}$$

then, integrating in time results in

$$\begin{aligned}\int_0^T \sum_{k=1}^{n}\left(\frac{d}{dt}\|\boldsymbol{u}_k\|_P^2\right) dt &= -\int_0^T \sum_{k=1}^{n}(u_{k,1} - u_{(k-1),N})^2\, dt, \\ \sum_{k=1}^{n}\|\boldsymbol{u}_k(T)\|_P^2 &= \sum_{k=1}^{n}\|\boldsymbol{u}_k(0)\|_P^2 - \int_0^T \sum_{k=1}^{n}(u_{k,1} - u_{(k-1),N})^2\, dt.\end{aligned}$$

The second term on the right hand side of the above equation is a negative semi-definite term, therefore,

$$\sum_{k=1}^{n}\|\boldsymbol{u}_k(T)\|_P^2 \leq \sum_{k=1}^{n}\|\boldsymbol{F}_k\|_P^2, \tag{3.14}$$

where $\boldsymbol{F}_k$ is the initial condition evaluated at the nodes of the k^{th} element. Thus, we have bounded the time derivative of the norm of the solution from above. Therefore, we claim that the semi-discrete scheme (3.12) is stable as we have shown the norm of the solution to be a decreasing function in time. This means that the norm is bounded by the data of the problem.

In section 3.3.1, we showed that using both upwind and symmetric SATs results in discretizations that can be algebraically manipulated into a consistent approximation to the integral form of the linear advection equation, discretized using a single element. The proofs of the single element case easily transfer to the multi-element case, and therefore, the discretization is conservative at the element level.

Now that we have motivated the use of the SBP-SAT technique to discretize the spatial term in the linear advection equation, we show the results we have obtained considering both the single and multi-element semi-discretizations. We will demonstrate the convergence properties of the scheme as well as the stability properties we have claimed for the scheme.

3.3.3 Results for the Linear Advection Equation

We have now motivated the use of the SBP-SAT technique to solve PDEs. Specifically, we will demonstrate the convergence properties of the single element scheme, (3.5), as well as the multi-element scheme, (3.12), through numerical experiments. To study the convergence properties of the schemes, we first need an exact solution to the linear advection equation that we can compare our numerical solution against.

We will take our exact solution to be $u_{EX} = \sin(x-t)$ on $x \in [0, 2\pi]$ and $t > 0$. Clearly, $\sin(x-t)$ is periodic on the domain and it can easily be substituted into (3.4) to see that it satisfies the PDE. Thus, we can write our PDE as follows:

$$\begin{aligned} \frac{\partial u}{\partial t} + \frac{\partial u}{\partial x} &= 0, x \in [0, 2\pi], t > 0, \\ u(0,t) &= u(2\pi, t), \\ u(x,0) &= \sin(x). \end{aligned} \tag{3.15}$$

To study the convergence rates of the schemes (3.5) and (3.12), we will use a third-order strong stability preserving Runge-Kutta (SSP-RK3) scheme, (5.32), to march in time from $t = 0s$ to $t = 1s$, with a time step of 10^{-5}. Then, we will compute the error vector, $\boldsymbol{E} = \boldsymbol{u}_{num} - \boldsymbol{u}_{EX}$, where, $\boldsymbol{u}_{num}$ is the numerical solution, and $\boldsymbol{u}_{EX}$ is the exact solution. Finally, the approximate L_2 error can be computed as follows:

$$L_2 = \left(\sum_{i=1}^{n} \boldsymbol{E}_i^{\mathrm{T}} \mathsf{P} \boldsymbol{E}_i \right)^{\frac{1}{2}}, \tag{3.16}$$

where, the sum over i represents the sum over all elements in the discretization. To display the results we will use log-log error plots as the convergence rates of the scheme can be seen in the slope of the line in the log-log error plot.

To begin, we will show the numerical results for the single element case. We use SBP operators of degree 1 through 4, and use 50, 100, 200, 400, and 800 nodes to discretize the spatial domain. Then, we will give the slope of the line of best fit in the last 3 points on the plot to determine the convergence rates of each degree. The results can be found in Figure (3.1).

It is clear from Figure (3.1) that the scheme, (3.5), achieves convergence on the order of $p + 1$ for a degree p SBP operator. We can show that this convergence order is also achieved in the multi-element case. In this case, we discretize the domain into multiple

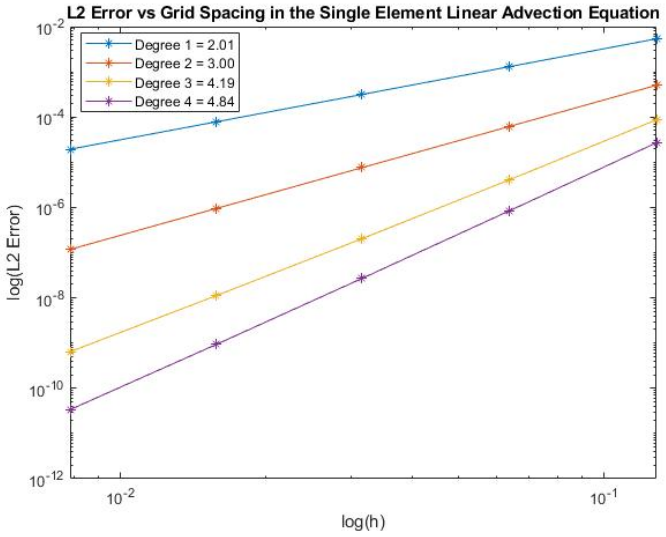

Figure 3.1: The convergence test on the linear advection equation discretized in space using (3.5). The domain was discretized using a single element with number of nodes = 50, 100, 200, 400, and 800.

elements and keep the number of nodes per element constant. We use 20 nodes per element and set our number of elements to 2, 4, 8, 16, and 32. The results can be found in Figure (3.2). Therefore, in both the single and multi-element case, we observe $p+1$ convergence using degree p SBP operators.

We can check the other properties of the semi-discretization. To do so, we will show that the stability property, (3.14), holds when running simulations. At each time step, we multiply the right hand side of (3.12) by $\boldsymbol{u}_k^{\mathrm{T}}\mathsf{P}$ and sum over all elements. As shown theoretically, this sum should be less than or equal to zero for all time steps. Figures (3.3), (3.4), (3.5), and (3.6) show the numerical result of this test in the case of degree 1, 2, 3, and 4 SBP operators, respectively. In each test, the domain is discretized into 32 elements with 20 nodes per element. As seen in figure (3.3), the time rate of change of the p-norm of the numerical solution, when discretizing with degree 1 SBP operators, is less than or equal to zero for all time. Similarly, in figure (3.4), it can be seen that when using degree 2 SBP operators, the time rate of change of the p-norm is less than or equal to zero for all time, however, it is several orders of magnitude less than the degree 1 case. Finally, in figures (3.5) and (3.6), we see that, when using degree 3 and 4 SBP operators, the time rate of change of the p-norm is machine zero. Therefore, the numerical solution satisfies the stability property that we demonstrated for the semi-discrete scheme using degree 1-4

SBP operators.

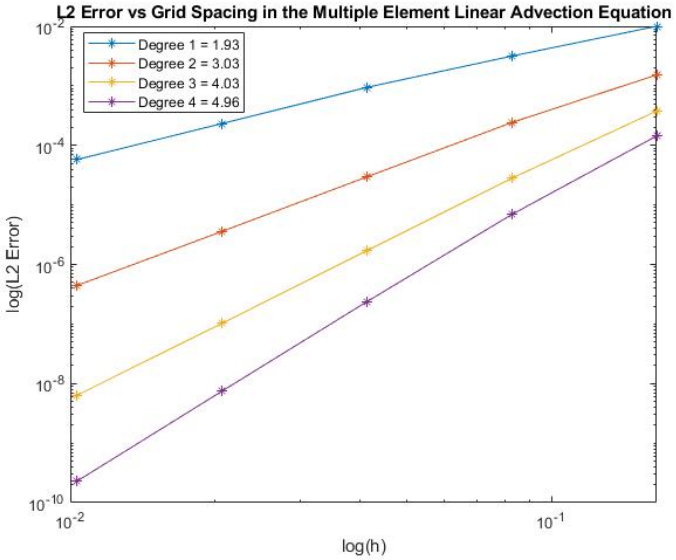

Figure 3.2: The convergence test on the linear advection equation discretized in space using (3.12). The domain was discretized using multiple elements = 2, 4, 8, 16, and 32 with number of nodes per element held constant at 20.

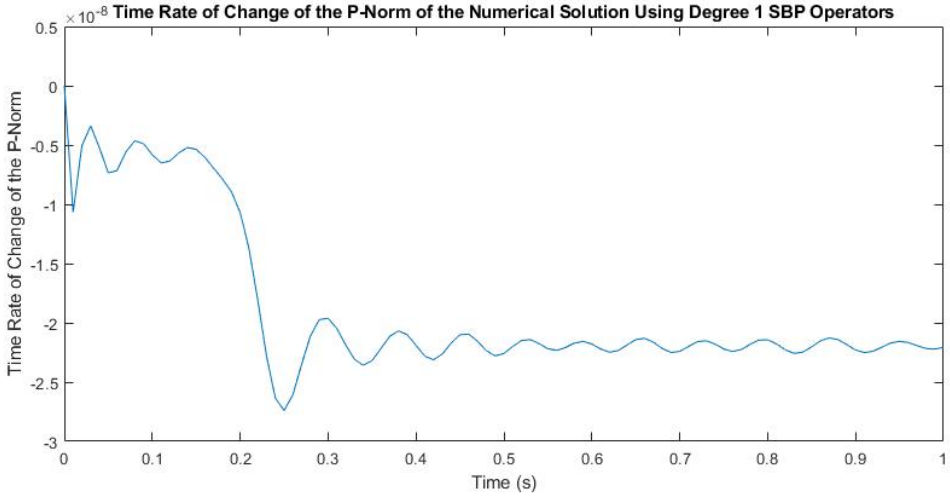

Figure 3.3: The stability test for the multi-element linear advection equation, (3.12), discretized using degree 1 SBP operators. The domain was discretized into 32 elements with 20 nodes per element. This plot shows the time rate of change of the p-norm of the solution vs time.

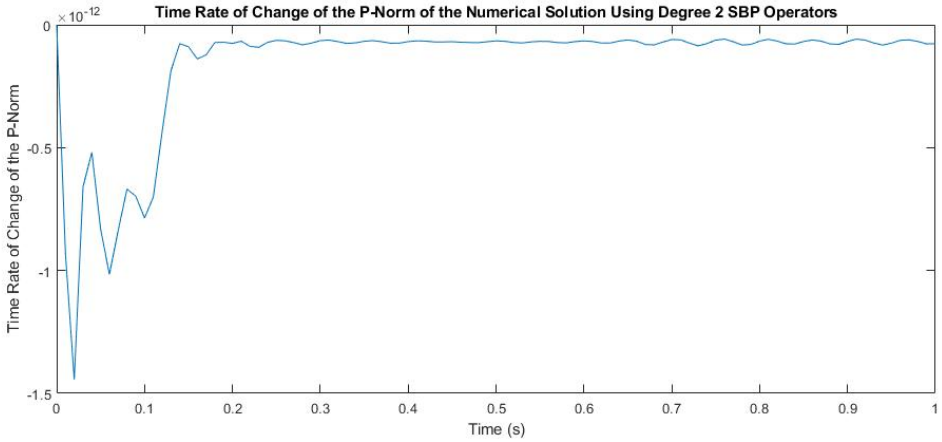

Figure 3.4: The stability test for the multi-element linear advection equation, (3.12), discretized using degree 2 SBP operators. The domain was discretized into 32 elements with 20 nodes per element. This plot shows the time rate of change of the p-norm of the solution vs time.

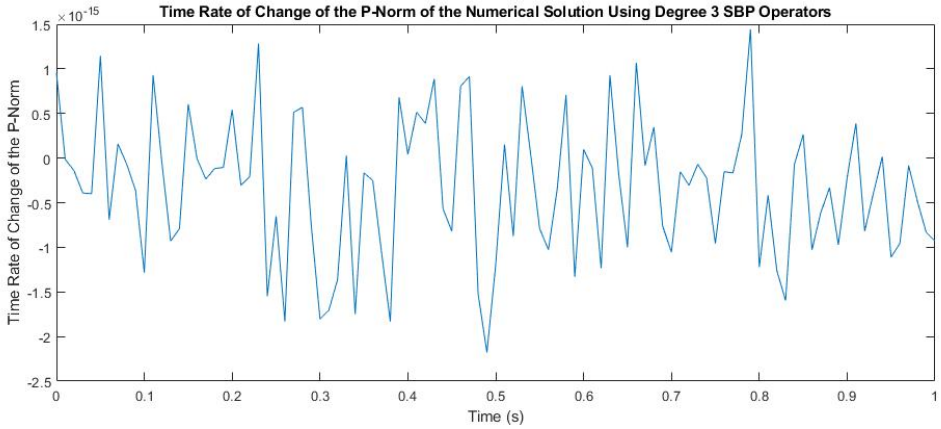

Figure 3.5: The stability test for the multi-element linear advection equation, (3.12), discretized using degree 3 SBP operators. The domain was discretized into 32 elements with 20 nodes per element. This plot shows the time rate of change of the p-norm of the solution vs time.

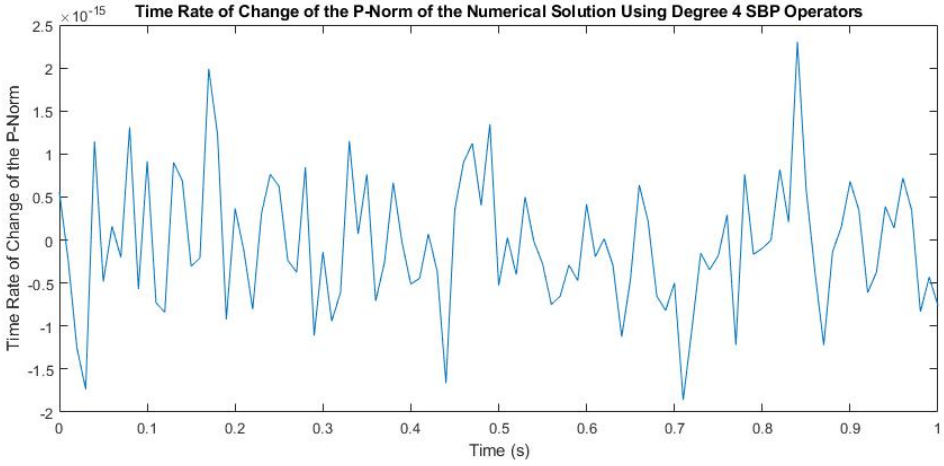

Figure 3.6: The stability test for the multi-element linear advection equation, (3.12), discretized using degree 4 SBP operators. The domain was discretized into 32 elements with 20 nodes per element. This plot shows the time rate of change of the p-norm of the solution vs time.

3.4 Special SBP Derivative Operator

In later chapters, we will study the isentropic Baer-Nunziato equations which contain variables, such as densities, that can get arbitrarily close to zero, but, can never be less than or equal to zero. To maintain this property, we will develop a positivity-preserving scheme for the Baer-Nunziato equations. In the construction of our scheme, we will use a special derivative operator.

Recall from Definition (3.2.1) that the SBP derivative matrix is defined as $\mathsf{D} = \mathsf{P}^{-1}\mathsf{Q}$. One can create a derivative matrix using the first-order Q matrix, which we will denote as Q_1, and a high-order P matrix, which we will denote as P_H. Indeed, using high-order P_H and first-order Q_1, the derivative matrix is constructed as

$$\mathsf{D}_1 = \mathsf{P}_H^{-1}\mathsf{Q}_1, \tag{3.17}$$

where,

$$\mathsf{Q}_1 = \begin{bmatrix} -1/2 & 1/2 & & & \\ -1/2 & 0 & 1/2 & & \\ & \ddots & \ddots & \ddots & \\ & & -1/2 & 0 & 1/2 \\ & & & -1/2 & 1/2 \end{bmatrix}.$$

It can be shown that discretizations using the derivative operator, (3.17), have a truncation error of $\mathcal{O}(h)$, by studying the integral form of a general conservation law. For this purpose, consider the following generic scalar conservation law with solution u and flux f, in the domain $x \in [x_L, x_R]$

$$\frac{\partial u}{\partial t} + \frac{\partial f}{\partial x} = 0.$$

Integrating in space over the domain results in

$$\begin{aligned} \int_{x_L}^{x_R} \frac{\partial u}{\partial t}\, dx + \int_{x_L}^{x_R} \frac{\partial f}{\partial x}\, dx = 0, \\ \int_{x_L}^{x_R} \frac{\partial u}{\partial t}\, dx + f\Big|_{x_L}^{x_R} = 0. \end{aligned} \tag{3.18}$$

We will show that our discretization of the strong formulation can be represented as a discretization of the integral form of the equations, and from this perspective, show that the truncation error is of order $\mathcal{O}(h)$. To do so, we define a set of intermediate points,

$\overline{\boldsymbol{x}} = [\overline{x}_0, \ldots, \overline{x}_N]$, with a similar definition in the multi element case, which defines bounding control volumes around each solution point $\boldsymbol{x} = [x_1, \ldots, x_N]$. Furthermore, $x_1 = \overline{x}_1$ and $x_N = \overline{x}_N$. These points, $\overline{\boldsymbol{x}}$, are called flux points [25, 62, 63]. The flux points form a grid whose spacing is equal to the entries in the diagonal norm matrix P_H, i.e.,

$$\Delta\overline{\boldsymbol{x}} = \mathsf{P}_H \mathbf{1},$$

where, the Δ operator is an $N \times (N+1)$ matrix defined as

$$\Delta = \begin{bmatrix} -1 & 1 & 0 & 0 & \ldots & 0 \\ 0 & -1 & 1 & 0 & \ldots & 0 \\ 0 & 0 & -1 & 1 & & 0 \\ & & \ddots & \ddots & \ddots & \\ & & & 0 & -1 & 1 \end{bmatrix}.$$

Fisher *et al.* [24] have shown that all one dimensional SBP first derivative operators can be recast into telescopic flux form

$$\mathsf{D}\boldsymbol{f} = \mathsf{P}^{-1}\mathsf{Q}\boldsymbol{f} = \mathsf{P}^{-1}\Delta\overline{\boldsymbol{f}}, \tag{3.19}$$

where $\overline{\boldsymbol{f}}$ is a flux vector of size (N+1) which is defined on the flux points. It is clear from (3.19) that $\mathsf{Q}\boldsymbol{f} = \Delta\overline{\boldsymbol{f}}$. For the degree 1 SBP operator, Q_1, we have

$$\overline{\boldsymbol{f}} = \left[f_1, \overline{f}_1, \ldots, \overline{f}_{N-1}, f_N\right]^{\mathrm{T}}, \tag{3.20}$$

where $\overline{\boldsymbol{f}}_i = \frac{1}{2}(f_{i+1} + f_i)$ for $i \in [1, N-1]$. Using this telescopic flux form, we can recast our scheme into a consistent approximation to (3.17) as follows

$$\begin{aligned} \frac{d\boldsymbol{u}_i}{dt} + (\mathsf{D}_1\boldsymbol{f})_i &= (\boldsymbol{SATs})_i, \\ \frac{d\boldsymbol{u}_i}{dt} + (\mathsf{P}_H^{-1}\mathsf{Q}_1\boldsymbol{f})_i &= (\boldsymbol{SATs})_i. \end{aligned}$$

Multiplying the above equation by $(\mathsf{P}_H)_{ii}$ results in

$$(\mathsf{P}_H)_{ii}\frac{d\boldsymbol{u}_i}{dt} + (\Delta\overline{\boldsymbol{f}})_i = (\mathsf{P}_H)_{ii}(\boldsymbol{SATs})_i. \tag{3.21}$$

In this form, it can be shown that discretizing in space using the special derivative operator, (3.17), results in first-order truncation error. Furthermore, it can be seen that the derivative operator (3.17) is degree zero, in that, it differentiates a constant exactly. This is easy to see from the telescopic flux form, since, for a constant solution, $\overline{\boldsymbol{f}}$ is constant, thus,

$$\mathsf{D}_1 = \mathsf{P}_H^{-1}\mathsf{Q}_1 = \mathsf{P}_H^{-1}\Delta\overline{\boldsymbol{f}} = 0.$$

Theorem 3.4.1. Discretization (3.21) has first-order truncation error in space using the derivative operator (3.17), that is

$$(\mathsf{P}_H)_{ii}\frac{d\boldsymbol{u}_i}{dt} + (\Delta\overline{\boldsymbol{f}})_i - (\mathsf{P}_H)_{ii}(\boldsymbol{SATs})_i = \int_{\overline{x}_{i-1}}^{\overline{x}_i} \frac{\partial u}{\partial t}dx + f\Big|_{\overline{x}_{i-1}}^{\overline{x}_i} + \mathcal{O}(h), \quad i = 1, 2, \ldots, N.$$

Proof: We will show that using the degree 1 SBP matrix, Q, in equation (3.21) results in a first-order approximation to (3.18), thus showing that the derivative operator, (3.17), results in a discretization with first-order truncation error. To do so, we will substitute the exact solution into (3.21). Note that the SAT term does not need to be considered since, when using the exact solution, this term vanishes. We first examine the interior nodes by expanding the spacial derivative term in (3.21) to find that

$$(\mathsf{P}_H)_{ii}\frac{d\boldsymbol{u}_i}{dt} + (\overline{\boldsymbol{f}}_i - \overline{\boldsymbol{f}}_{i-1}) = 0, \tag{3.22}$$

for $i = 2, 3, \ldots, N-1$. We now look to show the following 2 properties for the terms in (3.22): 1)

$$f(\overline{x}_i) - f(\overline{x}_{i-1}) = \overline{\boldsymbol{f}}_i - \overline{\boldsymbol{f}}_{i-1} + \mathcal{O}(h), \tag{3.23}$$

and 2)

$$\int_{\overline{x}_{i-1}}^{\overline{x}_i} \frac{du}{dt}\,dx = (\mathsf{P}_H)_{ii}\frac{d\boldsymbol{u}_i}{dt} + \mathcal{O}(h), \tag{3.24}$$

if these two properties hold, then (3.22) is a first-order approximation to the integral form over the domain $x \in [\overline{x}_{i-1}, \overline{x}_i]$. To prove property (3.23), consider (3.23); by expanding the terms on the right hand side using (3.20) to find that

$$\overline{\boldsymbol{f}}_i - \overline{\boldsymbol{f}}_{i-1} = \underbrace{\frac{1}{2}(f_i + f_{i+1})}_{1} - \underbrace{\frac{1}{2}(f_i + f_{i-1})}_{2}. \tag{3.25}$$

Then, using Taylor series of $f(x)$ centered around the flux points, we can find approximations of f_i, f_{i+1}, and f_{i-1} evaluated at the flux nodes. First, consider the flux node $\overline{x}_i$, this node is surrounded by the solution points x_i and x_{i+1}. Since $x_{i+1} - x_i = h$, we can say that $x_i = \overline{x}_i - \alpha h$ and $x_{i+1} = \overline{x}_i + \beta h$, where $\alpha + \beta = 1$. Therefore, taking a Taylor series approximation of $f(x)$ around $\overline{x}_i$ and evaluating at x_i one finds that

$$f_i = f(\overline{x}_i) + \frac{df}{dx}\bigg|_{\overline{x}_i}(-\alpha h) + \mathcal{O}(h^2),$$

and similarly, evaluating the Taylor series at x_{i+1} results in

$$f_{i+1} = f(\overline{x}_i) + \left.\frac{df}{dx}\right|_{\overline{x}_i} (\beta h) + \mathcal{O}(h^2).$$

Therefore, term 1 in (3.25) can be written as

$$\begin{aligned}\frac{1}{2}(f_i + f_{i+1}) &= f(\overline{x}_i) - \alpha \left.\frac{df}{dx}\right|_{\overline{x}_i} h + \beta \left.\frac{df}{dx}\right|_{\overline{x}_i} h + \mathcal{O}(h^2), \\ &= f(\overline{x}_i) + \mathcal{O}(h).\end{aligned}$$

A similar procedure can be carried out for the flux node $\overline{x}_{i-1}$ to find that term 2 in equation (3.25) can be written as

$$\frac{1}{2}(f_i + f_{i-1}) = f(\overline{x}_{i-1}) + \mathcal{O}(h).$$

Therefore, $\overline{\boldsymbol{f}}_i - \overline{\boldsymbol{f}}_{i-1} = f(\overline{x}_i) - f(\overline{x}_{i-1}) + \mathcal{O}(h)$ and (3.23) is satisfied. Now, all that remains to show is that (3.24) holds. To begin, note that, by the Leibniz integral rule we can rewrite (3.24) as

$$\frac{d}{dt}\int_{\overline{x}_{i-1}}^{\overline{x}_i} u\, dx = \frac{d}{dt}(\mathsf{P}_H)_{ii}\boldsymbol{u}_i + \mathcal{O}(h),$$

thus, we check that we can satisfy the equivalent condition

$$\int_{\overline{x}_{i-1}}^{\overline{x}_i} u\, dx = (\mathsf{P}_H)_{ii}\boldsymbol{u}_i + \mathcal{O}(h).$$

To this end, take a Taylor series approximation of u(x) around the solution point x_i, to find that

$$u(x) = \sum_{k=0}^{\infty} \left.\frac{\partial u^k}{\partial x^k}\right|_{x_i} \frac{(x - x_i)^k}{k!}.$$

Integrating across the domain results in

$$\begin{aligned}\int_{\overline{x}_{i-1}}^{\overline{x}_i} u\, dx &= \int_{\overline{x}_{i-1}}^{\overline{x}_i} \sum_{k=0}^{\infty} \left.\frac{\partial u^k}{\partial x^k}\right|_{x_i} \frac{(x - x_i)^k}{k!}\, dx, \\ &= \sum_{k=0}^{\infty} \left.\frac{\partial u^k}{\partial x^k}\right|_{x_i} \left(\frac{(\overline{x}_i - x_i)^{k+1}}{(k+1)!} - \frac{(\overline{x}_{i-1} - x_i)^{k+1}}{(k+1)!} \right), \\ &= u_i[(\overline{x}_i - x_i) - (\overline{x}_{i-1} - x_i)] + \sum_{k=1}^{\infty} \left.\frac{\partial u^k}{\partial x^k}\right|_{x_i} \left(\frac{(\overline{x}_i - x_i)^{k+1}}{(k+1)!} - \frac{(\overline{x}_{i-1} - x_i)^{k+1}}{(k+1)!} \right).\end{aligned}$$

The first term on the right hand side of the above equation gives

$$u_i[(\overline{x}_i - x_i) - (\overline{x}_{i-1} - x_i)] = u_i(\overline{x}_i - \overline{x}_{i-1}) = u_i(\mathsf{P}_H)_{ii},$$

where, it can be shown that the second term is $\mathcal{O}(h)$ as follows:

$$\sum_{k=1}^{\infty} \frac{\partial u^k}{\partial x^k}\bigg|_{x_i} \left(\frac{(\overline{x}_i - x_i)^{k+1}}{(k+1)!} - \frac{(\overline{x}_{i-1} - x_i)^{k+1}}{(k+1)!} \right) = \frac{1}{2}\frac{\partial u}{\partial x}\bigg|_{x_i} [(\overline{x}_i - x_i)^2 - (\overline{x}_{i-1} - x_i)^2],$$
$$+ \sum_{k=2}^{\infty} \frac{\partial u^k}{\partial x^k}\bigg|_{x_i} \left(\frac{(\overline{x}_i - x_i)^{k+1}}{(k+1)!} - \frac{(\overline{x}_{i-1} - x_i)^{k+1}}{(k+1)!} \right).$$

Then, expand the term $(\overline{x}_i - x_i)^2 - (\overline{x}_{i-1} - x_i)^2$ to find

$$\begin{aligned}(\overline{x}_i - x_i)^2 - (\overline{x}_{i-1} - x_i)^2 &= -2x_i(\overline{x}_i - \overline{x}_{i-1}) + \overline{x}_i^2 - \overline{x}_{i-1}^2, \\ &= -2x_i h(\tilde{\mathsf{P}}_H)_{ii} + \overline{x}_i^2 - \overline{x}_{i-1}^2, \\ &= \mathcal{O}(h).\end{aligned}$$

Therefore, we have that $\int_{\overline{x}_{i-1}}^{\overline{x}_i} u\,dx = (\mathsf{P}_H)_{ii}\boldsymbol{u}_i + \mathcal{O}(h),\ \forall\ i = 2, 3, \ldots, N-1$, which means both properties (3.23) and (3.24) hold on the interior nodes. All that remains to be show is that properties 1 and 2 hold on the boundary nodes $i = 1, N$. The analysis is the same for both nodes, therefore, we only detail node 1. Where we have that

$$(\mathsf{P}_H)_{11}\frac{\partial \boldsymbol{u}_1}{\partial t} + \left(\overline{\boldsymbol{f}_1} - f_1\right) = 0.$$

We immediately see that property 1 holds since, as shown previously, $f(\overline{x}_1) = \overline{\boldsymbol{f}_1} + \mathcal{O}(h)$, and $f_1 = f(x_1) = f(\overline{x}_0)$, thus, $f(\overline{x}_1) - f(\overline{x}_0) = \overline{\boldsymbol{f}_1} - \overline{\boldsymbol{f}_0} + \mathcal{O}(h)$. Then, the same proof for property 2 holds for both the first and last nodes. Therefore, we have that $\int_{\overline{x}_{i-1}}^{\overline{x}_i} u\,dx = (\mathsf{P}_H)_{ii}\boldsymbol{u}_i + \mathcal{O}(h)$ for $i = 1, N$. Thus, the derivative operator, (3.17), results in first-order truncation error. □

In compliment to theorem (3.4.1), we show numerically the convergence rate of discretizations using the special derivative operator. We do so by testing the multi-element convergence rates of the linear advection equation using this special derivative matrix. We will construct the derivative matrix using second, third, and fourth-order P, and show that the scheme (3.12) converges at first-order no matter the degree of P. Note that we do not include first-order P since this would simply return the regular first-order derivative operator, which has already been discussed in section 3.3.3. Our numerical experiments

demonstrate that the special derivative operator leads to solution convergence at first-order. This is not unreasonable, since, recollect in section 3.3.3, we demonstrated that degree p SBP operators result in $p+1$ convergence rates for the multi-element scheme (3.12). Thus, it is not unreasonable to expect the degree zero special derivative operator to lead to discretizations which converge at first-order. To run this test the domain is discretized into multiple elements with 20 nodes per element. After each run the approximate L_2 error, (3.16), is computed, then, the number of elements is doubled and the test is repeated. We complete this process for P matrix of order 2, 3, and 4 and then plot the results on a log-log plot. The convergence rate is determined by taking the line of best fit between the last 3 nodes. Figure (3.7) shows that no matter the order of the P matrix (for order greater than one), the special derivative operator, D_1, defined in (3.17), converges at first-order.

Finally, one might think that we see convergence using the special derivative operator only because we have accompanied it with upwind SATs, which allow the scheme to converge at $p+1$. Thus, we run the same test on the special derivative operator, but this time, use symmetric SATs to show that the scheme is still converging to the exact solution. Figure (3.8) shows the results of the linear advection equation discretized using regular SBP operators and symmetric SATs. The even degree operators achieve convergence on an order between $p+\frac{1}{2}$ and $p+1$. But, the odd degree SBP operators achieve convergence on the order of p. Then, running the same test using the special derivative operator and symmetric SATs, it can be seen from Figure (3.9), that the numerical solution converges to the exact solution as the grid is refined using degree 2, 3, and 4 norm matrix P. Therefore, the special derivative matrix, (3.17), converges at first-order.

In this chapter we have demonstrated the SBP properties and the accuracy of the operators through the model problem of the linear advection equation. For the remainder of this thesis, we will be studying the isentropic Baer-Nunizato model. Our goal is to develop an entropy-stable scheme that preserves positivity of the void fractions as well as the densities no matter how close the quantities get to zero. We also want our scheme to be high-order accurate for smooth solutions and have the capability to capture shocks. In the next chapter, we will make the first step to achieving our goal by developing a numerical scheme to handle the simplest possible solution to the Baer-Nunziato equations; that being a smooth solution with periodic boundary conditions. Such a solution conserves the entropy of the system, thus, we develop a high-order entropy-conservative scheme to solve the isentropic Baer-Nunziato model through the use of high-order SBP operators.

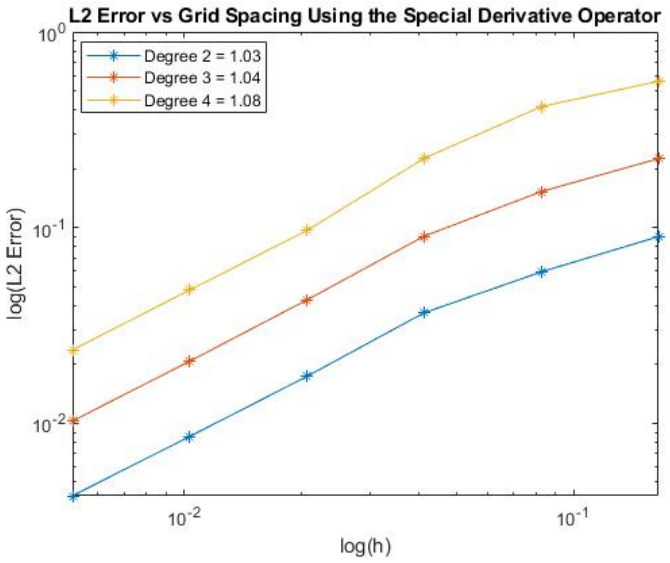

Figure 3.7: The convergence plot of the special first-order derivative operator using upwind SATs. This is a log-log plot of the L_2 error vs the grid spacing. The domain is discretized into multiple elements = 2, 4, 8, 16, and 32, with 20 nodes per element. The lines are labeled degree 2 through 4 and this indicates the degree of the P matrix that was used.

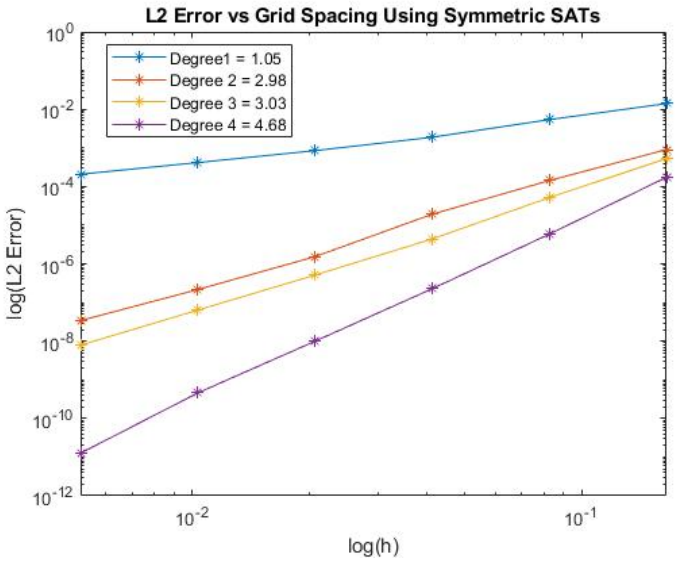

Figure 3.8: The convergence plot of multi-element linear advection equation using symmetric SATs instead of upwind SATs. The domain was discretized using multiple elements = 2, 4, 8, 16, and 32, with the number of nodes per element held constant at 20.

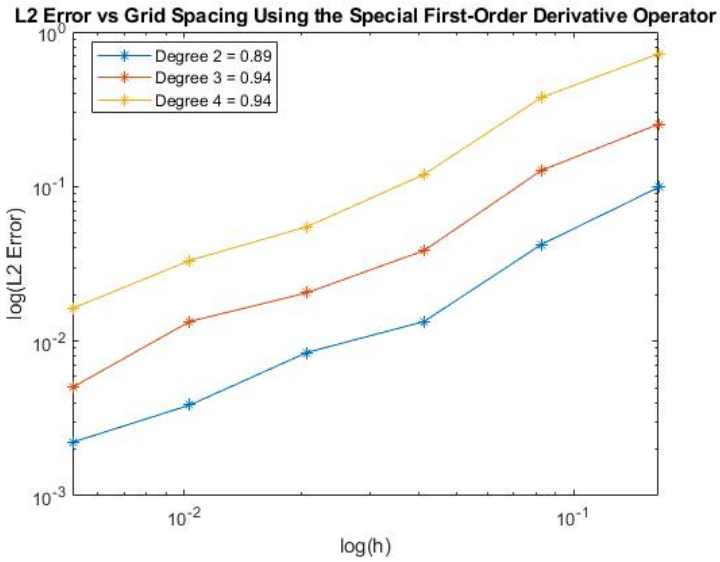

Figure 3.9: The convergence plot of the special first-order derivative operator using symmetric SATs. The lines are labeled according to the degree of the P matrix that was used.

Chapter 4

Entropy-Conservative Discretizations

4.1 Motivation

As is implied in the name, an entropy-conservative scheme is a scheme where the entropy of the system is conserved. The second law of thermodynamics for a closed system states that the change in entropy of a system is caused by entropy generation and entropy transfer. Entropy generation could occur in places such as across a discontinuity, thus, in this chapter we consider smooth solutions to the Baer-Nunziato equations (2.3). Entropy transfer occurs when there is heat or mass transferred in or out of the closed system. A mathematical model would reflect this transfer of heat or mass through the use of boundary conditions. We will take a systematic approach to solving the isentropic Baer-Nunziato equations where we will first create a scheme to handle smooth solutions and then use this scheme as a baseline to solve more difficult problems. Therefore, in this chapter we will develop an entropy-conservative scheme to solve the simplest possible problem; a smooth, periodic solution to the isentropic Baer-Nunziato model. Extending this scheme to non-periodic problems requires the formulation of entropy-stable boundary conditions, which is a non-trivial task and will not be dealt with in this thesis.

Many practical problems will contain shocks, discontinuities, and boundary conditions that will lead to the production of entropy in the system. An entropy-conservative scheme can serve as the foundation to which entropy-dissipative terms can be added, leading to an entropy-stable scheme. Entropy-stable schemes bound the mathematical entropy of a system from above, and have the capability to dissipate the entropy. Thus, they produce solutions that are physically correct in the presence of entropy generation, whereas an

entropy-conservative scheme would not produce a solution that is physically realizable. Therefore, entropy-stable schemes can be applied to shocked problems.

We have motivated the use of entropy-conservative/stable schemes from a physical point of view, but, they also serve a practical one as well. From a practical standpoint, we want to ensure that our numerical solution will not blow up, and as shown in section 2.2, we can convert a bound on the entropy of the system to an L_2 bound on the solution. Therefore, our starting point to study the Baer-Nunziato model numerically is to develop an entropy-conservative scheme in this chapter. However, we are interested in shocked problems and if the solution is not smooth, then physically the entropy of the system is not conserved. This means that, even if the entropy-conservative scheme were to converge, it would not converge to a physically realizable solution. Thus, in the next chapter, we take our entropy-conservative scheme, and add two entropy-dissipative terms to make it entropy-stable.

There exists an extensive body of work in the field that uses SBP operators to develop entropy-stable schemes for systems of nonlinear PDEs. For example, Fisher and Carpenter [25] combined the use of finite-difference SBP operators with the entropy-conservative numerical flux of Ismael and Roe [35], to create an entropy-stable, high-order scheme for the compressible Navier-Stokes equations. Furthermore, Hicken, Del Rey Fernández, and Zingg [32] have extended the SBP framework to handle general element types such as triangles and tetrahedra which can make SBP-SAT schemes easier to implement on complex domains. Renac [50] has developed a general framework to design high-order discretizations for nonconservative hyperbolic systems of the form (2.10) that satisfy the entropy inequality (2.7).

Recently, Upperman and Yamaleev [63] have developed a first-order entropy-stable positivity-preserving scheme for the Navier-Stokes equations. They use diagonal-norm SBP operators and re-write the scheme in a typical finite-volume manner, known as a flux-differencing form. In this flux-differencing form, combined with the Brenner regularization to the Navier-Stokes equations, they create an artificial dissipation operator that allows them to prove point-wise positivity of the thermodynamic variables. Upperman [62] then extends this work to high-order through the use of a mixing scheme, where the first-order positivity-preserving scheme is mixed with the high-order positivity-violating scheme to create a high-order positivity-preserving scheme. Alternatively, Rueda-Ramírez and Gassner [51] show that the existence of a flux-differencing form allows for the use of sub-cell limiting strategies which improve the robustness of the high-order scheme and can be used to preserve positivity.

In this chapter, we present a baseline entropy-conservative scheme for (2.3) using

diagonal-norm finite-difference SBP operators and the Hadamard formalism. This scheme is capable of handling smooth solutions to the Baer-Nunziato model with high-order accuracy through the use of high-order SBP operators. However, it has no positivity-preserving properties and is prone to spurious oscillations in the presence of discontinuities. In the following chapter, we will present a first-order entropy-stable scheme that addresses these limitations. Then, as in Upperman [62], we will mix the first-order entropy-stable positivity-preserving scheme, with the high-order entropy-conservative scheme constructed in this chapter to create a high-order entropy-stable positivity-preserving scheme for the Baer-Nunziato equations.

4.2 Entropy-Conservative Semi-Discrete Scheme

For the remainder of the thesis, we will study the isentropic Baer-Nunziato model which is a five equation model. Therefore, we will be studying vector valued functions. The SBP-SAT technique detailed in chapter 3 describes a one equation system. We can extend the SBP-SAT framework to a system of equations easily through the use of tensor products. Let us define the SBP operators for a one equation model as $\overline{\mathsf{L}}$, which can represent any of the SBP operators from Definition (3.2.1). Then, for a 5 equation model we define the SBP operator as $\mathsf{L} = \overline{\mathsf{L}} \otimes \mathsf{I}_5$, where I_5 is the 5x5 identity matrix. That is

$$\mathsf{P} = \overline{\mathsf{P}} \otimes \mathsf{I}_5,\ \mathsf{D} = \overline{\mathsf{D}} \otimes \mathsf{I}_5,\ \mathsf{Q} = \overline{\mathsf{Q}} \otimes \mathsf{I}_5,\ \mathsf{E} = \overline{\mathsf{E}} \otimes \mathsf{I}_5,\ \boldsymbol{t_L} = \overline{\boldsymbol{t_L}} \otimes \mathsf{I}_5,\ \boldsymbol{t_R} = \overline{\boldsymbol{t_R}} \otimes \mathsf{I}_5,\ \mathbf{1} = \overline{\mathbf{1}} \otimes \hat{\mathbf{1}},$$

where, $\hat{\mathbf{1}}$ is a vector of ones with 5 entries. Furthermore, to denote a quantity, $\boldsymbol{u}$, on node i within element j, we use the notation $\boldsymbol{u}_{j,i}$. The continuous entropy analysis performed in chapter 2.2 induces a "non-linear IBP rule"

$$\int_{x_L}^{x_R} \boldsymbol{w}^{\mathrm{T}} \left(\frac{\partial \boldsymbol{f}(\boldsymbol{u})}{\partial x} + \mathsf{c}(\boldsymbol{u}) \frac{\partial \boldsymbol{u}}{\partial x} \right) dx = q \Big|_{x_L}^{x_R}.$$

We recollect that $\boldsymbol{w}^{\mathrm{T}} = \frac{\partial \eta}{\partial u}$, are the entropy variables, η is the entropy, and q is the entropy flux. The SBP property alone is insufficient to mimic the above at the discrete level. Therefore, unlike the linear advection equation, where we could approximate the spatial derivative as $\frac{\partial u}{\partial x} \approx \mathsf{D}\boldsymbol{u}$, we will make use of the Hadamard product to approximate spatial derivatives as follows:

$$2\mathsf{D} \circ \mathsf{F}(\boldsymbol{u}, \boldsymbol{u})\mathbf{1} \approx \left(\frac{\partial \boldsymbol{f}(\boldsymbol{u})}{\partial x} + \mathsf{c}(\boldsymbol{u}) \frac{\partial \boldsymbol{u}}{\partial x} \right). \tag{4.1}$$

Note that the Hadamard product, $\circ$, is a binary operation that takes two matrices of the same size and returns a matrix composed of the product of the corresponding elements, i.e., $(\mathsf{A} \circ \mathsf{B})_{ij} = A_{ij}B_{ij}$. Later, we will prove that when using high-order SBP operators, (4.1) is high-order accurate, i.e., $\frac{\partial \boldsymbol{f}(\boldsymbol{u})}{\partial x} + \mathsf{c}(\boldsymbol{u})\frac{\partial \boldsymbol{u}}{\partial x} = 2\mathsf{D} \circ \mathsf{F}(\boldsymbol{u}, \boldsymbol{u})\mathbf{1} + \mathcal{O}\left(h^p\right)$. Furthermore, we will prove that (4.1) discretely mimics the non-linear IBP rule. In equation (4.1), $\mathsf{F}(\boldsymbol{u}, \boldsymbol{u})$ is a two-point flux function matrix, constructed block-wise, from the entropy-conservative two-point flux function of Renac [50], $\boldsymbol{f}^{(\boldsymbol{EC})}(\boldsymbol{u}_i, \boldsymbol{u}_j)$, such that F_{ij} is a 5x5 diagonal matrix, where its non-zero entries correspond to the entries of $\boldsymbol{f}^{(\boldsymbol{EC})}(\boldsymbol{u}_i, \boldsymbol{u}_j)$. The two point flux functions takes the form $\boldsymbol{f}^{(\boldsymbol{EC})}(\boldsymbol{u}_i, \boldsymbol{u}_j) = \boldsymbol{h}(\boldsymbol{u}_i, \boldsymbol{u}_j) - \boldsymbol{f}(\boldsymbol{u_i}) + \boldsymbol{b}(\boldsymbol{u}_i, \boldsymbol{u}_j)$ where,

$$\boldsymbol{h}\left(\boldsymbol{u}_i, \boldsymbol{u}_j\right) = \begin{bmatrix} 0 \\ \overline{\alpha_1}\,\overline{v_1}\hat{h}_1 \\ \overline{\alpha_1}\left(\overline{v_1}^2\hat{h}_1 + \overline{p_1}\right) \\ \overline{\alpha_2}\,\overline{v_2}\hat{h}_2 \\ \overline{\alpha_2}\left(\overline{v_2}^2\hat{h}_2 + \overline{p_2}\right) \end{bmatrix}, \boldsymbol{f}\left(\boldsymbol{u}_i\right) = \begin{bmatrix} 0 \\ \alpha_1\rho_1 v_1 \\ \alpha_1\left(\rho_1 v_1^2 + p_1\right) \\ \alpha_2\rho_2 v_2 \\ \alpha_2\left(\rho_2 v_2^2 + p_2\right) \end{bmatrix}, \tag{4.2}$$

$$\boldsymbol{b}\left(\boldsymbol{u}_i, \boldsymbol{u}_j\right) = \begin{bmatrix} v_{2i} \\ 0 \\ -p_{1i} \\ 0 \\ p_{1i} \end{bmatrix} \frac{\alpha_{1j} - \alpha_{1i}}{2},$$

$$\hat{h}_a\left(\rho_{ai}, \rho_{aj}\right) = \begin{cases} \frac{\Delta p_a(\rho_a)}{\Delta h_a(\rho_a)}, & \rho_{ai} \neq \rho_{aj}, \\ \rho_a, & \rho_{ai} = \rho_{aj} = \rho_a, \end{cases}, a = 1, 2, \tag{4.3}$$

and $\overline{u} = \frac{u_i + u_j}{2}$. The entropy-conservative two-point flux function can be re-written in fluctuation form, which will be used to prove entropy conservation,

$$\boldsymbol{f}^{(\boldsymbol{EC})}(\boldsymbol{u}_i, \boldsymbol{u}_j) = \boldsymbol{D}^{-}(\boldsymbol{u}_i, \boldsymbol{u}_j) - \boldsymbol{D}^{+}(\boldsymbol{u}_j, \boldsymbol{u}_i), \tag{4.4}$$

where

$$\boldsymbol{D}^{-}(\boldsymbol{u}_i, \boldsymbol{u}_j) = \frac{1}{2}\left(\boldsymbol{h}(\boldsymbol{u}_i, \boldsymbol{u}_j) - \boldsymbol{f}\left(\boldsymbol{u}_i\right) + \boldsymbol{b}\left(\boldsymbol{u}_i, \boldsymbol{u}_j\right)\right),$$
$$\boldsymbol{D}^{+}(\boldsymbol{u}_i, \boldsymbol{u}_j) = \frac{1}{2}\left(\boldsymbol{f}\left(\boldsymbol{u}_j\right) - \boldsymbol{h}(\boldsymbol{u}_i, \boldsymbol{u}_j) - \boldsymbol{b}\left(\boldsymbol{u}_j, \boldsymbol{u}_i\right)\right).$$

This equality holds since $\boldsymbol{h}(\boldsymbol{u}_i, \boldsymbol{u}_j) = \boldsymbol{h}(\boldsymbol{u}_j, \boldsymbol{u}_i)$. Furthermore, the fluctuation fluxes, $\boldsymbol{D}^{\pm}$, satisfy the following consistency property:

$$\boldsymbol{D}^{\pm}\left(\boldsymbol{u}, \boldsymbol{u}\right) = 0, \forall \boldsymbol{u} \in \Omega. \tag{4.5}$$

Here, we use the terminology of Castro *et al.* [10] and for the entropy-entropy flux pair (2.8), the fluctuation fluxes $\boldsymbol{D}^{\pm}$ satisfy

$$\boldsymbol{w}\left(\boldsymbol{u}_i\right)^{\mathrm{T}} \boldsymbol{D}^{-}(\boldsymbol{u}_i, \boldsymbol{u}_j) + \boldsymbol{w}\left(\boldsymbol{u}_j\right)^{\mathrm{T}} \boldsymbol{D}^{+}(\boldsymbol{u}_i, \boldsymbol{u}_j) = \frac{1}{2} q\left(\boldsymbol{u}_j\right) - \frac{1}{2} q\left(\boldsymbol{u}_i\right). \tag{4.6}$$

Later, we will make use of (4.6) to prove the high-order accuracy of (4.1) and to show that it discretely mimics the non-linear IBP rule (2.9). We weakly impose boundary conditions using the SBP-SAT technique [18]. Here, we only consider periodic problems and hence consider symmetric SATs, which have the following form for a single element discretization of the domain

$$\begin{aligned} \boldsymbol{SAT}\boldsymbol{s} = &- \mathsf{P}^{-1}\left(\boldsymbol{t}_{\boldsymbol{L}}\boldsymbol{t}_{\boldsymbol{L}}^{\mathrm{T}} \circ \mathsf{F}(\boldsymbol{u}, \boldsymbol{u})\mathbf{1} - \boldsymbol{t}_{\boldsymbol{L}}\boldsymbol{t}_{\boldsymbol{R}}^{\mathrm{T}} \circ \mathsf{F}(\boldsymbol{u}, \boldsymbol{u})\mathbf{1}\right) \\ &+ \mathsf{P}^{-1}\left(\boldsymbol{t}_{\boldsymbol{R}}\boldsymbol{t}_{\boldsymbol{R}}^{\mathrm{T}} \circ \mathsf{F}(\boldsymbol{u}, \boldsymbol{u})\mathbf{1} - \boldsymbol{t}_{\boldsymbol{R}}\boldsymbol{t}_{\boldsymbol{L}}^{\mathrm{T}} \circ \mathsf{F}(\boldsymbol{u}, \boldsymbol{u})\mathbf{1}\right), \end{aligned} \tag{4.7}$$

where $\boldsymbol{t}_{\boldsymbol{L}}$ and $\boldsymbol{t}_{\boldsymbol{R}}$ are defined in (3.3). Notice that this form of the symmetric SATs are very similar to those discussed in section 3.3.2 for the linear advection equation. We are only weakly enforcing inter-element coupling as we are not forcing the values at the element interfaces to be equal. Instead, we are penalizing the difference in the solution at an element interface. For example, take the first term in (4.7); in the case of a single element with N nodes, this reduces to $-\mathsf{P}^{-1}\boldsymbol{t}_{\boldsymbol{L}}\left(\mathsf{F}(u_1, u_1) - \mathsf{F}(u_1, u_N)\right)$. Since we are considering a periodic problem, for the first time step, after initializing the problem, we have that $u_1 = u_N$, meaning that the SAT term reduces to zero. The symmetric SAT only acts when numerical error is introduced into the solution, resulting in $u_1 \neq u_N$ and works to bring u_1 and u_N closer to the same value. Thus, in the case of a single element, the semi-discrete scheme reads

$$\frac{d\boldsymbol{u}}{dt} + 2\mathsf{D} \circ \mathsf{F}(\boldsymbol{u}, \boldsymbol{u})\mathbf{1} = \boldsymbol{SAT}\boldsymbol{s}. \tag{4.8}$$

However, this can be easily extended to multiple elements. To couple elements that are adjacent to each other, we re-use the symmetric SATs. Suppose the domain is discretized into n elements, then the semi-discrete scheme reads

$$
\begin{aligned}
\frac{d\boldsymbol{u_1}}{dt} + 2\mathsf{D} \circ \mathsf{F}(\boldsymbol{u_1}, \boldsymbol{u_1})\mathbf{1} = &- \mathsf{P}^{-1}\left(\boldsymbol{t_L}\boldsymbol{t_L}^{\mathrm{T}} \circ \mathsf{F}(\boldsymbol{u_1}, \boldsymbol{u_1})\mathbf{1} - \boldsymbol{t_L}\boldsymbol{t_R}^{\mathrm{T}} \circ \mathsf{F}(\boldsymbol{u_1}, \boldsymbol{u_n})\mathbf{1}\right) \\
&+ \mathsf{P}^{-1}\left(\boldsymbol{t_R}\boldsymbol{t_R}^{\mathrm{T}} \circ \mathsf{F}(\boldsymbol{u_1}, \boldsymbol{u_1})\mathbf{1} - \boldsymbol{t_R}\boldsymbol{t_L}^{\mathrm{T}} \circ \mathsf{F}(\boldsymbol{u_1}, \boldsymbol{u_2})\mathbf{1}\right), \\
\frac{d\boldsymbol{u_k}}{dt} + 2\mathsf{D} \circ \mathsf{F}(\boldsymbol{u_k}, \boldsymbol{u_k})\mathbf{1} = &- \mathsf{P}^{-1}\left(\boldsymbol{t_L}\boldsymbol{t_L}^{\mathrm{T}} \circ \mathsf{F}(\boldsymbol{u_k}, \boldsymbol{u_k})\mathbf{1} - \boldsymbol{t_L}\boldsymbol{t_R}^{\mathrm{T}} \circ \mathsf{F}(\boldsymbol{u_k}, \boldsymbol{u_{k-1}})\mathbf{1}\right) \\
&+ \mathsf{P}^{-1}\left(\boldsymbol{t_R}\boldsymbol{t_R}^{\mathrm{T}} \circ \mathsf{F}(\boldsymbol{u_k}, \boldsymbol{u_k})\mathbf{1} - \boldsymbol{t_R}\boldsymbol{t_L}^{\mathrm{T}} \circ \mathsf{F}(\boldsymbol{u_k}, \boldsymbol{u_{k+1}})\mathbf{1}\right), \\
\frac{d\boldsymbol{u_n}}{dt} + 2\mathsf{D} \circ \mathsf{F}(\boldsymbol{u_n}, \boldsymbol{u_n})\mathbf{1} = &- \mathsf{P}^{-1}\left(\boldsymbol{t_L}\boldsymbol{t_L}^{\mathrm{T}} \circ \mathsf{F}(\boldsymbol{u_n}, \boldsymbol{u_n})\mathbf{1} - \boldsymbol{t_L}\boldsymbol{t_R}^{\mathrm{T}} \circ \mathsf{F}(\boldsymbol{u_n}, \boldsymbol{u_{n-1}})\mathbf{1}\right) \\
&+ \mathsf{P}^{-1}\left(\boldsymbol{t_R}\boldsymbol{t_R}^{\mathrm{T}} \circ \mathsf{F}(\boldsymbol{u_n}, \boldsymbol{u_n})\mathbf{1} - \boldsymbol{t_R}\boldsymbol{t_L}^{\mathrm{T}} \circ \mathsf{F}(\boldsymbol{u_n}, \boldsymbol{u_1})\mathbf{1}\right),
\end{aligned} \tag{4.9}
$$

for $k \in [2, n-1]$. Note that $\boldsymbol{u_k}$ denotes the numerical solution on the k^{th} element. Now, we introduce a theorem which will provide us with a general formula that will be used to prove entropy conservation.

Theorem 4.2.1. Let a and b represent two elements in the discretization. Then, for any operator $\mathsf{A} = \overline{\mathsf{A}} \otimes \mathsf{I}_{\mathsf{M}}$, where M is the number of equations:

$$
\boldsymbol{w_a}^{\mathrm{T}}\mathsf{A} \circ \mathsf{F}\left(\boldsymbol{u_a}, \boldsymbol{u_b}\right)\mathbf{1} - \mathbf{1}^{\mathrm{T}}\mathsf{A} \circ \mathsf{F}^{\mathrm{T}}\left(\boldsymbol{u_b}, \boldsymbol{u_a}\right)\boldsymbol{w_b} = \overline{\mathbf{1}}^{\mathrm{T}}\overline{\mathsf{A}}\boldsymbol{q}_b - \boldsymbol{q}_a^{\mathrm{T}}\overline{\mathsf{A}}\,\overline{\mathbf{1}},
$$

where $\boldsymbol{u}_a$ and $\boldsymbol{u}_b$ denote the solution on the a^{th} and b^{th} elements respectively, and for example, $\boldsymbol{w}_a = \boldsymbol{w}(\boldsymbol{u_a})$ and $\boldsymbol{q}_a = q(\boldsymbol{u}_a)$.

Proof: We will rewrite the above expression in summation notation and use the form of the entropy-conservative two-point flux function in (4.4) to simplify the expression. Assume that each element has N nodes. Then, let $L = \boldsymbol{w_a}^{\mathrm{T}}\mathsf{A} \circ \mathsf{F}\left(\boldsymbol{u_a}, \boldsymbol{u_b}\right)\mathbf{1} - \mathbf{1}^{\mathrm{T}}\mathsf{A} \circ \mathsf{F}^{\mathrm{T}}\left(\boldsymbol{u_b}, \boldsymbol{u_a}\right)\boldsymbol{w_b}$, and with this definition we find that:

$$
\begin{aligned}
L &= \boldsymbol{w_a}^{\mathrm{T}}\mathsf{A} \circ \mathsf{F}\left(\boldsymbol{u_a}, \boldsymbol{u_b}\right)\mathbf{1} - \mathbf{1}^{\mathrm{T}}\mathsf{A} \circ \mathsf{F}^{\mathrm{T}}\left(\boldsymbol{u_b}, \boldsymbol{u_a}\right)\boldsymbol{w_b}, \\
&= \sum_{i=1}^{N}\left[\boldsymbol{w_{a,i}}^{\mathrm{T}}\sum_{j=1}^{N} A_{ij}\boldsymbol{f}^{(\boldsymbol{EC})}\left(\boldsymbol{u_{a,i}}, \boldsymbol{u_{b,j}}\right) - \sum_{j=1}^{N}\mathsf{A}_{ij}\boldsymbol{f}^{(\boldsymbol{EC})^{\mathrm{T}}}\left(\boldsymbol{u_{b,j}}, \boldsymbol{u_{a,i}}\right)\boldsymbol{w_{b,j}}\right].
\end{aligned}
$$

Note that $\boldsymbol{f}^{(\boldsymbol{EC})^{\mathrm{T}}}\left(\boldsymbol{u}_{\boldsymbol{b},\boldsymbol{j}}, \boldsymbol{u}_{\boldsymbol{a},\boldsymbol{i}}\right) \boldsymbol{w}_{\boldsymbol{b},\boldsymbol{j}}$ is a scalar value and hence can be written as $\boldsymbol{w}_{\boldsymbol{b},\boldsymbol{j}}{}^{\mathrm{T}} \boldsymbol{f}^{(\boldsymbol{EC})}\left(\boldsymbol{u}_{\boldsymbol{b},\boldsymbol{j}}, \boldsymbol{u}_{\boldsymbol{a},\boldsymbol{i}}\right)$, therefore,

$$L=\sum_{i=1}^{N} \sum_{j=1}^{N} \mathsf{A}_{ij}\left[\boldsymbol{w}_{\boldsymbol{a},\boldsymbol{i}}{}^{\mathrm{T}} \boldsymbol{f}^{(\boldsymbol{EC})}\left(\boldsymbol{u}_{\boldsymbol{a},\boldsymbol{i}}, \boldsymbol{u}_{\boldsymbol{b},\boldsymbol{j}}\right)-\boldsymbol{w}_{\boldsymbol{b},\boldsymbol{j}}{}^{\mathrm{T}} \boldsymbol{f}^{(\boldsymbol{EC})}\left(\boldsymbol{u}_{\boldsymbol{b},\boldsymbol{j}}, \boldsymbol{u}_{\boldsymbol{a},\boldsymbol{i}}\right)\right].$$

Recall from (4.4) that $\boldsymbol{f}^{(\boldsymbol{EC})}\left(\boldsymbol{u}_{\boldsymbol{a},\boldsymbol{i}}, \boldsymbol{u}_{\boldsymbol{b},\boldsymbol{j}}\right)=\boldsymbol{D}^{-}\left(\boldsymbol{u}_{\boldsymbol{a},\boldsymbol{i}}, \boldsymbol{u}_{\boldsymbol{b},\boldsymbol{j}}\right)-\boldsymbol{D}^{+}\left(\boldsymbol{u}_{\boldsymbol{b},\boldsymbol{j}}, \boldsymbol{u}_{\boldsymbol{a},\boldsymbol{i}}\right)$. Inserting this into the above equation results in

$$\begin{aligned}
L=&\sum_{i=1}^{N} \sum_{j=1}^{N} \mathsf{A}_{ij} \boldsymbol{w}_{\boldsymbol{a},\boldsymbol{i}}{}^{\mathrm{T}}\left[\boldsymbol{D}^{-}\left(\boldsymbol{u}_{\boldsymbol{a},\boldsymbol{i}}, \boldsymbol{u}_{\boldsymbol{b},\boldsymbol{j}}\right)-\boldsymbol{D}^{+}\left(\boldsymbol{u}_{\boldsymbol{b},\boldsymbol{j}}, \boldsymbol{u}_{\boldsymbol{a},\boldsymbol{i}}\right)\right] \\
&-\sum_{i=1}^{N} \sum_{j=1}^{N} \mathsf{A}_{ij} \boldsymbol{w}_{\boldsymbol{b},\boldsymbol{j}}{}^{\mathrm{T}}\left[\boldsymbol{D}^{-}\left(\boldsymbol{u}_{\boldsymbol{b},\boldsymbol{j}}, \boldsymbol{u}_{\boldsymbol{a},\boldsymbol{i}}\right)-\boldsymbol{D}^{+}\left(\boldsymbol{u}_{\boldsymbol{a},\boldsymbol{i}}, \boldsymbol{u}_{\boldsymbol{b},\boldsymbol{j}}\right)\right], \\
=&\sum_{i=1}^{N} \sum_{j=1}^{N} \mathsf{A}_{ij}\left[\boldsymbol{w}_{\boldsymbol{a},\boldsymbol{i}}{}^{\mathrm{T}} \boldsymbol{D}^{-}\left(\boldsymbol{u}_{\boldsymbol{a},\boldsymbol{i}}, \boldsymbol{u}_{\boldsymbol{b},\boldsymbol{j}}\right)+\boldsymbol{w}_{\boldsymbol{b},\boldsymbol{j}}{}^{\mathrm{T}} \boldsymbol{D}^{+}\left(\boldsymbol{u}_{\boldsymbol{a},\boldsymbol{i}}, \boldsymbol{u}_{\boldsymbol{b},\boldsymbol{j}}\right)\right] \\
&-\sum_{i=1}^{N} \sum_{j=1}^{N} \mathsf{A}_{ij}\left[\boldsymbol{w}_{\boldsymbol{b},\boldsymbol{j}}{}^{\mathrm{T}} \boldsymbol{D}^{-}\left(\boldsymbol{u}_{\boldsymbol{b},\boldsymbol{j}}, \boldsymbol{u}_{\boldsymbol{a},\boldsymbol{i}}\right)+\boldsymbol{w}_{\boldsymbol{a},\boldsymbol{i}}{}^{\mathrm{T}} \boldsymbol{D}^{+}\left(\boldsymbol{u}_{\boldsymbol{b},\boldsymbol{j}}, \boldsymbol{u}_{\boldsymbol{a},\boldsymbol{i}}\right)\right].
\end{aligned}$$

Substituting (4.6) gives

$$\begin{aligned}
L=&\sum_{i=1}^{N} \sum_{j=1}^{N} \overline{\mathsf{A}}_{ij}\left[\frac{1}{2}(q(\boldsymbol{u}_{b,j})-q(\boldsymbol{u}_{a,i}))-\frac{1}{2}(q(\boldsymbol{u}_{a,i})-q(\boldsymbol{u}_{b,j}))\right], \\
=&\overline{\mathbf{1}}^{\mathrm{T}} \overline{\mathsf{A}} \boldsymbol{q}_{b}-\boldsymbol{q}_{a}^{\mathrm{T}} \overline{\mathsf{A}}\, \overline{\mathbf{1}}. \square
\end{aligned}$$

Now, we will prove the accuracy of the spatial discretization in (4.1), by following Renac's proof in [50], but changing the notation to fit that of this thesis. Furthermore, with theorem (4.2.1) in hand, we can also prove that (4.1) discretely mimics the non-linear IBP rule (2.9).

Theorem 4.2.2. Assuming the fluctuation fluxes (4.6) have the following form

$$\boldsymbol{D}^{\pm}\left(\boldsymbol{u}_{i}, \boldsymbol{u}_{j}\right)=2 \mathbf{A}^{\pm}\left(\boldsymbol{u}_{i}, \boldsymbol{u}_{j}\right) \Delta \boldsymbol{u}, \tag{4.10a}$$

$$\mathbf{A}\left(\boldsymbol{u}_{i}, \boldsymbol{u}_{j}\right)=\mathbf{A}^{-}\left(\boldsymbol{u}_{i}, \boldsymbol{u}_{j}\right)+\mathbf{A}^{+}\left(\boldsymbol{u}_{i}, \boldsymbol{u}_{j}\right), \tag{4.10b}$$

$$\mathbf{A}\left(\boldsymbol{u}_{i}, \boldsymbol{u}_{j}\right)+\mathbf{A}\left(\boldsymbol{u}_{j}, \boldsymbol{u}_{i}\right)=\mathsf{A}\left(\boldsymbol{u}_{i}\right)+\mathsf{A}\left(\boldsymbol{u}_{j}\right), \tag{4.10c}$$

$$\mathbf{A}\left(\boldsymbol{u}, \boldsymbol{u}\right)=\mathsf{A}\left(\boldsymbol{u}\right), \tag{4.10d}$$

for all $\boldsymbol{u}_{i/j} \in \Omega$, where we assume that the domain is discretized using a single element, hence, we drop the element indices and the i and j indices denote the node label, and $\Delta \boldsymbol{u} = \boldsymbol{u}_j - \boldsymbol{u}_i$. Then, $2\mathsf{D} \circ \mathsf{F}(\boldsymbol{u}, \boldsymbol{u})\mathbf{1}$ is a high-order approximation to the spatial derivatives of smooth solutions. That is

$$\mathsf{A}(\boldsymbol{u}) \frac{\partial \boldsymbol{u}}{\partial x} = \frac{\partial \boldsymbol{f}(\boldsymbol{u})}{\partial x} + \mathsf{c}(\boldsymbol{u}) \frac{\partial \boldsymbol{u}}{\partial x} = 2\mathsf{D} \circ \mathsf{F}(\boldsymbol{u}, \boldsymbol{u})\mathbf{1} + \mathcal{O}\left(h^p\right).$$

Furthermore, when multiplied by the entropy variables and discretely integrated over the domain, $2\mathsf{D} \circ \mathsf{F}(\boldsymbol{u}, \boldsymbol{u})\mathbf{1}$ discretely mimics the non-linear IBP rule (2.9) as follows

$$2\boldsymbol{w}^{\mathrm{T}} \mathsf{P} \mathsf{D} \circ \mathsf{F}\mathbf{1} = q_N - q_1,$$

where $q_N = q(x_N)$ and $q_1 = q(x_1)$ when the domain is discretized into N nodes.

Proof: We will show that $2\mathsf{D} \circ \mathsf{F}(\boldsymbol{u}, \boldsymbol{u})\mathbf{1}$ is a high-order approximation of $\frac{\partial \boldsymbol{f}(\boldsymbol{u})}{\partial x} + \mathsf{c}(\boldsymbol{u}) \frac{\partial \boldsymbol{u}}{\partial x}$ at all solution points, where we assume that we are on a single element for ease of notation and hence, drop the element indices. For any two-functions $a(x)$ and $b(x)$, we can take the derivative of $(ab)(x)$, and evaluate it at a point x_i as follows

$$\left.\frac{d(ab)(x)}{dx}\right|_{x=x_i} = \left.\frac{da(x)}{dx}\right|_{x=x_i} b(x_i) + a(x_i) \left.\frac{db(x)}{dx}\right|_{x=x_i}.$$

Discretizing the right hand side of the above with a degree p SBP operator, D, results in

$$\begin{aligned} \left.\frac{d(ab)(x)}{dx}\right|_{x=x_i} &= \left.\frac{da(x)}{dx}\right|_{x=x_i} b(x_i) + a(x_i) \left.\frac{db(x)}{dx}\right|_{x=x_i}, \\ &= (\mathsf{D}a)_i b_i + a_i (\mathsf{D}b)_i + \mathcal{O}\left(h^p\right), \\ &= (\sum_{j=1}^{N} \mathsf{D}_{ij} a_j) b_i + a_i (\sum_{j=1}^{N} \mathsf{D}_{ij} b_j) + \mathcal{O}\left(h^p\right). \end{aligned} \tag{4.11}$$

Now, consider the Hadamard product in summation notation

$$2\mathsf{D} \circ \mathsf{F}(\boldsymbol{u}, \boldsymbol{u})\mathbf{1} = 2 \sum_{j=1}^{N} \mathsf{D}_{ij} \boldsymbol{f}^{(\boldsymbol{EC})}(\boldsymbol{u}_i, \boldsymbol{u}_j),$$

substituting the form of the alternate entropy-conservative flux (4.4) leads to

$$2\mathsf{D} \circ \mathsf{F}(\boldsymbol{u}, \boldsymbol{u})\mathbf{1} = 2 \sum_{j=1}^{N} \mathsf{D}_{ij} \left(\boldsymbol{D}^{-}(\boldsymbol{u}_i, \boldsymbol{u}_j) - \boldsymbol{D}^{+}(\boldsymbol{u}_j, \boldsymbol{u}_i) \right),$$

substituting (4.10a) into the above equation for $\boldsymbol{D}^{\pm}$ results in

$$2\mathsf{D} \circ \mathsf{F}(\boldsymbol{u}, \boldsymbol{u})\mathbf{1} = \sum_{j=1}^{N} \mathsf{D}_{ij} \left[\mathbf{A}^{-}(\boldsymbol{u}_i, \boldsymbol{u}_j) \left(\boldsymbol{u}_j - \boldsymbol{u}_i \right) - \mathbf{A}^{+}(\boldsymbol{u}_j, \boldsymbol{u}_i) \left(\boldsymbol{u}_i - \boldsymbol{u}_j \right) \right],$$

rearranging the equation one finds that

$$2\mathsf{D} \circ \mathsf{F}(\boldsymbol{u}, \boldsymbol{u})\mathbf{1} = \sum_{j=1}^{N} \mathsf{D}_{ij} \left[\mathbf{A}^{-}(\boldsymbol{u}_i, \boldsymbol{u}_j) + \mathbf{A}^{+}(\boldsymbol{u}_j, \boldsymbol{u}_i) \right] \left[\boldsymbol{u}_j - \boldsymbol{u}_i \right]. \tag{4.12}$$

To proceed, we begin by applying (4.11) in the following context

$$\sum_{j=1}^{N} \mathsf{D}_{ij} \mathbf{A}^{-}(\boldsymbol{u}_i, \boldsymbol{u}_j) \boldsymbol{u}_j = \mathbf{A}^{-}(\boldsymbol{u}_i, \boldsymbol{u}_i) \sum_{j=1}^{N} \mathsf{D}_{ij} \boldsymbol{u}_j + \boldsymbol{u}_i \sum_{j=1}^{N} \mathsf{D}_{ij} \mathbf{A}^{-}(\boldsymbol{u}_i, \boldsymbol{u}_j) + \mathcal{O}\left(h^p\right).$$

Rearranging the equation gives

$$\sum_{j=1}^{N} \mathsf{D}_{ij} \mathbf{A}^{-}(\boldsymbol{u}_i, \boldsymbol{u}_j) \left[\boldsymbol{u}_j - \boldsymbol{u}_i \right] = \mathbf{A}^{-}(\boldsymbol{u}_i, \boldsymbol{u}_i) \sum_{j=1}^{N} \mathsf{D}_{ij} \boldsymbol{u}_j + \mathcal{O}\left(h^p\right),$$

then, using the accuracy property of SBP operators results in

$$\sum_{j=1}^{N} \mathsf{D}_{ij} \mathbf{A}^{-}(\boldsymbol{u}_i, \boldsymbol{u}_j) \left[\boldsymbol{u}_j - \boldsymbol{u}_i \right] = \mathbf{A}^{-}(\boldsymbol{u}_i, \boldsymbol{u}_i) \frac{\partial \boldsymbol{u}}{\partial x}\bigg|_{x=x_i} + \mathcal{O}\left(h^p\right). \tag{4.13}$$

Applying the same rule to $\sum_{j=1}^{N} \mathsf{D}_{ij} \mathbf{A}^{+}(\boldsymbol{u}_j, \boldsymbol{u}_i) \boldsymbol{u}_j$, we find that

$$\sum_{j=1}^{N} \mathsf{D}_{ij} \mathbf{A}^{+}(\boldsymbol{u}_j, \boldsymbol{u}_i) \left[\boldsymbol{u}_j - \boldsymbol{u}_i \right] = \mathbf{A}^{+}(\boldsymbol{u}_i, \boldsymbol{u}_i) \sum_{j=1}^{N} \mathsf{D}_{ij} \boldsymbol{u}_j + \mathcal{O}\left(h^p\right).$$

Again, using the accuracy property of SBP operators results in

$$\sum_{j=1}^{N} \mathsf{D}_{ij} \mathbf{A}^{+}(\boldsymbol{u}_j, \boldsymbol{u}_i) \left[\boldsymbol{u}_j - \boldsymbol{u}_i \right] = \mathbf{A}^{+}(\boldsymbol{u}_i, \boldsymbol{u}_i) \frac{\partial \boldsymbol{u}}{\partial x}\bigg|_{x=x_i} + \mathcal{O}\left(h^p\right). \tag{4.14}$$

Recall equation (4.12):

$$2\mathsf{D} \circ \mathsf{F}(\boldsymbol{u}, \boldsymbol{u})\mathbf{1} = \sum_{j=1}^{N} \mathsf{D}_{ij} \left[\mathbf{A}^{-}(\boldsymbol{u}_i, \boldsymbol{u}_j) + \mathbf{A}^{+}(\boldsymbol{u}_j, \boldsymbol{u}_i) \right] \left[\boldsymbol{u}_j - \boldsymbol{u}_i \right],$$

and apply (4.13) and (4.14) to the above equation resulting in

$$2\mathsf{D} \circ \mathsf{F}(\boldsymbol{u}, \boldsymbol{u})\mathbf{1} = \left(\mathbf{A}^{-}(\boldsymbol{u}_i, \boldsymbol{u}_i) + \mathbf{A}^{+}(\boldsymbol{u}_i, \boldsymbol{u}_i)\right) \frac{\partial \boldsymbol{u}}{\partial x}\bigg|_{x=x_i} + \mathcal{O}\left(h^p\right).$$

In this form, (4.10b) can be applied to the above equation to find that

$$2\mathsf{D} \circ \mathsf{F}(\boldsymbol{u}, \boldsymbol{u})\mathbf{1} = \mathbf{A}(\boldsymbol{u}_i, \boldsymbol{u}_i)\frac{\partial \boldsymbol{u}}{\partial x}\bigg|_{x=x_i} + \mathcal{O}\left(h^p\right),$$

where finally, (4.10d) can be applied to the above equation resulting in

$$2\mathsf{D} \circ \mathsf{F}(\boldsymbol{u}, \boldsymbol{u})\mathbf{1} = \mathsf{A}\left(\boldsymbol{u}_i\right) \frac{\partial \boldsymbol{u}}{\partial x}\bigg|_{x=x_i} + \mathcal{O}\left(h^p\right).$$

Therefore, $2\mathsf{D} \circ \mathsf{F}(\boldsymbol{u}, \boldsymbol{u})\mathbf{1}$ is a high-order approximation to the spatial derivative of smooth solutions to (2.10). What remains to be shown is that $2\mathsf{D} \circ \mathsf{F}(\boldsymbol{u}, \boldsymbol{u})\mathbf{1}$ can be used to discretely mimic the non-linear IBP rule that arises in the continuous entropy analysis, i.e.,

$$\int_{x_L}^{x_R} \boldsymbol{w}^{\mathrm{T}} \left(\frac{\partial \boldsymbol{f}(\boldsymbol{u})}{\partial x} + \mathsf{c}(\boldsymbol{u}) \frac{\partial \boldsymbol{u}}{\partial x} \right) dx = q\Big|_{x_L}^{x_R}.$$

The discrete counter part of multiplying the entropy variables and integrating over the domain is left multiplication of $2\mathsf{D} \circ \mathsf{F}(\boldsymbol{u}, \boldsymbol{u})\mathbf{1}$ by $\boldsymbol{w}^{\mathrm{T}}\mathsf{P}$. We show that doing so results in the difference in the entropy flux function, q, between the first and last nodes. Begin by left multiplying $2\mathsf{D} \circ \mathsf{F}(\boldsymbol{u}, \boldsymbol{u})\mathbf{1}$ by $\boldsymbol{w}^{\mathrm{T}}\mathsf{P}$ to find that

$$\begin{aligned} \boldsymbol{w}^{\mathrm{T}}\mathsf{P}\left(2\mathsf{D} \circ \mathsf{F}(\boldsymbol{u}, \boldsymbol{u})\mathbf{1}\right) &= 2\boldsymbol{w}^{\mathrm{T}}\mathsf{Q} \circ \mathsf{F}(\boldsymbol{u}, \boldsymbol{u})\mathbf{1}, \\ &= \left(\boldsymbol{w}^{\mathrm{T}}\mathsf{Q} \circ \mathsf{F}\mathbf{1} + \boldsymbol{w}^{\mathrm{T}}\mathsf{Q} \circ \mathsf{F}\mathbf{1}\right). \end{aligned}$$

Note that $\mathsf{F} = \mathsf{F}(\boldsymbol{u}, \boldsymbol{u})$, is used for ease of notation, therefore,

$$2\boldsymbol{w}^{\mathrm{T}}\mathsf{P}\mathsf{D} \circ \mathsf{F}\mathbf{1} = \left(\boldsymbol{w}^{\mathrm{T}}\mathsf{Q} \circ \mathsf{F}\mathbf{1} + \mathbf{1}^{\mathrm{T}}\mathsf{F}^{\mathrm{T}} \circ \mathsf{Q}^{\mathrm{T}}\boldsymbol{w}\right).$$

The Hadamard product is symmetric, i.e., $\mathsf{A} \circ \mathsf{B} = \mathsf{B} \circ \mathsf{A}$, thus,

$$2\boldsymbol{w}^{\mathrm{T}}\mathsf{P}\mathsf{D} \circ \mathsf{F}\mathbf{1} = \left(\boldsymbol{w}^{\mathrm{T}}\mathsf{Q} \circ \mathsf{F}\mathbf{1} + \mathbf{1}^{\mathrm{T}}\mathsf{Q}^{\mathrm{T}} \circ \mathsf{F}^{\mathrm{T}}\boldsymbol{w}\right).$$

Recall the property of SBP operators: $\mathsf{Q}^{\mathrm{T}} = \mathsf{E} - \mathsf{Q}$. Substituting this into the above expression gives

$$2\boldsymbol{w}^{\mathrm{T}}\mathsf{PD} \circ \mathsf{F}\mathbf{1} = \left(\boldsymbol{w}^{\mathrm{T}}\mathsf{Q} \circ \mathsf{F}\mathbf{1} - \mathbf{1}^{\mathrm{T}}\mathsf{Q} \circ \mathsf{F}^{\mathrm{T}}\boldsymbol{w} + \mathbf{1}^{\mathrm{T}}\mathsf{E} \circ \mathsf{F}^{\mathrm{T}}\boldsymbol{w}\right).$$

Using theorem (4.2.1) on the first two terms on the right hand side results in

$$2\boldsymbol{w}^{\mathrm{T}}\mathsf{PD} \circ \mathsf{F}\mathbf{1} = \overline{\mathbf{1}}^{\mathrm{T}}\overline{\mathsf{Q}}\boldsymbol{q} - \overline{\mathbf{1}}^{\mathrm{T}}\overline{\mathsf{Q}\,\boldsymbol{q}} + \boldsymbol{w}^{\mathrm{T}}\mathsf{E} \circ \mathsf{F}\mathbf{1}.$$

Furthermore, since the second term on the right hand side is a scalar, we can take it's transpose. Thus,

$$2\boldsymbol{w}^{\mathrm{T}}\mathsf{PD} \circ \mathsf{F}\mathbf{1} = \overline{\mathbf{1}}^{\mathrm{T}}\overline{\mathsf{Q}}\boldsymbol{q} - \cancel{\boldsymbol{q}^{\mathrm{T}}\overline{\mathsf{Q}}\,\overline{\mathbf{1}}} + \boldsymbol{w}^{\mathrm{T}}\mathsf{E} \circ \mathsf{F}\mathbf{1}.$$

Where we have cancelled the middle term since and SBP operator, Q, of any order, will result in $\overline{\mathsf{Q}}\mathbf{1} = 0$. Thus,

$$2\boldsymbol{w}^{\mathrm{T}}\mathsf{PD} \circ \mathsf{F}\mathbf{1} = \overline{\mathbf{1}}^{\mathrm{T}}\overline{\mathsf{Q}}\boldsymbol{q} + \boldsymbol{w}^{\mathrm{T}}\mathsf{E} \circ \mathsf{F}\mathbf{1},$$

replacing E with $\mathsf{E} = \boldsymbol{t_R}\boldsymbol{t_R}^{\mathrm{T}} - \boldsymbol{t_L}\boldsymbol{t_L}^{\mathrm{T}}$ results in

$$2\boldsymbol{w}^{\mathrm{T}}\mathsf{PD} \circ \mathsf{F}\mathbf{1} = \overline{\mathbf{1}}^{\mathrm{T}}\overline{\mathsf{Q}}\boldsymbol{q} + \mathbf{1}^{\mathrm{T}}\boldsymbol{t_R}\boldsymbol{t_R}^{\mathrm{T}} \circ \mathsf{F}\boldsymbol{w}_i - \mathbf{1}^{\mathrm{T}}\boldsymbol{t_L}\boldsymbol{t_L}^{\mathrm{T}} \circ \mathsf{F}\boldsymbol{w}_i.$$

Using (3.3), we can write

$$\boldsymbol{t_R}\boldsymbol{t_R}^{\mathrm{T}} \circ \mathsf{F} = \mathrm{diag}(0, \ldots, 0, F(u_{i,N}, u_{i,N})),$$

and similarly

$$\boldsymbol{t_L}\boldsymbol{t_L}^{\mathrm{T}} \circ \mathsf{F} = \mathrm{diag}(F(u_{i,1}, u_{i,1}), 0, \ldots, 0).$$

Then, equations (4.4) and (4.5), give $F(u_{i,N}, u_{i,N}) = F(u_{i,1}, u_{i,1}) = 0$. Plugging this into the above equation gives

$$\begin{aligned} 2\boldsymbol{w}^{\mathrm{T}}\mathsf{PD} \circ \mathsf{F}\mathbf{1} &= \overline{\mathbf{1}}^{\mathrm{T}}\overline{\mathsf{Q}}\boldsymbol{q}, \\ &= \overline{\mathbf{1}}^{\mathrm{T}}\left(\overline{\mathsf{E}} - \overline{\mathsf{Q}}^{\mathrm{T}}\right)\boldsymbol{q}, \\ &= \overline{\mathbf{1}}^{\mathrm{T}}\overline{\mathsf{E}}\boldsymbol{q} - \cancel{\overline{\mathbf{1}}^{\mathrm{T}}\overline{\mathsf{Q}}^{\mathrm{T}}\boldsymbol{q}}, \\ 2\boldsymbol{w}^{\mathrm{T}}\mathsf{PD} \circ \mathsf{F}\mathbf{1} &= q_N - q_1. \end{aligned}$$

Therefore, the Hadamard product, (4.1), discretely mimics the non-linear IBP rule (2.9). □

With Theorems (4.2.1) and (4.2.2) in hand, we can now prove that the semi-discrete scheme is entropy-conservative.

Theorem 4.2.3. Let $\boldsymbol{w}_i$ be the entropy variables associated with an entropy function η, on an element i, such that $\frac{\partial \eta_i}{\partial \boldsymbol{u}_i} = \boldsymbol{w}_i^{\mathrm{T}}$. Then, the semi-discrete scheme (4.9), which is discretized into n elements, satisfies the following equality when left multiplied by $\boldsymbol{w}_i^{\mathrm{T}}\mathsf{P}$,

$$\sum_{i=1}^{n} \overline{\mathbf{1}}^{\mathrm{T}} \overline{\mathsf{P}} \frac{d\boldsymbol{\eta}_i}{dt} = 0,$$

where $\mathsf{P} = \overline{\mathsf{P}} \otimes \mathsf{I}_5$, and $\boldsymbol{\eta}_i = \eta(\boldsymbol{u}_i)$. That is, the semi-discrete scheme, (4.9), is entropy-conservative.

Proof: We mimic the steps taken in the continuous proof of entropy conservation at the discrete level and show that the total entropy over the domain remains constant over all time, i.e.,

$$\frac{d}{dt}\int_{x_L}^{x_R} \eta dx = q(x_L) - q(x_R) = 0,$$

in the case of a periodic problem. As the discrete analog to multiplying the equations by the entropy variables and integrating over the domain, we left multiply (4.9) by $\boldsymbol{w}^{\mathrm{T}}\mathsf{P}$. For element $i = 1, 2 \ldots, n$ we find the time derivative term on the left hand side of (4.9)

$$\begin{aligned}
\boldsymbol{w}_i^{\mathrm{T}}\mathsf{P}\frac{d\boldsymbol{u}_i}{dt} &= \sum_{j=1}^{N} \boldsymbol{w}_{i,j}\overline{\mathsf{P}}_{jj}\frac{d\boldsymbol{u}_{i,j}}{dt}, \\
&= \sum_{j=1}^{N} \overline{\mathsf{P}}_{jj}\frac{d\eta_{i,j}}{d\boldsymbol{u}_{i,j}}\frac{d\boldsymbol{u}_{i,j}}{dt}, \\
&= \sum_{j=1}^{N} \overline{\mathsf{P}}_{jj}\frac{d\eta_{i,j}}{dt}, \\
\boldsymbol{w}_i^{\mathrm{T}}\mathsf{P}\frac{d\boldsymbol{u}_i}{dt} &= \overline{\mathbf{1}}^{\mathrm{T}}\overline{\mathsf{P}}\frac{d\boldsymbol{\eta}_i}{dt}.
\end{aligned}$$

The second term on the left hand side of (4.9) can be simplified following the same steps as in the proof of theorem (4.2.2). We re-use the notation $\mathsf{F}(\boldsymbol{u}_i, \boldsymbol{u}_j) = \mathsf{F}_{ij}$, to find that

$$2\boldsymbol{w}_i^{\mathrm{T}}\mathsf{PD} \circ \mathsf{F}_{ii}\mathbf{1} = \mathbf{1}^{\mathrm{T}}\overline{\mathsf{Q}}q_i + \mathbf{1}^{\mathrm{T}}\boldsymbol{t_R}\boldsymbol{t_R}^{\mathrm{T}} \circ \mathsf{F}_{ii}\boldsymbol{w}_i - \mathbf{1}^{\mathrm{T}}\boldsymbol{t_L}\boldsymbol{t_L}^{\mathrm{T}} \circ \mathsf{F}_{ii}\boldsymbol{w}_i.$$

Thus, after left multiplying (4.9) by $\boldsymbol{w}^{\mathrm{T}}\mathsf{P}$ we find for an element $i = 1, 2, \ldots, n$,

$$\begin{aligned}
\mathbf{1}^{\mathrm{T}}\overline{\mathsf{P}}\frac{d\eta_i}{dt} + \mathbf{1}^{\mathrm{T}}\overline{\mathsf{Q}}q_i + \cancel{\mathbf{1}^{\mathrm{T}}\boldsymbol{t_R}\boldsymbol{t_R}^{\mathrm{T}} \circ \mathsf{F}_{ii}\boldsymbol{w}_i} - \cancel{\mathbf{1}^{\mathrm{T}}\boldsymbol{t_L}\boldsymbol{t_L}^{\mathrm{T}} \circ \mathsf{F}_{ii}\boldsymbol{w}_i} &= -\boldsymbol{w}_i^{\mathrm{T}}\left(\cancel{\boldsymbol{t_L}\boldsymbol{t_L}^{\mathrm{T}} \circ \mathsf{F}_{ii}\mathbf{1}} - \boldsymbol{t_L}\boldsymbol{t_R}^{\mathrm{T}} \circ \mathsf{F}_{i(i-1)}\mathbf{1}\right) \\
&\quad + \boldsymbol{w}_i^{\mathrm{T}}\left(\cancel{\boldsymbol{t_R}\boldsymbol{t_R}^{\mathrm{T}} \circ \mathsf{F}_{ii}\mathbf{1}} - \boldsymbol{t_R}\boldsymbol{t_L}^{\mathrm{T}} \circ \mathsf{F}_{i(i+1)}\mathbf{1}\right), \\
\mathbf{1}^{\mathrm{T}}\overline{\mathsf{P}}\frac{d\boldsymbol{\eta}_i}{dt} + \mathbf{1}^{\mathrm{T}}\overline{\mathsf{Q}}q_i &= +\boldsymbol{w}_i^{\mathrm{T}}\left(\boldsymbol{t_L}\boldsymbol{t_R}^{\mathrm{T}} \circ \mathsf{F}_{i(i-1)}\mathbf{1}\right) \\
&\quad - \boldsymbol{w}_i^{\mathrm{T}}\left(\boldsymbol{t_R}\boldsymbol{t_L}^{\mathrm{T}} \circ \mathsf{F}_{i(i+1)}\mathbf{1}\right).
\end{aligned} \tag{4.15}$$

Note that if $i = 1$, then, in the above equation, $(i-1) = n$. Similarly, if $i = n$, then $(i+1) = 1$, since we are considering a periodic domain. To prove entropy conservation over the entire domain we must sum over all elements. The remaining SAT terms from (4.15) can be shown to sum to

$$SAT = \sum_{i=1}^{n}\left[\boldsymbol{w}_i^{\mathrm{T}}\left(\boldsymbol{t_L}\boldsymbol{t_R}^{\mathrm{T}} \circ \mathsf{F}_{i(i-1)}\mathbf{1}\right) - \boldsymbol{w}_i^{\mathrm{T}}\left(\boldsymbol{t_R}\boldsymbol{t_L}^{\mathrm{T}} \circ \mathsf{F}_{i(i+1)}\mathbf{1}\right)\right].$$

Expanding the sum and gathering similar F_{ij} terms results in

$$\begin{aligned}
SAT &= \sum_{i=1}^{n}\left[\boldsymbol{w}_i^{\mathrm{T}}\left(\boldsymbol{t_L}\boldsymbol{t_R}^{\mathrm{T}} \circ \mathsf{F}_{i(i-1)}\mathbf{1}\right) - \boldsymbol{w}_{i-1}^{\mathrm{T}}\left(\boldsymbol{t_R}\boldsymbol{t_L}^{\mathrm{T}} \circ \mathsf{F}_{(i-1)i}\mathbf{1}\right)\right], \\
&= \sum_{i=1}^{n}\left[\boldsymbol{w}_i^{\mathrm{T}}\boldsymbol{t_L}\boldsymbol{t_R}^{\mathrm{T}} \circ \mathsf{F}_{i(i-1)}\mathbf{1} - \mathbf{1}^{\mathrm{T}}\boldsymbol{t_L}\boldsymbol{t_R}^{\mathrm{T}} \circ \mathsf{F}_{(i-1)i}^{\mathrm{T}}\boldsymbol{w}_{i-1}\right].
\end{aligned}$$

Now, these operators are in the form of theorem (4.2.1), thus, they can be re-written in terms of the entropy flux function

$$\begin{aligned}
SAT &= \sum_{i=1}^{n}\left[\overline{\mathbf{1}}^{\mathrm{T}}\overline{t_L}\,\overline{t_R}^{\mathrm{T}}\boldsymbol{q}_{(i-1)} - \boldsymbol{q}_i^{\mathrm{T}}\overline{t_L}\,\overline{t_R}^{\mathrm{T}}\overline{\mathbf{1}}\right], \\
&= \sum_{i=1}^{n}\left[q_{(i-1),N} - q_{i,1}\right].
\end{aligned}$$

Expanding out the sum and gathering like terms results in

$$SAT = \sum_{i=1}^{n}\left[q_{i,N} - q_{i,1}\right],$$

where, $q_{i,j}$ stands for the entropy flux function evaluated on the j^{th} node of the i^{th} element. Next, we sum the term $\overline{\mathbf{1}}^{\mathrm{T}}\overline{\mathsf{Q}}\boldsymbol{q}_i$ from (4.15) over all elements to find that

$$\begin{aligned}
\sum_{i=1}^{n}\overline{\mathbf{1}}^{\mathrm{T}}\overline{\mathsf{Q}}\boldsymbol{q}_i &= \sum_{i=1}^{n}\overline{\mathbf{1}}^{\mathrm{T}}\left(\overline{\mathsf{E}}-\overline{\mathsf{Q}}^{\mathrm{T}}\right)\boldsymbol{q}_i, \\
&= \sum_{i=1}^{n}\left[\overline{\mathbf{1}}^{\mathrm{T}}\overline{\mathsf{E}}\boldsymbol{q}_i - \cancel{\overline{\mathbf{1}}^{\mathrm{T}}\overline{\mathsf{Q}}^{\mathrm{T}}\boldsymbol{q}_i}\right], \\
\sum_{i=1}^{n}\overline{\mathbf{1}}^{\mathrm{T}}\overline{\mathsf{Q}}\boldsymbol{q}_i &= \sum_{i=1}^{n}\left[q_{i,N}-q_{i,1}\right].
\end{aligned}$$

Therefore, summing (4.15) over all elements leaves us with:

$$\begin{aligned}
\sum_{i=1}^{n}\overline{\mathbf{1}}^{\mathrm{T}}\overline{\mathsf{P}}\frac{d\boldsymbol{\eta}_i}{dt}+\sum_{i=1}^{n}\left[q_{i,N}-q_{i,1}\right] &= \sum_{i=1}^{n}\left[q_{i,N}-q_{i,1}\right], \\
\sum_{i=1}^{n}\overline{\mathbf{1}}^{\mathrm{T}}\overline{\mathsf{P}}\frac{d\boldsymbol{\eta}_i}{dt} &= 0.
\end{aligned}$$

Therefore, (4.9) is a semi-discrete entropy-conservative discretization of the Baer-Nunziato model. It can achieve high order accuracy for smooth solutions through the use of high-order SBP operators. □

In this chapter, we developed a high-order entropy-conservative scheme which solves the isentropic Baer-Nunziato equations for smooth, periodic solutions. We have used the Hadamard formalism, (4.1), to discretize the spatial terms in the isentropic Baer-Nunziato equations since the SBP property alone is insufficient to mimic the "non-linear IBP rule," (2.9), that arises from the continuous entropy analysis. Furthermore, we have introduced the symmetric SATs, (4.7), which are used to enforce periodic boundary conditions as well as couple adjacent elements. Since we are interested in studying the bubble collapse problem in relation to HIFU, we are interested in studying discontinuous solutions to the isentropic Baer-Nunziato equations, since the collapse introduces a shock into the system. The entropy-conservative scheme, (4.9), is not capable of handling this case since, around a shock, the mathematical entropy of the system must dissipate according to the second law of thermodynamics. Thus, the entropy-conservative scheme will not produce solutions that are physically relevant. Furthermore, this scheme has no positivity-preserving properties and, as such, could produce solutions that contain negative void fractions and densities, which is not only nonphysical, but, will also cause the code to crash. Therefore, in the next

chapter, we detail a first-order scheme that is entropy-stable and positivity-preserving. We will introduce a novel dissipation operator, which is an entropy-dissipative term, to the numerical scheme, thus, dissipating the entropy around a discontinuity. Furthermore, this dissipation operator will have tuneable dissipation coefficients that can be selected such that the first-order scheme is provably node-wise positivity-preserving, which, to the authors knowledge, is a novel contribution to the solution of the isentropic Baer-Nunziato equations. Finally, we will detail a mixing scheme that will combine the high-order entropy-conservative scheme, (4.9), detailed in chapter 4, with the first-order entropy-stable positivity preserving scheme, detailed in section 5.1, to achieve a high-order entropy-stable positivity-preserving scheme.

Chapter 5

Entropy-Stable Positivity-Preserving Scheme

In the previous chapter we detailed a high-order entropy-conservative scheme for the isentropic Baer-Nunziato model. It is capable of handling smooth solutions, but is prone to developing spurious oscillations around discontinuities, as is the case with other nonlinear hyperbolic systems [41]. Furthermore, at discontinuities, the physical entropy of the system must increase to satisfy the second law of thermodynamics and the entropy-conservative scheme detailed in the previous chapter conserves entropy. Meaning that, at discontinuities, the entropy-conservative scheme, (4.9), is physically incorrect. As we are interested in studying the bubble collapse problem in relation to HIFU, we wish to study discontinuous solutions to the Baer-Nunziato model. It is well known that the mathematical entropy of a system must be dissipated around a shock [41], hence, we add appropriate numerical dissipation to ensure mathematical entropy dissipation. This concept is known as entropy stability. In this chapter we present a scheme that is capable of handing discontinuous solutions through the use of entropy-dissipative terms. Furthermore, we would like to be able to handle void fractions and densities that get arbitrarily close to zero. However, as values get close to zero, the base numerical scheme, (4.9), may not preserve the positivity of void fractions and densities. These quantities need to remain positive not only to make physical sense, but our stability estimate depends on the strict convexity of the entropy. The entropy function, (2.8), is strictly convex if and only if the void fractions and densities are strictly positive. Thus, in this chapter, we seek a high-order entropy-stable positivity-preserving scheme for the isentropic Baer-Nunziato model.

To begin, we detail a first-order entropy-stable positivity-preserving scheme. The positivity-preserving properties result from the use of a first-order entropy-dissipative term

which was inspired by the work of Upperman and Yamaleev [63], who used the Brenner regularization of the Navier-Stokes equations to construct a dissipation operator which can guarantee the node-wise positivity of density and temperature in the Navier-Stokes equations. Then, to attain high-order accuracy, we leverage the work of Upperman [62] and take a convex combination of the first-order positivity-preserving entropy-stable scheme and the high-order positivity-violating entropy-conservative scheme, (4.9), to attain a high-order positivity-preserving entropy-stable scheme. Finally, we include the algorithm and implementation details.

5.1 First-Order Entropy-Stable Positivity-Preserving Scheme

We now present a first-order entropy-stable positivity-preserving scheme for the isentropic Baer-Nunziato model (2.3). For the remainder of this thesis, we will use $\boldsymbol{v} = [\alpha_1 \ \rho_1 \ v_1 \ \rho_2 \ v_2]^{\mathrm{T}}$ as the vector of primitive variables and $\boldsymbol{u} = [\alpha_1 \ \alpha_1\rho_1 \ \alpha_1\rho_1 v_1 \ \alpha_2\rho_2 \ \alpha_2\rho_2 v_2]^{\mathrm{T}}$ as the vector of conserved variables.

The first-order entropy-stable positivity-preserving semi-discrete scheme can be written as follows

$$\frac{d\boldsymbol{u}}{dt} + 2\mathsf{D}_1 \circ \mathsf{F}(\boldsymbol{u}, \boldsymbol{u})\mathbf{1} = \tilde{\mathsf{P}}_H^{-1}(\mathsf{Diss} \circ \mathsf{M})\boldsymbol{v} + \boldsymbol{u}^{EID} + \boldsymbol{SATs}. \tag{5.1}$$

This semi-discrete scheme is the same as (4.9) with the addition of an artificial dissipation operator

$$\boldsymbol{ADO} = \tilde{\mathsf{P}}_H^{-1}(\mathsf{Diss} \circ \mathsf{M})\boldsymbol{v}, \tag{5.2}$$

and the element interface dissipation $\boldsymbol{u}^{EID}$. It is important to note that while (4.9) can attain high-order accuracy through the use of high-order SBP operators, (5.1) attains only first-order accuracy. This is because we use a specific derivative operator in (5.1). The derivative operator, D_1, defined in (3.17), is constructed as $\mathsf{P}_H^{-1}\mathsf{Q}_1$, where, P_H is a high-order norm matrix and Q_1 is the first-order Q matrix. The reason (5.1) needs to use this specific derivative operator will become clear when proving the positivity-preserving properties of the scheme. For the remainder of this chapter, we drop the subscript of the derivative matrix, i.e., $\mathsf{D}_1 = \mathsf{D}$. Furthermore, we use a high-order mass matrix P_H so that we can prove entropy-stability of the high-order mixed scheme detailed in the next section.

The artificial dissipation operator, (5.2), is broken into 3 parts: the undivided high-order SBP mass matrix $\tilde{\mathsf{P}}_H$ (i.e., $\mathsf{P}_H = h\tilde{\mathsf{P}}_H$), the Hadamard product between Diss and M,

and the primitive variables $\boldsymbol{v}$. For the remainder of this thesis, we will assume that the SBP mass matrix is of high-order and write $\mathsf{P}_H = h\tilde{\mathsf{P}}_H = \mathsf{P} = h\tilde{\mathsf{P}}$. Note that:

$$\mathsf{Diss} = \begin{bmatrix} -2 & 1 & 0 & 0 & \dots & 0 \\ 1 & -2 & 1 & 0 & \dots & 0 \\ 0 & 1 & -2 & 1 & & 0 \\ & & \ddots & \ddots & \ddots & \\ & & & 1 & -2 & 1 \\ & & & & 1 & -2 \end{bmatrix}, \tag{5.3}$$

and M is a symmetric block matrix that has the form

$$\mathsf{M} = \begin{bmatrix} \mathsf{M}_{11} & \mathsf{M}_{12} & 0 & 0 & \dots & 0 \\ \mathsf{M}_{12} & \mathsf{M}_{22} & \mathsf{M}_{23} & 0 & \dots & 0 \\ 0 & \mathsf{M}_{23} & \mathsf{M}_{33} & \mathsf{M}_{34} & \dots & 0 \\ & & \ddots & \ddots & \ddots & \\ & & & \mathsf{M}_{(n-1)(n-2)} & \mathsf{M}_{(n-1)(n-1)} & \mathsf{M}_{(n-1)n} \\ & & & & \mathsf{M}_{(n-1)n} & \mathsf{M}_{nn} \end{bmatrix}, \tag{5.4}$$

where,

$$\mathsf{M}_{11} = \frac{\mathsf{M}_{12}}{2}, \;\; \mathsf{M}_{nn} = \frac{\mathsf{M}_{(n-1)n}}{2}, \;\; \forall\, i \neq 1, n \;\; \mathsf{M}_{ii} = \frac{\mathsf{M}_{(i-1)i} + \mathsf{M}_{i(i+1)}}{2}. \tag{5.5}$$

Then, for $i \neq j$

$$\mathsf{M}_{ij} = \begin{bmatrix} \sigma_1 & 0 & 0 & 0 & 0 \\ \sigma_2\overline{\rho_1} & \sigma_2\overline{\alpha_1} & 0 & 0 & 0 \\ \sigma_2\overline{\rho_1}\,\overline{v_1} & \sigma_2\overline{\alpha_1}\,\overline{v_1} & 0 & 0 & 0 \\ -\sigma_4\overline{\rho_2} & 0 & 0 & \sigma_4\overline{\alpha_2} & 0 \\ -\sigma_4\overline{\rho_2}\,\overline{v_2} & 0 & 0 & \sigma_4\overline{\alpha_2}\,\overline{v_2} & 0 \end{bmatrix}, \tag{5.6}$$

where,

$$\overline{\rho_1} = \frac{(\rho_1)_i + (\rho_1)_j}{2},$$

with similar definitions for the other averages in (5.6). Also, σ_1, σ_2, and σ_4 are positive constants and their value will be determined in order to enforce positivity.

The artificial dissipation operator adds volume dissipation within an element, and as such, only deals with nodes on the same element. On the other hand, the element interface dissipation, $\boldsymbol{u}^{EID}$, which uses the same framework as the artificial dissipation operator,

requires some different notation as we will be using values from two adjacent elements. For the i^{th} element we find that

$$\boldsymbol{u}^{EID} = \tilde{\mathsf{P}}^{-1}[-\mathsf{M}^{i}_{N1}\Delta^{i}\boldsymbol{v}, 0, \ldots, 0, \mathsf{M}^{(\mathsf{i+1})}_{\mathsf{N1}}\Delta^{(i+1)}\boldsymbol{v}]^{\mathrm{T}}. \tag{5.7}$$

Where M^{i}_{N1} is the same operator, M, as introduced in (5.4), except, its entries are computed using $\boldsymbol{v}_{i,1}$ and $\boldsymbol{v}_{(i-1),N}$, and $\Delta^{i}\boldsymbol{v} = \boldsymbol{v}_{i,1} - \boldsymbol{v}_{(i-1),N}$. Furthermore, the dissipation coefficients, $\sigma_a,\ a \in \{1, 2, 4\}$, are calculated by scaling the maximum absolute value of the eigenvalues of the flux Jacobian, which is described in the appendix A. We will now prove that the artificial dissipation operator, (5.2), vanishes for a constant solution.

Theorem 5.1.1. The artificial dissipation operator, as defined in (5.2), vanishes for a constant solution, that is, when given a constant solution, $\tilde{\mathsf{P}}^{-1}\left(\mathsf{Diss} \circ \mathsf{M}\right)\boldsymbol{v} = 0$.

Proof: The artificial dissipation operator is comprised of terms of the form $\tilde{\mathsf{P}}_{ii}\mathsf{M}_{ij}\Delta\boldsymbol{v}$, i.e.,

$$\tilde{\mathsf{P}}^{-1}\left(\mathsf{Diss} \circ \mathsf{M}\right)\boldsymbol{v} = \tilde{\mathsf{P}}^{-1}\begin{bmatrix} \mathsf{M}_{12}(\boldsymbol{v}_2 - \boldsymbol{v}_1) \\ \vdots \\ -\mathsf{M}_{(i-1)i}(\boldsymbol{v}_i - \boldsymbol{v}_{i-1}) + \mathsf{M}_{i(i+1)}(\boldsymbol{v}_{i+1} - \boldsymbol{v}_i) \\ \vdots \\ -\mathsf{M}_{(N-1)N}(\boldsymbol{v}_N - \boldsymbol{v}_{N-1}) \end{bmatrix}. \tag{5.8}$$

Written in the above form, it is clear that the artificial dissipation operator vanishes for a constant solution. A constant solution implies that the primitive variables, $\boldsymbol{v}$, are constant. Since the operator can be written as a sum of differences in the primitive variables between adjacent nodes, when given a constant solution, these values are all zero. Thus, the artificial dissipation operator, (5.2), vanishes when given a constant solution. □

In addition to the above theorem, the artificial dissipation operator is consistent with the volume dissipation added by Upperman and Yamaleev [63] to their discretization for the Navier-Stokes equations. In their work, first-order accuracy is easily seen by converting the discretizations into a telescopic flux form. Additionally, from the analysis performed in section 3.4, it seems reasonable to assume that the artificial dissipation operator should converge to 0 at first-order. Here, we do not present the analysis, however, in chapter 6, we present numerical tests which confirm that the artificial dissipation operator converges to zero at first-order. Furthermore, the artificial dissipation operator has been constructed so that it is an entropy-stable term. We will now prove a relation between the entropy variables, the operator M_{ij}, and the primitive variables that will help us prove that the artificial dissipation operator, (5.2), is entropy-stable.

Theorem 5.1.2. For all admissible states $\boldsymbol{u} \in \Omega$, and all $i = 1, 2, \ldots, N-1$, there exists σ_1, σ_2, and σ_4 such that

$$\Delta\alpha_1 \left[\sigma_2\overline{\rho_1}\Delta h_1 - \sigma_1\Delta p_1\right] > 0 \text{ and } \Delta\alpha_1 \left[\sigma_1\Delta p_2 - \sigma_4\overline{\rho_2}\Delta h_2\right] > 0,$$

and therefore

$$\Delta\boldsymbol{w}^{\mathrm{T}}\mathsf{M}_{\mathsf{i(i+1)}}\Delta\boldsymbol{v} \geq 0,$$

where $\Delta\boldsymbol{w} = \boldsymbol{w_{i+1}} - \boldsymbol{w_i}$ and $\Delta\boldsymbol{v} = \boldsymbol{v_{i+1}} - \boldsymbol{v_i}$, with similar definitions for other variables.

Proof: To prove that $\Delta\boldsymbol{w}^{\mathrm{T}}\mathsf{M}_{\mathsf{i(i+1)}}\Delta\boldsymbol{v} \geq 0$, we first carry through the multiplication using arbitrary nodes i and $i+1$. Then, by placing lower bounds on the values of the dissipation coefficients, that correspond to the magnitude of the density, we will be able to show that the contraction is greater than or equal to zero for all nodes $i \in [1, N-1]$. We have

$$\Delta\boldsymbol{w} = \begin{bmatrix} \Delta p_2 - \Delta p_1 \\ \Delta h_1 - \overline{v_1}\Delta v_1 \\ \Delta v_1 \\ \Delta h_2 - \overline{v_2}\Delta v_2 \\ \Delta v_2 \end{bmatrix}, \mathsf{M}_{\mathsf{i(i+1)}}\Delta\boldsymbol{v} = \begin{bmatrix} \sigma_1\Delta\alpha_1 \\ \sigma_2\overline{\rho_1}\Delta\alpha_1 + \sigma_2\overline{\alpha_1}\Delta\rho_1 \\ \sigma_2\overline{\rho_1}\,\overline{v_1}\Delta\alpha_1 + \sigma_2\overline{\alpha_1}\,\overline{v_1}\Delta\rho_1 \\ -\sigma_4\overline{\rho_2}\Delta\alpha_1 + \sigma_4\overline{\alpha_2}\Delta\rho_2 \\ -\sigma_4\overline{\rho_2}\overline{v_2}\Delta\alpha_1 + \sigma_4\overline{\alpha_2}\overline{v_2}\Delta\rho_2 \end{bmatrix}. \tag{5.9}$$

Carrying through the multiplication and gathering like terms gives

$$\begin{aligned} \Delta\boldsymbol{w}^{\mathrm{T}}\mathsf{M}_{\mathsf{i(i+1)}}\Delta\boldsymbol{v} =& \Delta\alpha_1 \left[\sigma_2\overline{\rho_1}\Delta h_1 - \sigma_1\Delta p_1\right] + \Delta\alpha_1 \left[\sigma_1\Delta p_2 - \sigma_4\overline{\rho_2}\Delta h_2\right] + \\ & \Delta\rho_1[\sigma_2\overline{\alpha_1}]\Delta h_1 + \Delta\rho_2[\sigma_4\overline{\alpha_2}]\Delta h_2 + \\ & \Delta\alpha_1 \cancel{\left[\sigma_2\overline{\rho_1}\,\overline{v_1} - \sigma_2\overline{\rho_1}\,\overline{v_1}\right]}\Delta v_1 + \Delta\alpha_1\cancel{[\sigma_4\overline{\rho_2}\,\overline{v_2} - \sigma_4\overline{\rho_2}\,\overline{v_2}]}\Delta v_2 + \\ & \Delta\rho_1 \cancel{\left[\sigma_2\overline{\alpha_1}\,\overline{v_1} - \sigma_2\overline{\alpha_1}\,\overline{v_1}\right]}\Delta v_1 + \Delta\rho_2 \cancel{\left[\sigma_4\overline{\alpha_2}\,\overline{v_2} - \sigma_4\overline{\alpha_2}\,\overline{v_2}\right]}\Delta v_2. \end{aligned} \tag{5.10}$$

The last four terms in (5.10) are always zero as the interior of the terms exactly cancel out. Then, it is possible to show that the terms on the second line of (5.10) are also greater than or equal to zero under the assumptions that σ_2, σ_4, $\overline{\alpha_1}$, and $\overline{\alpha_2}$ are positive. This results because we are considering ideal gases, meaning that the change in enthalpy, $\Delta h_i = \left(\frac{k\gamma_i}{\gamma_i - 1}\right)\Delta\left(\rho_i^{\gamma_i - 1}\right)$, has the same sign as the change in density, $\Delta\rho_i$.

All that remains is to ensure that the terms in the first line of (5.10) are positive. These terms can always be made positive, if they are not positive already, by increasing one of the dissipation coefficients (σ_1,σ_2, or σ_4). We will show the proof for the case where $\Delta\alpha_1$, Δp_1, and Δp_2 are positive. Note that the sign of Δh_1 is equal to the sign of Δp_1 and

likewise for the second phase since we are considering polytropic ideal gas. One can ensure the positivity of the second term in (5.10) by choosing

$$\begin{aligned}\Delta\alpha_1\left[\sigma_1\Delta p_2-\sigma_4\overline{\rho_2}\Delta h_2\right]&>0,\\ \sigma_1\Delta p_2-\sigma_4\overline{\rho_2}\Delta h_2&>0,\\ \sigma_1\Delta p_2&>\sigma_4\overline{\rho_2}\Delta h_2,\\ \sigma_1&>\frac{\sigma_4\overline{\rho_2}\Delta h_2}{\Delta p_2},\end{aligned}$$

then, considering the above restriction on σ_1 chose

$$\begin{aligned}\Delta\alpha_1\left[\sigma_2\overline{\rho_1}\Delta h_1-\sigma_1\Delta p_1\right]&>0,\\ \sigma_2\overline{\rho_1}\Delta h_1-\sigma_1\Delta p_1&>0,\\ \sigma_2\overline{\rho_1}\Delta h_1&>\sigma_1\Delta p_1,\\ \sigma_2&>\frac{\sigma_1\Delta p_1}{\overline{\rho_1}\Delta h_1}.\end{aligned}$$

A similar procedure can be carried for the case where $\Delta\alpha_1<0$. Furthermore, for an ideal gas, these constraints that are placed onto the dissipation coefficients will not cause the coefficients to grow uncontrollably as $\frac{\Delta p}{\Delta h}$ is on the order of magnitude of density. This property will become important when discussing the positivity-preservation algorithm. □

We can now use Theorem (5.1.2) to show that the artificial dissipation operator and the element interface dissipation are entropy-dissipative terms. With this we can conclude that the first-order scheme (5.1) is entropy-stable.

Theorem 5.1.3. Left multiplying the artificial dissipation operator, defined in (5.2), on some element i, by the entropy variables $\boldsymbol{w}_i^{\mathrm{T}}$, and the SBP norm matrix P, results in

$$\boldsymbol{w}_i^{\mathrm{T}}\mathsf{P}\tilde{\mathsf{P}}^{-1}(\mathsf{Diss}\circ\mathsf{M})\boldsymbol{v}_i\leq 0.$$

Furthermore, left multiplying the element interface dissipation, defined in (5.7), by $\boldsymbol{w}_i^{\mathrm{T}}\mathsf{P}$ and summing over all elements $i=1,2,\ldots,n$ leads to

$$\sum_{i=1}^{n}\boldsymbol{w}_i^{\mathrm{T}}\mathsf{P}\boldsymbol{u}_i^{EID}\leq 0.$$

Hence, the first-order scheme, (5.1), is entropy-stable, i.e., $\sum_{i=1}^{n}\overline{\mathbf{1}}^{\mathrm{T}}\overline{\mathsf{P}}\frac{d\boldsymbol{\eta}_i}{dt}\leq 0$, where $\mathsf{P}=\overline{\mathsf{P}}\otimes\mathsf{I}_5$ and $\boldsymbol{\eta}_i=\eta(\boldsymbol{u}_i)$.

Proof: From theorem (4.2.3), (4.9) is entropy-conservative. Furthermore, (5.1) is simply (4.9) with the addition of the artificial dissipation operator, (5.2), and element interface dissipation (5.7). Therefore, to prove that (5.1) is entropy-stable all that needs to be shown is that (5.2) and (5.7) are entropy-dissipative.

The artificial dissipation operator can be shown to be entropy-stable over each element individually, meaning that, when summed over all elements, the total contribution of the dissipation operator is also entropy-stable. Therefore, it is sufficient to show that (5.2) is entropy-stable in a single element with N nodes. To do this, we take a similar approach as in the proof that (4.9) is entropy-conservative. We left multiply the artificial dissipation operator by $\boldsymbol{w}^{\mathrm{T}}\mathsf{P}$, except this time show that the contraction is less than or equal to zero. Note that $\mathsf{P}\tilde{\mathsf{P}}^{-1} = h$, where h is the grid spacing.

$$\boldsymbol{w}^{\mathrm{T}}\mathsf{P}\tilde{\mathsf{P}}^{-1}(\mathsf{Diss}\circ\mathsf{M})\boldsymbol{v} = h\boldsymbol{w}^{\mathrm{T}}(\mathsf{Diss}\circ\mathsf{M})\boldsymbol{v},$$

$$h\boldsymbol{w}^{\mathrm{T}}(\mathsf{Diss}\circ\mathsf{M})\boldsymbol{v} = h\begin{bmatrix}\boldsymbol{w}_1\\ \boldsymbol{w}_2\\ \boldsymbol{w}_3\\ \vdots\\ \boldsymbol{w}_N\end{bmatrix}^{\mathrm{T}}\begin{bmatrix}-2\mathsf{M}_{11} & \mathsf{M}_{12} & 0 & 0 & \dots & 0\\ \mathsf{M}_{21} & -2\mathsf{M}_{22} & \mathsf{M}_{23} & 0 & \dots & 0\\ 0 & \mathsf{M}_{32} & -2\mathsf{M}_{33} & \mathsf{M}_{34} & \dots & 0\\ & \ddots & \ddots & \ddots & & \\ 0 & 0 & 0 & \dots & \mathsf{M}_{(\mathsf{N}-1)\mathsf{N}} & -2\mathsf{M}_{\mathsf{NN}}\end{bmatrix}\begin{bmatrix}\boldsymbol{v}_1\\ \boldsymbol{v}_2\\ \boldsymbol{v}_3\\ \vdots\\ \boldsymbol{v}_N\end{bmatrix},$$

$$= h\begin{bmatrix}\boldsymbol{w}_1\\ \boldsymbol{w}_2\\ \boldsymbol{w}_3\\ \vdots\\ \boldsymbol{w}_N\end{bmatrix}^{\mathrm{T}}\begin{bmatrix}-2\mathsf{M}_{11}\boldsymbol{v}_1 + \mathsf{M}_{12}\boldsymbol{v}_2\\ \mathsf{M}_{12}\boldsymbol{v}_1 - 2\mathsf{M}_{22}\boldsymbol{v}_2 + \mathsf{M}_{23}\boldsymbol{v}_3\\ \mathsf{M}_{23}\boldsymbol{v}_2 - 2\mathsf{M}_{33}\boldsymbol{v}_3 + \mathsf{M}_{34}\boldsymbol{v}_4\\ \vdots\\ \mathsf{M}_{(\mathsf{N}-1)\mathsf{N}}\boldsymbol{v}_{(N-1)} - 2\mathsf{M}_{\mathsf{NN}}\boldsymbol{v}_N\end{bmatrix}.$$

Carrying out the multiplication and substituting in the form of M_{ii} from (5.5) $\forall\ i = 1, 2, \dots, N$ we find that

$$\begin{aligned}\boldsymbol{w}^{\mathrm{T}}\mathsf{P}\tilde{\mathsf{P}}^{-1}(\mathsf{Diss}\circ\mathsf{M})\boldsymbol{v} &= -h\sum_{i=1}^{N-1}\left(\boldsymbol{w}_{(i+1)} - \boldsymbol{w}_i\right)^{\mathrm{T}}\mathsf{M}_{\mathsf{i}(\mathsf{i}+1)}\left(\boldsymbol{v}_{(i+1)} - \boldsymbol{v}_i\right),\\ &= -h\sum_{i=1}^{N-1}\Delta\boldsymbol{w}^{\mathrm{T}}\mathsf{M}_{\mathsf{i}(\mathsf{i}+1)}\Delta\boldsymbol{v},\end{aligned}$$

by theorem (5.1.2), $\Delta\boldsymbol{w}^{\mathrm{T}}\mathsf{M}_{\mathsf{i}(\mathsf{i}+1)}\Delta\boldsymbol{v} \geq 0\ \forall\ i = 1, 2, \dots, N-1$. Thus,

$$\boldsymbol{w}^{\mathrm{T}}\mathsf{P}\tilde{\mathsf{P}}^{-1}(\mathsf{Diss}\circ\mathsf{M})\boldsymbol{v} = -h\sum_{i=1}^{N-1}\Delta\boldsymbol{w}^{\mathrm{T}}\mathsf{M}_{\mathsf{i}(\mathsf{i}+1)}\Delta\boldsymbol{v} \leq 0.$$

Therefore, $\boldsymbol{w}^{\mathrm{T}}\mathsf{P}\tilde{\mathsf{P}}^{-1}(\mathsf{Diss}\circ\mathsf{M})\boldsymbol{v} \leq 0$ in each element. Hence, the artificial dissipation operator is an entropy-dissipative term. All that remains to be shown is that the element interface dissipation is entropy-dissipative. To demonstrate that the interface term (5.7) results in entropy dissipation, we need to contract with the entropy on each element and then sum the results over all elements. Assume the domain has been discretized into n elements with N nodes per element. Thus, left multiplying (5.7) by $\boldsymbol{w}^{\mathrm{T}}\mathsf{P}$ and summing over all elements gives

$$\sum_{i=1}^{n} \boldsymbol{w}_i^{\mathrm{T}}\mathsf{P}\boldsymbol{u}_i^{EID} = \sum_{i=1}^{n} \boldsymbol{w}_i^{\mathrm{T}}\mathsf{P}\tilde{\mathsf{P}}^{-1}[-\mathsf{M}_{N1}^{i}\Delta^{i}\boldsymbol{v}, 0, \ldots, 0, \mathsf{M}_{\mathsf{N1}}^{(\mathrm{i+1})}\Delta^{(i+1)}\boldsymbol{v}]^{\mathrm{T}}.$$

Here, in the case of a periodic problem, when $i = n$, $(i+1) = 1$. Therefore,

$$\begin{aligned}
\sum_{i=1}^{n} \boldsymbol{w}_i^{\mathrm{T}}\mathsf{P}\boldsymbol{u}_i^{EID} &= h\sum_{i=1}^{n} -\boldsymbol{w}_{i,1}\mathsf{M}_{N1}^{i}\Delta^{i}\boldsymbol{v} + \boldsymbol{w}_{i,N}\mathsf{M}_{\mathsf{N1}}^{(\mathrm{i+1})}\Delta^{(i+1)}\boldsymbol{v}, \\
&= h\sum_{i=1}^{n}(\boldsymbol{w}_{(i-1),N} - \boldsymbol{w}_{i,1})\mathsf{M}_{N1}^{i}\Delta^{i}\boldsymbol{v}, \\
&= -h\sum_{i=1}^{n}(\boldsymbol{w}_{i,1} - \boldsymbol{w}_{(i-1),N})\mathsf{M}_{N1}^{i}\Delta^{i}\boldsymbol{v}, \\
\sum_{i=1}^{n} \boldsymbol{w}_i^{\mathrm{T}}\mathsf{P}\boldsymbol{u}_i^{EID} &= -h\sum_{i=1}^{n}\Delta^{i}\boldsymbol{w}\mathsf{M}_{N1}^{i}\Delta^{i}\boldsymbol{v}.
\end{aligned}$$

By theorem (5.1.2), $\Delta^{i}\boldsymbol{w}\mathsf{M}_{N1}^{i}\Delta^{i}\boldsymbol{v} \geq 0$, thus, $\sum_{i=1}^{N} \boldsymbol{w}_i^{\mathrm{T}}\mathsf{P}\boldsymbol{u}_i^{EID} \leq 0$. Therefore, both the artificial dissipation, (5.2), and the element interface dissipation are entropy-dissipative, meaning (5.1) is entropy-stable, since it is the sum of an entropy-conservative scheme, (4.9), and two entropy-dissipative terms. □

For the isentropic Baer-Nunziato model, we require positivity in α_1, ρ_1, α_2 and ρ_2. In numerical simulations we compute α_2 as $1-\alpha_1$. Therefore, to maintain positivity of α_2 we require α_1 to be bounded above by 1. That is, $\alpha_1 \in (0,1)$, $\rho_1, \rho_2 > 0$. This is equivalent to requiring positivity in equations 1, 2, and 4 of (2.3) since the vector of conserved variables is $[\alpha_1, \alpha_1\rho_1, \alpha_1\rho_1 v_1, \alpha_2\rho_2, \alpha_2\rho_2 v_2]^{\mathrm{T}}$. We will take (5.1) and analyze only equations 1, 2, and 4 for positivity.

First, we can write (5.1) in a simplified form by substituting the form of the first-order SBP operator Q_1, which will allow us to prove node-wise positivity of the scheme. We will

prove positivity on an element by element basis, thus, for the following discussion we are only considering one element, j, and element indices will not be used for ease of notation. Using first-order Q_1 SBP-finite-difference operators one finds that

$$2\mathsf{D} \circ \mathsf{F}(\boldsymbol{u},\boldsymbol{u})\mathbf{1} = 2(\mathsf{P}^{-1}\mathsf{Q}) \circ \mathsf{F}(\boldsymbol{u},\boldsymbol{u})\mathbf{1} = \mathsf{P}^{-1}(2\mathsf{Q}_1) \circ \mathsf{F}(\boldsymbol{u},\boldsymbol{u})\mathbf{1} = \frac{1}{h}\tilde{\mathsf{P}}^{-1} \begin{bmatrix} \boldsymbol{f}_{12}^{(EC)} \\ \vdots \\ \boldsymbol{f}_{i(i+1)}^{(EC)} - \boldsymbol{f}_{i(i-1)}^{(EC)} \\ \vdots \\ -\boldsymbol{f}_{N(N-1)}^{(EC)} \end{bmatrix}.$$

Furthermore, the artificial dissipation operator can be written as

$$\tilde{\mathsf{P}}^{-1}\left(\mathsf{Diss} \circ \mathsf{M}\right)\boldsymbol{v} = \tilde{\mathsf{P}}^{-1} \begin{bmatrix} \mathsf{M}_{12}(\boldsymbol{v}_2 - \boldsymbol{v}_1) \\ \vdots \\ -\mathsf{M}_{(i-1)i}(\boldsymbol{v}_i - \boldsymbol{v}_{i-1}) + \mathsf{M}_{i(i+1)}(\boldsymbol{v}_{(i+1)} - \boldsymbol{v}_i) \\ \vdots \\ -\mathsf{M}_{(N-1)N}(\boldsymbol{v}_N - \boldsymbol{v}_{N-1}) \end{bmatrix}.$$

Finally, we will pull the P term out of the SATs as follows

$$\boldsymbol{SATs} = \mathsf{P}^{-1}\overline{\boldsymbol{SATs}} = \frac{1}{h}\tilde{\mathsf{P}}^{-1}\overline{\boldsymbol{SATs}}.$$

For ease of notation we absorb the $\frac{1}{h}$ term into the SATs as well as the Hadamard product term so that $\frac{1}{h}\boldsymbol{f}_{ij}^{(EC)} = \boldsymbol{f}_{ij}$ and $\frac{1}{h}\overline{\boldsymbol{SATs}} = \boldsymbol{S}$. Plugging the above into (5.1) we can rewrite the scheme nodewise as follows:

$$\begin{aligned} \frac{d\boldsymbol{u}_1}{dt} =& \frac{1}{\tilde{P}_{11}}\left[-\boldsymbol{f}_{12} + \mathsf{M}_{12}(\boldsymbol{v}_2 - \boldsymbol{v}_1) - \mathsf{M}_{N1}^{j}\Delta^{j}\boldsymbol{v} + \boldsymbol{S}\right], \\ \frac{d\boldsymbol{u}_i}{dt} =& -\frac{1}{\tilde{P}_{ii}}\left[\boldsymbol{f}_{i(i+1)} - \mathsf{M}_{i(i+1)}(\boldsymbol{v}_{(i+1)} - \boldsymbol{v}_i)\right] + \frac{1}{\tilde{P}_{ii}}\left[\boldsymbol{f}_{i(i-1)} - \mathsf{M}_{(i-1)i}(\boldsymbol{v}_i - \boldsymbol{v}_{i-1})\right], \\ \frac{d\boldsymbol{u}_N}{dt} =& \frac{1}{\tilde{P}_{NN}}\left[\boldsymbol{f}_{N(N-1)} - \mathsf{M}_{(N-1)N}(\boldsymbol{v}_N - \boldsymbol{v}_{N-1}) + \mathsf{M}_{N1}^{(j+1)}\Delta^{(j+1)}\boldsymbol{v} + \boldsymbol{S}\right], \end{aligned} \tag{5.11}$$

where $i = 2, 3, \ldots, N-1$. The scheme (5.11) is now written in a form such that, when marching in time using the explicit forward Euler discretization, we can prove that positivity of the densities and void fractions will be preserved. Positivity is preserved under certain restrictions on the dissipation coefficients as well as the allowable time step.

Theorem 5.1.4. Consider the semi-discrete scheme (5.11) with the explicit forward Euler discretization in time on a single element, with a time step of Δt:

$$\begin{aligned}
\boldsymbol{u}_1^{n+1} =& \boldsymbol{u}_1^n - \frac{\Delta t}{\tilde{P}_{11}}\left[\boldsymbol{f}_{12} - \mathsf{M}_{12}(\boldsymbol{v}_2 - \boldsymbol{v}_1) + \mathsf{M}_{N1}^j \Delta^j \boldsymbol{v} - \boldsymbol{S}\right], \\
\boldsymbol{u}_i^{n+1} =& \boldsymbol{u}_i^n - \frac{\Delta t}{\tilde{P}_{ii}}\left[\boldsymbol{f}_{i(i+1)} - \mathsf{M}_{i(i+1)}(\boldsymbol{v}_{(i+1)} - \boldsymbol{v}_i)\right] + \frac{\Delta t}{\tilde{P}_{ii}}\left[\boldsymbol{f}_{i(i-1)} - \mathsf{M}_{(i-1)i}(\boldsymbol{v}_i - \boldsymbol{v}_{i-1})\right], \\
\boldsymbol{u}_N^{n+1} =& \boldsymbol{u}_N^n + \frac{\Delta t}{\tilde{P}_{NN}}\left[\boldsymbol{f}_{N(N-1)} - \mathsf{M}_{(N-1)N}(\boldsymbol{v}_N - \boldsymbol{v}_{N-1}) + \mathsf{M}_{N1}^{(j+1)} \Delta^{(j+1)} \boldsymbol{v} + \boldsymbol{S}\right].
\end{aligned} \tag{5.12}$$

Assuming that $\boldsymbol{u}^n$ is in the admissible set and under certain choices for σ_1, σ_2, and σ_4, defined below, the above first-order scheme preserves the positivity of ρ_1, ρ_2, α_1, and α_2 under the CFL-like condition:

$$\begin{cases} \Delta t < \frac{\tilde{P}_{ii}}{2\Gamma} & i = 1, N \\ \Delta t < \frac{\tilde{P}_{ii}}{4\Gamma} & i = 2, 3, \ldots, N-1 \end{cases},$$

where $\Gamma = \max(\sigma_1,\sigma_2,\sigma_4)$. Assuming that each element is discretized using N nodes, the dissipation coefficients σ_1, σ_2, and σ_4 are selected as follows:
For $i = 1$ choose the dissipation coefficients such that:

$$\begin{aligned}
\sigma_1 &\geq \max\left(\frac{|f_{12}^{(1)} + \overline{\sigma}\Delta^j u^{(1)} - S^{(1)}|}{u_1^{(1)} + u_2^{(1)}}, \frac{|\overline{\sigma}\Delta^j(\alpha_2) + S^{(1)} - f_{12}^{(1)}|}{(\alpha_2)_1 + (\alpha_2)_2}\right), \\
\sigma_a &\geq \frac{|f_{12}^{(a)} + \overline{\sigma}\Delta^j u^{(a)} - S^{(a)}|}{u_1^{(a)} + u_2^{(a)}}, \quad a = 2, 4.
\end{aligned} \tag{5.13}$$

For $i = 2, 3, \ldots, N-1$ choose the dissipation coefficients such that:

$$\begin{aligned}
\sigma_1 &\geq \max\left(\frac{|f_{i(i+1)}^{(1)}|}{u_i^{(1)} + u_{i+1}^{(1)}}, \frac{|f_{i(i-1)}^{(1)}|}{u_i^{(1)} + u_{i-1}^{(1)}}, \frac{|f_{i(i+1)}^{(1)}|}{(\alpha_2)_i + (\alpha_2)_{(i+1)}}, \frac{|f_{i(i-1)}^{(1)}|}{(\alpha_2)_i + (\alpha_2)_{(i-1)}}\right), \\
\sigma_a &\geq \max\left(\frac{|f_{i(i+1)}^{(a)}|}{u_i^{(a)} + u_{i+1}^{(a)}}, \frac{|f_{i(i-1)}^{(a)}|}{u_i^{(a)} + u_{i-1}^{(a)}}\right), \quad a = 2, 4.
\end{aligned} \tag{5.14}$$

For $i = N$ choose the dissipation coefficients such that:

$$\begin{aligned}\sigma_1 &\geq \max\left(\frac{|f^{(1)}_{N(N-1)} + \overline{\sigma}\Delta^{(j+1)}u^{(1)} + S^{(1)}|}{u^{(1)}_N + u^{(1)}_{N-1}}, \frac{|f^{(1)}_{N(N-1)} - \overline{\sigma}\Delta^{(j+1)}(\alpha_2) + S^{(1)}|}{(\alpha_2)_N + (\alpha_2)_{(N-1)}}\right),\\ \sigma_a &\geq \frac{|f^{(a)}_{N(N-1)} + \overline{\sigma}\Delta^{(j+1)}u^{(a)} + S^{(a)}|}{u^{(a)}_N + u^{(a)}_{N-1}}, \quad a = 2, 4.\end{aligned} \tag{5.15}$$

Proof: To prove the node-wise positivity of the numerical scheme we will make use of the design of the artificial dissipation operator (5.2). Notice that the operator M has been designed so that when multiplied by the change in primitive variables it returns the change in conserved variables in the relevant equations as follows,

$$\mathsf{M}_{ij}\Delta\boldsymbol{v} = \begin{bmatrix} \sigma_1\Delta\alpha_1 \\ \sigma_2\overline{\rho_1}\Delta\alpha_1 + \sigma_2\overline{\alpha_1}\Delta\rho_1 \\ \sigma_2\overline{\rho_1}\,\overline{v_1}\Delta\alpha_1 + \sigma_2\overline{\alpha_1}\,\overline{v_1}\Delta\rho_1 \\ -\sigma_4\overline{\rho_2}\Delta\alpha_1 + \sigma_4\overline{\alpha_2}\Delta\rho_2 \\ -\sigma_4\overline{\rho_2 v_2}\Delta\alpha_1 + \sigma_4\overline{\alpha_2 v_2}\Delta\rho_2 \end{bmatrix} = \begin{bmatrix} \sigma_1\Delta\alpha_1 \\ \sigma_2\Delta\left(\alpha_1\rho_1\right) \\ \sigma_2\overline{v_1}\Delta\left(\alpha_1\rho_1\right) \\ \sigma_4\Delta\left(\alpha_2\rho_2\right) \\ \sigma_4\overline{v_2}\Delta\left(\alpha_2\rho_2\right) \end{bmatrix} = \begin{bmatrix} \sigma_1\Delta u^{(1)} \\ \sigma_2\Delta u^{(2)} \\ \sigma_2\overline{v_1}\Delta u^{(2)} \\ \sigma_4\Delta u^{(4)} \\ \sigma_4\overline{v_2}\Delta u^{(4)} \end{bmatrix},$$

where $u^{(a)}$ denotes the a^{th} conserved variable in the 5 equation isentropic Baer-Nunziato model. The analysis on equations 1, 2, and 4 is identical, thus, here we perform them all at once, i.e.,

$$\begin{aligned} u_1^{n+1(a)} =& u_1^{n(a)} - \frac{\Delta t}{\tilde{P}_{11}}\left[f^{(a)}_{12} - \left[\mathsf{M}_{12}(\boldsymbol{v}_2 - \boldsymbol{v}_1)\right]^{(a)} + \left[\mathsf{M}^j_{N1}\Delta^j\boldsymbol{v}\right]^{(a)} - S^{(a)}\right],\\ u_i^{n+1(a)} =& u_i^{n(a)} - \frac{\Delta t}{\tilde{P}_{ii}}\left[f^{(a)}_{i(i+1)} - \left[\mathsf{M}_{i(i+1)}(\boldsymbol{v}_{(i+1)} - \boldsymbol{v}_i)\right]^{(a)}\right] + \frac{\Delta t}{\tilde{P}_{ii}}\left[f^{(a)}_{i(i-1)} - \left[\mathsf{M}_{(i-1)i}(\boldsymbol{v}_i - \boldsymbol{v}_{i-1})\right]^{(a)}\right],\\ u_N^{n+1(a)} =& u_N^{n(a)} + \frac{\Delta t}{\tilde{P}_{NN}}\left[f^{(a)}_{N(N-1)} - \left[\mathsf{M}_{(N-1)N}(\boldsymbol{v}_N - \boldsymbol{v}_{N-1})\right]^{(a)} + \left[\mathsf{M}^{(j+1)}_{N1}\Delta^{(j+1)}\boldsymbol{v}\right]^{(a)} + S^{(a)}\right], \end{aligned} \tag{5.16}$$

for $a \in \{1, 2, 4\}$. For the rest of the proof we will omit the (a) symbol and assume that, unless stated otherwise, the analysis holds for equations 1, 2, and 4. Suppose we are on node i, define $\Delta^+ b = b_{i+1} - b_i$ and $\Delta^- b = b_i - b_{i-1}$ for some quantity b. First, let's study

the interior nodes:

$$\begin{aligned} u_i^{n+1} &= u_i^n - \frac{\Delta t}{\tilde{P}_{ii}}\left[f_{i(i+1)} - \mathsf{M}_{i(i+1)}(\boldsymbol{v}_{(i+1)} - \boldsymbol{v}_i)\right] + \frac{\Delta t}{\tilde{P}_{ii}}\left[f_{i(i-1)} - \mathsf{M}_{(i-1)i}(\boldsymbol{v}_i - \boldsymbol{v}_{i-1})\right], \\ &= u_i^n - \frac{\Delta t}{\tilde{P}_{ii}}\left[f_{i(i+1)} - \sigma\Delta^+ u\right] + \frac{\Delta t}{\tilde{P}_{ii}}\left[f_{i(i-1)} - \sigma\Delta^- u\right], \\ &= \left[\frac{u_i^n}{2} - \frac{\Delta t}{\tilde{P}_{ii}}\left(f_{i(i+1)} - \sigma\Delta^+ u\right)\right] + \left[\frac{u_i^n}{2} + \frac{\Delta t}{\tilde{P}_{ii}}\left(f_{i(i-1)} - \sigma\Delta^- u\right)\right]. \end{aligned} \tag{5.17}$$

To maintain positivity at the next time step we can maintain positivity of each term on the right hand side of (5.17). Consider the first term on the right hand side; we want to determine restrictions on σ and Δt such that $\frac{u_i^n}{2} - \frac{\Delta t}{\tilde{P}_{ii}}\left(f_{i(i+1)} - \sigma\Delta^+ u\right) > 0$. We will determine such restrictions as follows,

$$\begin{aligned} \frac{u_i^n}{2} - \frac{\Delta t}{\tilde{P}_{ii}}\left(f_{i(i+1)} - \sigma\Delta^+ u\right) &\geq \frac{u_i^n}{2} - \frac{\Delta t}{\tilde{P}_{ii}}\left(|f_{i(i+1)}| - \sigma\Delta^+ u\right), \\ &= \frac{u_i^n}{2} - \frac{2\sigma\Delta t}{\tilde{P}_{ii}}\left(\frac{|f_{i(i+1)}|}{2\sigma} - \frac{\Delta^+ u}{2}\right), \\ &\geq \frac{u_i^n}{2} - \frac{2\sigma\Delta t}{\tilde{P}_{ii}}\left(u_A - \frac{\Delta^+ u}{2}\right). \end{aligned}$$

Note that this is true if and only if $u_A \geq \frac{|f_{i(i+1)}|}{2\sigma}$ or $\sigma \geq \frac{|f_{i(i+1)}|}{2u_A}$, where $u_A = \frac{u_i + u_{i+1}}{2}$. We assume that positivity was maintained on the previous time step, therefore, u_A is guaranteed to be positive. Furthermore, $u_A - \frac{\Delta^+ u}{2} = u_i^n$. Thus,

$$\begin{aligned} \frac{u_i^n}{2} - \frac{\Delta t}{\tilde{P}_{ii}}\left(f_{i(i+1)} - \sigma\Delta^+ u\right) &\geq \frac{u_i^n}{2} - \frac{2\sigma\Delta t}{\tilde{P}_{ii}}\left(u_i^n\right), \\ &= u_i^n\left(\frac{1}{2} - \frac{2\sigma\Delta t}{\tilde{P}_{ii}}\right) > 0. \end{aligned}$$

The solution at time step n, $\boldsymbol{u}^n$, is in the set of admissible states, thus, all we need to do is choose a time step, Δt, such that $\frac{1}{2} - \frac{2\sigma\Delta t}{\tilde{P}_{ii}} > 0$. Therefore, by choosing $\sigma \geq \frac{|f_{i(i+1)}|}{2u_A}$ and $\Delta t < \frac{\tilde{P}_{ii}}{4\sigma}$, we can maintain positivity in the first term on the right hand side. Now,

lets perform the same exercise with the second term on the right hand side of (5.17):

$$\begin{aligned}\frac{u_i^n}{2}+\frac{\Delta t}{\tilde{P}_{ii}}\left(f_{i(i-1)}-\sigma\Delta^- u\right) &= \frac{u_i^n}{2}-\frac{\Delta t}{\tilde{P}_{ii}}\left(-f_{i(i-1)}+\sigma\Delta^- u\right),\\ &\geq \frac{u_i^n}{2}-\frac{\Delta t}{\tilde{P}_{ii}}\left(|f_{i(i-1)}|+\sigma\Delta^- u\right),\\ &= \frac{u_i^n}{2}-\frac{2\sigma\Delta t}{\tilde{P}_{ii}}\left(\frac{|f_{i(i-1)}|}{2\sigma}+\frac{\Delta^- u}{2}\right),\\ &\geq \frac{u_i^n}{2}-\frac{2\sigma\Delta t}{\tilde{P}_{ii}}\left(u_A+\frac{\Delta^- u}{2}\right).\end{aligned}$$

Note that, this is true if and only if $u_A \geq \frac{|f_{i(i-1)}|}{2\sigma}$ or $\sigma \geq \frac{|f_{i(i-1)}|}{2u_A}$, where $u_A = \frac{u_i+u_{i-1}}{2}$. Furthermore, $u_A + \frac{\Delta^- u}{2} = u_i^n$, thus,

$$\begin{aligned}\frac{u_i^n}{2}+\frac{\Delta t}{\tilde{P}_{ii}}\left(f_{i(i-1)}-\sigma\Delta^- u\right) &\geq \frac{u_i^n}{2}-\frac{2\sigma\Delta t}{\tilde{P}_{ii}}\left(u_i^n\right),\\ &= u_i^n\left(\frac{1}{2}-\frac{2\sigma\Delta t}{\tilde{P}_{ii}}\right) > 0.\end{aligned}$$

Therefore, to maintain positivity in the second half of the equation we need $\sigma \geq \frac{|f_{i(i-1)}|}{2u_A}$ and the same CFL-like condition $\Delta t < \frac{\tilde{P}_{ii}}{4\sigma}$. Therefore, to maintain positivity on an interior node i, we need to choose σ such that

$$\sigma \geq \max\left(\frac{|f_{i(i+1)}|}{u_i+u_{i+1}}, \frac{|f_{i(i-1)}|}{u_i+u_{i-1}}\right).$$

Furthermore, we must take a time step, Δt, such that

$$\Delta t < \frac{\tilde{P}_{ii}}{4\sigma}.$$

It is crucial that Δt does not become arbitrarily small and this happens when σ becomes arbitrarily large. Later, we will prove that σ cannot grow uncontrollably. Now, all that remains is to prove positivity at the first and last nodes. The procedure is similar for both

nodes and so we will only show the proof for node 1.

$$
\begin{aligned}
u_1^{n+1} &= u_1^n - \frac{\Delta t}{\tilde{P}_{11}} \left(f_{12} - \mathsf{M}_{12}(\boldsymbol{v}_2 - \boldsymbol{v}_1) + \mathsf{M}_{N1}^j \Delta^j \boldsymbol{v} - S \right), \\
&= u_1^n - \frac{\Delta t}{\tilde{P}_{11}} \left[f_{12} - \sigma \Delta^+ u + \overline{\sigma} \Delta^j u - S \right], \\
&= u_1^n - \frac{2\sigma \Delta t}{\tilde{P}_{11}} \left(\frac{f_{12}}{2\sigma} - \frac{\Delta^+ u}{2} + \frac{\overline{\sigma} \Delta^j u}{2\sigma} - \frac{S}{2\sigma} \right), \\
&\geq u_1^n - \frac{2\sigma \Delta t}{\tilde{P}_{11}} \left(\frac{|f_{12} + \overline{\sigma} \Delta^j u - S|}{2\sigma} - \frac{\Delta^+ u}{2} \right), \\
&\geq u_1^n - \frac{2\sigma \Delta t}{\tilde{P}_{11}} \left(u_A - \frac{\Delta^+ u}{2} \right), \\
&= u_1^n - \frac{2\sigma \Delta t}{\tilde{P}_{11}} (u_1^n), \\
&= u_1^n \left(1 - \frac{2\sigma \Delta t}{\tilde{P}_{11}} \right) > 0.
\end{aligned}
$$

Note that $2\mathsf{M}_{N1}^j \Delta^j = 2\overline{\sigma} \Delta^j u$ where σ does not have to equal $\overline{\sigma}$, meaning we can use a different dissipation coefficient for the element interface dissipation. Above we have assumed that σ has been selected such that $\sigma \geq \frac{|f_{12} + \overline{\sigma} \Delta^j u - S|}{2u_A}$. Therefore, to maintain positivity on node 1, we pick a time step such that

$$\Delta t < \frac{\tilde{P}_{11}}{2\sigma},$$

with

$$\sigma \geq \frac{|f_{12} + \overline{\sigma} \Delta^j u - S|}{2u_A}.$$

Similarly, it can be shown that we can maintain positivity on node N with

$$\sigma \geq \frac{|f_{N(N-1)} + \overline{\sigma} \Delta^{(j+1)} u + S|}{2u_A},$$

and a time step

$$\Delta t < \frac{\tilde{P}_{NN}}{2\sigma}.$$

The above approach will preserve the positivity of ρ_1, ρ_2, and α_1. However, we also need to maintain positivity of α_2. Since α_1 and α_2 must satisfy the closure law $\alpha_1 + \alpha_2 =$

1, maintaining positivity in α_2 is equivalent to maintaining boundedness on α_1, namely, $\alpha_1 < 1$. To maintain boundedness on α_1, we use the first equation in the isentropic Baer-Nunziato model since it describes the evolution of α_1.

$$1 > \left(u_i^{(1)}\right)^{n+1},$$
$$1 - \left(u_i^{(1)}\right)^{n+1} > 0.$$

From here we can substitute the form of (5.16) for $\left(u_i^{(1)}\right)^{n+1}$. The analysis is similar to the proof of positivity so we only outline the analysis performed for node 1. Furthermore, all terms in the update equation for u_i^{n+1} are at time level n, thus, we drop the superscript "n".

$$1 - u_1^{(1)} + \frac{\Delta t}{\tilde{P}_{11}}\left[f_{12}^{(1)} - \sigma\Delta^+ u^{(1)} + \overline{\sigma}\Delta^j u^{(1)} - S^{(1)}\right] > 0.$$

It is informative to substitute $\alpha_1 = u^{(1)}$ into the above expression to find that

$$1 - \alpha_1 + \frac{\Delta t}{\tilde{P}_{11}}\left[f_{12}^{(1)} - \sigma\Delta^+(\alpha_1) + \overline{\sigma}\Delta^j u^{(1)} - S^{(1)}\right] > 0.$$

Recall, $\alpha_2 = 1 - \alpha_1$, thus, $\Delta^{\pm}(\alpha_1) = -\Delta^{\pm}(\alpha_2)$. Therefore,

$$\alpha_2 + \frac{\Delta t}{\tilde{P}_{11}}\left[f_{12}^{(1)} + \sigma\Delta^+(\alpha_2) + \overline{\sigma}\Delta^j u^{(1)} - S^{(1)}\right] > 0,$$
$$\alpha_2 - \frac{\Delta t}{\tilde{P}_{11}}\left[-f_{12}^{(1)} - \sigma\Delta^+(\alpha_2) - \overline{\sigma}\Delta^j u^{(1)} + S^{(1)}\right] > 0.$$

From here, the same analysis from earlier can be performed to find a lower bound on the dissipation coefficient, σ, and an upper bound on the allowable time step to maintain positivity of α_2 and therefore, maintain an upper bound on α_1. The dissipation coefficient and time step restriction to maintain boundedness of α_1 can be summarized as follows: For $i = 2, 3, \ldots, N-1$:

$$\sigma_1 \geq \max\left(\frac{|f_{i(i+1)}^{(1)}|}{(\alpha_2)_i + (\alpha_2)_{(i+1)}}, \frac{|f_{i(i-1)}^{(1)}|}{(\alpha_2)_i + (\alpha_2)_{(i-1)}}\right),$$
$$\Delta t < \frac{\tilde{P}_{ii}}{4\sigma_1}.$$

For $i = 1$:

$$\sigma_1 \geq \frac{|\overline{\sigma}\Delta^j(\alpha_2) + S^{(1)} - f_{12}^{(1)}|}{(\alpha_2)_1 + (\alpha_2)_2},$$
$$\Delta t < \frac{\tilde{P}_{11}}{2\sigma_1},$$

For $i = N$:

$$\sigma_1 \geq \frac{|f_{N(N-1)}^{(1)} - \overline{\sigma}\Delta^{(j+1)}(\alpha_2) + S^{(1)}|}{(\alpha_2)_N + (\alpha_2)_{(N-1)}},$$
$$\Delta t < \frac{\tilde{P}_{NN}}{2\sigma_1}.$$

Therefore, to preserve node-wise positivity of ρ_1, ρ_2, α_1, and α_2 in the first-order scheme, we first go node by node and select the largest value of σ_1, σ_2, and σ_4 based on equations (5.13),(5.14), and (5.15). Then, letting $\Gamma = \max(\sigma_1, \sigma_2, \sigma_4)$, we calculate the time step restriction required to maintain positivity as:

$$\begin{cases} \Delta t < \frac{\tilde{P}_{ii}}{2\Gamma} & i = 1, N \\ \Delta t < \frac{\tilde{P}_{ii}}{4\Gamma} & i = 2, 3, \ldots, N-1 \end{cases}. \square \tag{5.18}$$

It is very important that none of the dissipation coefficients, σ's, grow uncontrollably as the time step restriction shrinks proportionally to the inverse of the dissipation coefficients. Thus, if the coefficients were to become very large, it would not only destroy the accuracy of the numerical solution by adding large amounts of artificial dissipation, but, it would cause the time step to become arbitrarily small, which is not of practical use in running simulations. However, using the entropy-conservative two-point flux function of Renac [50], it can be shown that the dissipation coefficients will not grow uncontrollably.

The value of the dissipation coefficients are calculated by $\sigma_a \geq \frac{|f_{ij}^{(a)}|}{2u_A^{(a)}}$, where $j = i + 1$ or $j = i - 1$. We now prove that this cannot grow uncontrollably no matter how close the positive quantities get to zero. First we begin with σ_1

$$\sigma_1 \geq \frac{|f_{ij}^{(1)}|}{2u_A^{(1)}} = \frac{|(v_2)_i[(\alpha_1)_j - (\alpha_1)_i]|}{(\alpha_1)_j + (\alpha_1)_i},$$
$$= |(v_2)_i| \frac{|(\alpha_1)_j - (\alpha_1)_i|}{(\alpha_1)_j + (\alpha_1)_i}.$$

The term $\frac{|(\alpha_1)_j-(\alpha_1)_i|}{(\alpha_1)_j+(\alpha_1)_i}$, is bound between 0 and 1 given $\alpha_1 \in (0,1)$, therefore, the only thing that could cause σ_1 to grow uncontrollably is if the magnitude of the velocity of phase 2 were to grow uncontrollably. The entropy stability properties of the scheme imply a bound on the norm of the solution, thus, the velocity of phase 2 will not diverge for finite time. Now, we consider σ_2

$$\begin{aligned}\sigma_2 \geq \frac{|f_{ij}^{(2)}|}{2u_A^{(2)}} &= \frac{|\overline{\alpha_1}\,\overline{v_1}\hat{h}_1 - (\alpha_1)_i(\rho_1)_i(v_1)_i|}{(\alpha_1\rho_1)_j + (\alpha_1\rho_1)_i}, \\ &\leq \frac{|\overline{\alpha_1}\,\overline{v_1}\hat{h}_1|}{(\alpha_1\rho_1)_j + (\alpha_1\rho_1)_i} + \frac{|(\alpha_1)_i(\rho_1)_i(v_1)_i|}{(\alpha_1\rho_1)_j + (\alpha_1\rho_1)_i}, \\ &= |\overline{v_1}|\frac{\overline{\alpha_1}\hat{h}_1}{(\alpha_1\rho_1)_j + (\alpha_1\rho_1)_i} + |(v_1)_i|\frac{(\alpha_1\rho_1)_i}{(\alpha_1\rho_1)_j + (\alpha_1\rho_1)_i}.\end{aligned}$$

It is clear that unless $(v_1)_i$ were to diverge that the second term on the right hand side of the above equation will not diverge. Then, considering the first term, $\hat{h}_1 = \frac{(p_1)_j-(p_1)_i}{(h_1)_j-(h_1)_i}$, in the case of an ideal gas, this simplifies to $\frac{\gamma_1-1}{\gamma_1}\frac{(\rho_1)_j^{\gamma_1}-(\rho_1)_i^{\gamma_1}}{(\rho_1)_j^{\gamma_1-1}-(\rho_1)_i^{\gamma_1-1}}$, therefore,

$$\frac{\overline{\alpha_1}\hat{h}_1}{(\alpha_1\rho_1)_j + (\alpha_1\rho_1)_i} = R,$$

where,

$$R = \frac{\gamma_1 - 1}{\gamma_1}\frac{(\alpha_1)_j(\rho_1)_j^{\gamma_1} - (\alpha_1)_i(\rho_1)_i^{\gamma_1} - (\alpha_1)_j(\rho_1)_i^{\gamma_1} + (\alpha_1)_i(\rho_1)_j^{\gamma_1}}{2\left[(\alpha_1)_j(\rho_1)_j^{\gamma_1} - (\alpha_1)_i(\rho_1)_i^{\gamma_1} - (\alpha_1)_j(\rho_1)_j(\rho_1)_i^{\gamma_1-1} + (\alpha_1)_i(\rho_1)_i(\rho_1)_j^{\gamma_1-1}\right]}.$$

This function will not diverge as the void fraction and density go to zero, thus, σ_2 will not diverge since the stability properties of the scheme ensure that the velocities will remain bounded, for finite time. The restrictions on σ_4 mimic the restrictions on σ_2, except they use phase 2 quantities instead of phase 1 quantities. Therefore, the analysis performed for σ_2 will hold for σ_4. Thus, the dissipation coefficients, σ_1, σ_2, and σ_4, cannot diverge, meaning that the allowable time step to maintain positivity will not become arbitrarily small.

We have thus far discussed entropy stability and positivity preservation; however, there are other important properties one might want to preserve. For example, Abgrall and Karni [2] show that if care is not taken in the discretization of the non-conservative terms in

(2.3), then oscillations may occur across interfaces separating fluids with different material properties. As we are interested in studying the bubble collapse problem, this is a point which needs to be addressed. In compressible, multiphase flows, a guideline for creating suitable discretizations is provided by Abgrall's criterion [1], which states that a two-phase flow that is uniform in pressure and velocity must remain uniform as the system evolves in time. We will now show that (5.1) satisfies Abgrall's criterion.

Theorem 5.1.5. The first-order entropy-stable positivity-preserving scheme, (5.1), satisfies Abgrall's criterion, which is formulated as follows. Assume that the velocity of both phases are uniform and equal and the pressure of both phases are also uniform and equal at time $t^{(n)}$, that is

$$(v_a)_{j,i} = v, (p_a)_{j,i} = p, a = 1, 2, \quad \forall j = 1, 2, \ldots, n, \quad \forall i = 1, 2, \ldots, N, \tag{5.19}$$

where v and p are given constants that are not necessarily equal, then, given equal dissipation coefficients, i.e., $\sigma_1 = \sigma_2 = \sigma_4 = \sigma$, the velocity and pressure remain uniform and equal at time $t^{(n+1)}$.

Proof: The proof is the same on all elements and so we will drop the index j for ease of notation. Furthermore, if we are assuming equal and uniform pressure, that means that the densities, ρ_1 and ρ_2, are also uniform, but not necessarily equal since the pressures are calculated as $p_a = k\rho_a^{\gamma_a}$. Under these assumptions it can be shown that the entropy-conservative flux simplifies to

$$\boldsymbol{f}^{(\boldsymbol{EC})}(\boldsymbol{u}_i, \boldsymbol{u}_j) = \begin{bmatrix} 1 \\ \rho_1 \\ \rho_1 v \\ -\rho_2 \\ -\rho_2 v \end{bmatrix} v\Delta\alpha_1. \tag{5.20}$$

Now, we will show the proof on the interior nodes, but it can easily be extended to the boundary nodes. On the interior nodes $\tilde{\mathsf{P}}^{-1}(\mathsf{Diss}\circ\mathsf{M})\boldsymbol{v} = \frac{1}{\tilde{P}_{ii}}\left(-\mathsf{M}_{(i-1)i}\Delta\boldsymbol{v}_i + \mathsf{M}_{i(i+1)}\Delta\boldsymbol{v}_{i+1}\right)$, where $\Delta\boldsymbol{v}_i = \boldsymbol{v}_i - \boldsymbol{v_{i-1}}$ and

$$\mathsf{M}_{ij}\Delta v = \begin{bmatrix} \sigma_1\Delta\alpha_1 \\ \sigma_2\rho_1\Delta\alpha_1 \\ \sigma_2\rho_1 v\Delta\alpha_1 \\ -\sigma_4\rho_2\Delta\alpha_1 \\ -\sigma_4\rho_2 v\Delta\alpha_1 \end{bmatrix}.$$

If the velocities and pressures are uniform, we set $\sigma_1 = \sigma_2 = \sigma_4 = \sigma = \max(\sigma_1, \sigma_2, \sigma_4)$. This allows us to simplify the above to

$$\mathsf{M}_{ij}\Delta v = \begin{bmatrix} 1 \\ \rho_1 \\ \rho_1 v \\ -\rho_2 \\ -\rho_2 v \end{bmatrix} \sigma \Delta \alpha_1. \tag{5.21}$$

Note that setting all of the dissipation coefficients to be $\sigma = \max(\sigma_1, \sigma_2, \sigma_4)$ does not effect the positivity preserving properties of the scheme since we simply need to select the dissipation coefficients to be greater than or equal to a minimum value that was determined in theorem (5.16). Thus, by selecting the largest value of σ_1, σ_2, and σ_4, we ensure that the condition is met for all equations.

On the interior we have $\boldsymbol{u}_t = \tilde{\mathsf{P}}^{-1}(\mathsf{Diss} \circ \mathsf{M})\boldsymbol{v} - 2\mathsf{D} \circ \mathsf{F}(\boldsymbol{u}, \boldsymbol{u})\,\mathbf{1}$. Plugging in the above we find that

$$\boldsymbol{u}_t = \begin{bmatrix} 1 \\ \rho_1 \\ \rho_1 v \\ -\rho_2 \\ -\rho_2 v \end{bmatrix} \left(\frac{\sigma\Delta(\alpha_1)_{i+1}}{\tilde{P}_{ii}} - \frac{\sigma\Delta(\alpha_1)_{i+1}}{\tilde{P}_{ii}} - v\sum_{i=1}^{N} \mathsf{D}_{\mathsf{ij}}[(\alpha_1)_j - (\alpha_1)_i] \right) = \begin{bmatrix} 1 \\ \rho_1 \\ \rho_1 v \\ -\rho_2 \\ -\rho_2 v \end{bmatrix} R,$$

where $R = \left(\frac{\sigma\Delta(\alpha_1)_{i+1}}{\tilde{P}_{ii}} - \frac{\sigma\Delta(\alpha_1)_{i+1}}{\tilde{P}_{ii}} - v\sum_{i=1}^{N} \mathsf{D}_{\mathsf{ij}}[(\alpha_1)_j - (\alpha_1)_i] \right)$. Now, assuming a forward Euler discretization is used to march in time, the update on each of the 5 equations is

$$(\alpha_1)_i^{(n+1)} - (\alpha_1)_i^{(n)} = R, \tag{5.22a}$$

$$(\alpha_1)_i^{(n+1)} \left[(\rho_1)_i^{(n+1)} - (\rho_1) \right] + \rho_1 \left[(\alpha_1)_i^{(n+1)} - (\alpha_1)_i^{(n)} \right] = \rho_1 R, \tag{5.22b}$$

$$(\alpha_1\rho_1)_i^{(n+1)} \left[(v_1)_i^{(n+1)} - v \right] + v \left[(\alpha_1\rho_1)_i^{(n+1)} - (\alpha_1)_i^{(n)}\rho_1 \right] = \rho_1 v R, \tag{5.22c}$$

$$(\alpha_2)_i^{(n+1)} \left[(\rho_2)_i^{(n+1)} - (\rho_2) \right] + \rho_2 \left[(\alpha_2)_i^{(n+1)} - (\alpha_2)_i^{(n)} \right] = -\rho_2 R, \tag{5.22d}$$

$$(\alpha_2\rho_2)_i^{(n+1)} \left[(v_2)_i^{(n+1)} - v \right] + v \left[(\alpha_2\rho_2)_i^{(n+1)} - (\alpha_2)_i^{(n)}\rho_2 \right] = -\rho_2 v R. \tag{5.22e}$$

Then, (5.22b) - $\rho_1\times$(5.22a), implies $(\rho_1)_i^{(n+1)} = \rho_1$. This allows us to show (5.22c) -$\rho_1 v\times$(5.22a), gives $(v_1)_i^{(n+1)} = v$. Then, completing the same procedure using (5.22d) and (5.22e), we find that $(\rho_2)_i^{(n+1)} = \rho_2$ and $(v_2)_i^{(n+1)} = v$. □

Using theorem (5.1.5), we immediately find that the high-order entropy-conservative scheme, (4.9), also satisfies Abgrall's criterion.

Corollary 1. The high-order entropy-conservative scheme, (4.9), satisfies Abgrall's criterion as defined in theorem (5.1.5).

Proof: The proof follows immediately from theorem (5.1.5) by dropping the term (5.21). This leads to the following semi-discrete scheme

$$\boldsymbol{u}_t = \begin{bmatrix} 1 \\ \rho_1 \\ \rho_1 v \\ -\rho_2 \\ -\rho_2 v \end{bmatrix} \left(-v \sum_{i=1}^{N} \mathsf{D_{ij}} [(\alpha_1)_j - (\alpha_1)_i] \right) = \begin{bmatrix} 1 \\ \rho_1 \\ \rho_1 v \\ -\rho_2 \\ -\rho_2 v \end{bmatrix} R,$$

where R is now defined as $R = -v \sum_{i=1}^{N} \mathsf{D_{ij}} [(\alpha_1)_j - (\alpha_1)_i]$. From here, the same analysis performed in theorem (5.1.5) holds, and we have that the high-order entropy-conservative scheme, (4.9), satisfies Abgrall's criterion. □

In section 2.2, we showed that, at the continuous level, having a bound on the entropy of the solution corresponds to a bound on the L_2 norm of the solution itself. We now show that for the first-order entropy-stable positivity-preserving scheme (5.1), a bound on the discrete entropy, leads to a bound on the discrete solution.

Theorem 5.1.6. The discrete L_2 norm of the first-order entropy-stable positivity-preserving scheme, defined in (5.1), is bounded by the data of the problem as follows

$$\|\boldsymbol{u}\|_P^2 \leq 2\frac{C}{\eta''_{min}} + \|\boldsymbol{u}_0\|_P^2,$$

where η''_{min} is the minimum value of the Hessian of the entropy function in space and time, $\boldsymbol{u}_0$ is a constant state which lies in the set of admissible states, and C is a constant such that $\frac{C}{\eta''_{min}} \geq \sum_{j=1}^{N} (\overline{\mathsf{P}}_H)_{jj} (\boldsymbol{u}_j - \boldsymbol{u}_0)^{\mathrm{T}} (\boldsymbol{u}_j - \boldsymbol{u}_0)$.

Proof: To begin, we define a new discrete entropy at all nodes $j = 1, 2, \ldots, N$

$$\overline{\eta}_j = \eta_j - \eta(\boldsymbol{u}_0) - \eta'(\boldsymbol{u}_0)^{\mathrm{T}} (\boldsymbol{u}_j - \boldsymbol{u}_0),$$

such that $\overline{\boldsymbol{\eta}} = [\overline{\eta}_1, \ldots, \overline{\eta}_N]^{\mathrm{T}}$ and $\eta' = \frac{\partial \eta}{\partial \boldsymbol{u}}$. Note that $\boldsymbol{u}_0$ is a constant, non-zero state. We choose the state $\boldsymbol{u}_0$ such that $\alpha_i = (\alpha_i)_0 > 0$ and $\rho_i = (\rho_i)_0 > 0$ for $i = 1, 2$. Then,

define the new entropy variables $\overline{\boldsymbol{w}}^{\mathrm{T}} = \frac{d\overline{\eta}}{d\boldsymbol{u}} = \eta' - \eta'(\boldsymbol{u}_0)$, where $\overline{\boldsymbol{w}}_x = \boldsymbol{w}_x$. To find a bound on the new discrete entropy of the system, we will multiply the first-order entropy-stable positivity-preserving scheme, (5.1), by $\overline{\boldsymbol{w}_i}^{\mathrm{T}}\mathsf{P}_H$, where $\overline{\boldsymbol{w}_i}$ is the new entropy variables defined on the i^{th} element. Then, we will sum over all elements to find a bound on the new discrete entropy for the entire system. On the i^{th} element we find that

$$\underbrace{\overline{\boldsymbol{w}}^{\mathrm{T}}\mathsf{P}_H\frac{d\boldsymbol{u}}{dt}}_{1} + \underbrace{2\overline{\boldsymbol{w}}^{\mathrm{T}}\mathsf{Q}\circ\mathsf{F}(\boldsymbol{u},\boldsymbol{u})\mathbf{1}}_{2} = \underbrace{h\overline{\boldsymbol{w}}^{\mathrm{T}}(\mathsf{Diss}\circ\mathsf{M})\boldsymbol{v}}_{3} + \underbrace{\overline{\boldsymbol{w}}^{\mathrm{T}}\mathsf{P}_H\boldsymbol{u}^{EID}}_{4} + \underbrace{\overline{\boldsymbol{w}}^{\mathrm{T}}\mathsf{P}_H\boldsymbol{SATs}}_{5}, \tag{5.23}$$

where we have dropped the element index. Term 1 can be recast as follows

$$\begin{aligned}
\overline{\boldsymbol{w}}^{\mathrm{T}}\mathsf{P}_H\frac{d\boldsymbol{u}}{dt} &= \sum_{j=1}^{N}\overline{\boldsymbol{w}}_j(\mathsf{P}_H)_{jj}\frac{d\boldsymbol{u}_j}{dt},\\
&= \sum_{j=1}^{N}(\mathsf{P}_H)_{jj}\frac{d\overline{\eta}_j}{d\boldsymbol{u}_j}\frac{d\boldsymbol{u}_j}{dt},\\
&= \sum_{j=1}^{N}(\overline{\mathsf{P}}_H)_{jj}\frac{d\overline{\eta}_j}{dt},\\
\overline{\boldsymbol{w}}^{\mathrm{T}}\mathsf{P}_H\frac{d\boldsymbol{u}}{dt} &= \overline{\mathbf{1}}^{\mathrm{T}}\overline{\mathsf{P}}_{\mathsf{H}}\frac{d\overline{\boldsymbol{\eta}}}{dt}.
\end{aligned}$$

Next, consider term 3, here we break apart the new entropy function into its components, i.e., $\overline{\boldsymbol{w}}^{\mathrm{T}} = \eta' - \eta'(\boldsymbol{u}_0) = \boldsymbol{w}^{\mathrm{T}} - \boldsymbol{w}_0^{\mathrm{T}}$. Therefore, term 3 can be written as

$$h\overline{\boldsymbol{w}}^{\mathrm{T}}(\mathsf{Diss}\circ\mathsf{M})\boldsymbol{v} = h\boldsymbol{w}^{\mathrm{T}}(\mathsf{Diss}\circ\mathsf{M})\boldsymbol{v} - h\boldsymbol{w}_0^{\mathrm{T}}(\mathsf{Diss}\circ\mathsf{M})\boldsymbol{v},$$

where the first term on the right hand side of the above equation has been proven to be less than or equal to zero in theorem (5.1.3). Thus,

$$\begin{aligned}
h\overline{\boldsymbol{w}}^{\mathrm{T}}(\mathsf{Diss}\circ\mathsf{M})\boldsymbol{v} &\leq -h\boldsymbol{w}_0^{\mathrm{T}}(\mathsf{Diss}\circ\mathsf{M})\boldsymbol{v},\\
&= -h\sum_{j=1}^{N-1}((\boldsymbol{w}_0)_{j+1} - (\boldsymbol{w}_0)_j)^{\mathrm{T}}\mathsf{M}_{j,(j+1)}(\boldsymbol{v}_{j+1} - \boldsymbol{v}_j).
\end{aligned}$$

Since $\boldsymbol{w}_0$ is a constant, $(\boldsymbol{w}_0)_{j+1} - (\boldsymbol{w}_0)_j = 0$, thus, term 3 is bounded as follows

$$h\overline{\boldsymbol{w}}^{\mathrm{T}}(\mathsf{Diss}\circ\mathsf{M})\boldsymbol{v} \leq 0.$$

A similar process can be carried out for term 4 and when summed over all elements one finds that

$$\sum_{i=1}^{n} \overline{\boldsymbol{w}}_i^{\mathrm{T}} \mathsf{P}_H \boldsymbol{u}_i^{EID} \leq 0.$$

With these changes, we can re-write (5.23) as

$$\begin{aligned}
\overline{\mathbf{1}}^{\mathrm{T}} \overline{\mathsf{P}}_{\mathsf{H}} \frac{d\overline{\boldsymbol{\eta}}}{dt} + 2\overline{\boldsymbol{w}}^{\mathrm{T}} \mathsf{Q} \circ \mathsf{F}(\boldsymbol{u}, \boldsymbol{u}) \mathbf{1} &\leq \overline{\boldsymbol{w}}^{\mathrm{T}} \mathsf{P}_H \boldsymbol{SATs}, \\
\overline{\mathbf{1}}^{\mathrm{T}} \overline{\mathsf{P}}_{\mathsf{H}} \frac{d\overline{\boldsymbol{\eta}}}{dt} + 2(\cancel{\boldsymbol{w}^{\mathrm{T}}} - \boldsymbol{w}_0)^{\mathrm{T}} \mathsf{Q} \circ \mathsf{F}(\boldsymbol{u}, \boldsymbol{u}) \mathbf{1} &\leq (\cancel{\boldsymbol{w}^{\mathrm{T}}} - \boldsymbol{w}_0)^{\mathrm{T}} \mathsf{P}_H \boldsymbol{SATs}, \\
\underbrace{\overline{\mathbf{1}}^{\mathrm{T}} \overline{\mathsf{P}}_{\mathsf{H}} \frac{d\overline{\boldsymbol{\eta}}}{dt}}_{1} - \underbrace{2\boldsymbol{w}_0^{\mathrm{T}} \mathsf{Q} \circ \mathsf{F}(\boldsymbol{u}, \boldsymbol{u}) \mathbf{1}}_{2} &\leq - \underbrace{\boldsymbol{w}_0^{\mathrm{T}} \mathsf{P}_H \boldsymbol{SATs}}_{5},
\end{aligned}$$

where the $\boldsymbol{w}^{\mathrm{T}}$ terms cancel in terms 2 and 5 as is shown in the proof of theorem (4.2.3). Next, consider the remainder of term 2. Here, we will write $\mathsf{F}(\boldsymbol{u}, \boldsymbol{u}) = \mathsf{F}$ for ease of notation.

$$\begin{aligned}
2\boldsymbol{w}_0^{\mathrm{T}} \mathsf{Q} \circ \mathsf{F} \mathbf{1} &= \boldsymbol{w}_0^{\mathrm{T}} \mathsf{Q} \circ \mathsf{F} \mathbf{1} + \boldsymbol{w}_0^{\mathrm{T}} \mathsf{Q} \circ \mathsf{F} \mathbf{1}, \\
&= \boldsymbol{w}_0^{\mathrm{T}} \mathsf{Q} \circ \mathsf{F} \mathbf{1} + \mathbf{1}^{\mathrm{T}} \mathsf{F}^{\mathrm{T}} \circ \mathsf{Q}^{\mathrm{T}} \boldsymbol{w}_0.
\end{aligned}$$

Now, we use the SBP property $\mathsf{Q}^{\mathrm{T}} = \mathsf{E} - \mathsf{Q}$ to find that

$$2\boldsymbol{w}_0^{\mathrm{T}} \mathsf{Q} \circ \mathsf{F} \mathbf{1} = \boldsymbol{w}_0^{\mathrm{T}} \mathsf{Q} \circ \mathsf{F} \mathbf{1} + \mathbf{1}^{\mathrm{T}} \mathsf{F}^{\mathrm{T}} \circ (\mathsf{E} - \mathsf{Q}) \boldsymbol{w}_0,$$

where, by considering the entropy-conservative flux in fluctuation form, (4.4), coupled with the consistency property, (4.5), we obtain $\mathbf{1}^{\mathrm{T}} \mathsf{F}^{\mathrm{T}} \circ \mathsf{E} \boldsymbol{w}_0 = 0$. This results in

$$\begin{aligned}
2\boldsymbol{w}_0^{\mathrm{T}} \mathsf{Q} \circ \mathsf{F} \mathbf{1} &= \boldsymbol{w}_0^{\mathrm{T}} \mathsf{Q} \circ \mathsf{F} \mathbf{1} - \mathbf{1}^{\mathrm{T}} \mathsf{F}^{\mathrm{T}} \circ \mathsf{Q} \boldsymbol{w}_0, \\
&= \boldsymbol{w}_0^{\mathrm{T}} \mathsf{Q} \circ \mathsf{F} \mathbf{1} - \mathbf{1}^{\mathrm{T}} \mathsf{Q} \circ \mathsf{F}^{\mathrm{T}} \boldsymbol{w}_0,
\end{aligned}$$

where the last equality holds using the symmetry of the Hadamard product. Next, we expand the right hand side in summation notation to obtain

$$2\boldsymbol{w}_0^{\mathrm{T}} \mathsf{Q} \circ \mathsf{F} \mathbf{1} = \sum_{i=1}^{N} \left[\boldsymbol{w}_0^{\mathrm{T}} \sum_{j=1}^{N} \mathsf{Q}_{ij} \mathsf{F}_{ij} - \sum_{j=1}^{N} \mathsf{Q}_{ij} \mathsf{F}_{ij}^{\mathrm{T}} \boldsymbol{w}_0 \right].$$

Since $\mathsf{F}_{ij}^{\mathrm{T}}\boldsymbol{w}_0$ is a scalar value, we can take its transpose to find that

$$\begin{aligned}
2\boldsymbol{w}_0^{\mathrm{T}}\mathsf{Q}\circ\mathsf{F}\mathbf{1} &= \sum_{i=1}^{N}\left[\boldsymbol{w}_0^{\mathrm{T}}\sum_{j=1}^{N}\mathsf{Q}_{ij}\mathsf{F}_{ij} - \sum_{j=1}^{N}\mathsf{Q}_{ij}\boldsymbol{w}_0^{\mathrm{T}}\mathsf{F}_{ij}\right], \\
&= \boldsymbol{w}_0^{\mathrm{T}}\sum_{i=1}^{N}\left[\sum_{j=1}^{N}\mathsf{Q}_{ij}\mathsf{F}_{ij} - \sum_{j=1}^{N}\mathsf{Q}_{ij}\mathsf{F}_{ij}\right], \\
2\boldsymbol{w}_0^{\mathrm{T}}\mathsf{Q}\circ\mathsf{F}\mathbf{1} &= 0.
\end{aligned}$$

The same procedure can be taken to study term 5 to obtain

$$\boldsymbol{w}_0^{\mathrm{T}}\mathsf{P}_H\boldsymbol{S}\boldsymbol{A}\boldsymbol{T}\boldsymbol{s} = 0,$$

thus, combining these results, and summing over all elements we find that

$$\sum_{i=1}^{n}\overline{\boldsymbol{w}}_i^{\mathrm{T}}\mathsf{P}_H\frac{d\boldsymbol{u}_i}{dt} = \sum_{i=1}^{n}\overline{\mathbf{1}}^{\mathrm{T}}\overline{\mathsf{P}}_H\frac{d\overline{\boldsymbol{\eta}}_i}{dt} \leq 0. \tag{5.24}$$

We drop the element indices and consider a single element for the rest of the analysis, however, this can be easily extended to multiple elements. Now, we modify the definition of the new entropy from (2.14) to reflect that we are at the discrete level, that is

$$\overline{\eta}_j = \eta_j - \eta(\boldsymbol{u}_0) - \eta'(\boldsymbol{u}_0)^{\mathrm{T}}(\boldsymbol{u}_j - \boldsymbol{u}_0) = \frac{1}{2}(\boldsymbol{u}_j - \boldsymbol{u}_0)^{\mathrm{T}}\eta''(\boldsymbol{u}_j(\theta))(\boldsymbol{u}_j - \boldsymbol{u}_0), \tag{5.25}$$

where the index j, denotes the node label, thus, $j = 1, 2, \ldots, N$. Furthermore, the analysis performed in chapter 2.2 holds in the discrete case, thus, $\eta''(\boldsymbol{u}_j(\theta))$ has real and positive eigenvalues. Now, integrate (5.24) in time from $t = 0$ to $t = T$ to find that

$$\begin{aligned}
\overline{\mathbf{1}}^{\mathrm{T}}\overline{\mathsf{P}}_H\overline{\boldsymbol{\eta}}(T) &\leq \overline{\mathbf{1}}^{\mathrm{T}}\overline{\mathsf{P}}_H\overline{\boldsymbol{\eta}}(0), \\
\sum_{j=0}^{N}(\overline{\mathsf{P}}_H)_{jj}(\overline{\eta}_j(T)) &\leq \sum_{j=0}^{N}(\overline{\mathsf{P}}_H)_{jj}(\overline{\eta}_j(0)),
\end{aligned}$$

then, substitute (5.25) into the left hand side of the above equation to obtain

$$\frac{1}{2}\sum_{j=1}^{N}(\overline{\mathsf{P}}_H)_{jj}(\boldsymbol{u}_j - \boldsymbol{u}_0)^{\mathrm{T}}\eta''(\boldsymbol{u}_j(\theta(T)))(\boldsymbol{u}_j - \boldsymbol{u}_0) \leq \sum_{j=0}^{N}(\overline{\mathsf{P}}_H)_{jj}(\overline{\eta}_j(0)).$$

Therefore, we can say that $\sum_{j=1}^{N}(\overline{\mathsf{P}}_H)_{jj}(\boldsymbol{u}_j-\boldsymbol{u}_0)^{\mathrm{T}}\eta''(\boldsymbol{u}_j(\theta(T)))(\boldsymbol{u}_j-\boldsymbol{u}_0)\leq C$, and from this we can deduce

$$\sum_{j=1}^{N}(\overline{\mathsf{P}}_H)_{jj}(\boldsymbol{u}_j-\boldsymbol{u}_0)^{\mathrm{T}}\eta''_{min}(\boldsymbol{u}_j-\boldsymbol{u}_0)=\eta''_{min}\sum_{j=1}^{N}(\overline{\mathsf{P}}_H)_{jj}(\boldsymbol{u}_j-\boldsymbol{u}_0)^{\mathrm{T}}(\boldsymbol{u}_j-\boldsymbol{u}_0)\leq C. \tag{5.26}$$

Using the same algebraic manipulations as in (2.16) we find that

$$\sum_{j=1}^{N}\boldsymbol{u}_j^{\mathrm{T}}(\overline{\mathsf{P}}_H)_{jj}\boldsymbol{u}_j\leq 2\sum_{j=1}^{N}(\overline{\mathsf{P}}_H)_{jj}(\boldsymbol{u}_j-\boldsymbol{u}_0)^{\mathrm{T}}(\boldsymbol{u}_j-\boldsymbol{u}_0)+2\sum_{j=1}^{N}\boldsymbol{u}_0^{\mathrm{T}}(\overline{\mathsf{P}}_H)_{jj}\boldsymbol{u}_0,$$

then, using (5.26), we obtain

$$\begin{aligned}\boldsymbol{u}^{\mathrm{T}}\mathsf{P}\boldsymbol{u}&\leq 2\frac{C}{\eta''_{min}}+2\boldsymbol{u}_0^{\mathrm{T}}\mathsf{P}\boldsymbol{u}_0,\\ \|\boldsymbol{u}\|_P^2&\leq 2\frac{C}{\eta''_{min}}+\|\boldsymbol{u}_0\|_P^2.\end{aligned}$$

Therefore, by bounding the discrete entropy of the solution, it is possible to obtain a bound on the discrete norm of the solution itself. □
We also immediately have the following corollary for the high-order entropy-conservative scheme.

Corollary 2. The discrete L_2 norm of the entropy-conservative scheme is bounded by the data of the problem as follows

$$\|\boldsymbol{u}\|_P^2=2\frac{C}{\eta''_{min}}+\|\boldsymbol{u}_0\|_P^2,$$

with the same definitions for η''_{min}, $\boldsymbol{u}_0$, and C as in theorem (5.1.6).

Proof: If we drop the entropy-dissipative terms from (5.1), we recover the high-order entropy-conservative scheme (when replacing the special SBP derivative operator in (5.1) with a high-order SBP operator). From theorem (5.1.6), we immediately have that the high-order entropy conservative scheme (4.9) satisfies

$$\|\boldsymbol{u}\|_P^2=2\frac{C}{\eta''_{min}}+\|\boldsymbol{u}_0\|_P^2,$$

where we have an equality in the above expression because the terms in (4.9) conserve entropy at the discrete level, thus, we do not insert the inequality as done in theorem (5.1.6). □

Through the use of the novel artificial dissipation operator, (5.2), we have developed a first-order scheme that is entropy-stable and preserves the positivity of the void fractions as well as densities. We used the entropy-conservative scheme, (4.9), as a base to which element interface dissipation, as well as the artificial dissipation operator were added to dissipate entropy in the system. To complete our goal of developing a high-order entropy-stable positivity-preserving scheme to solve the isentropic Baer-Nunziato equations, we detail a mixing scheme in the next section which will mix the high-order entropy-conservative scheme, (4.9), with the first-order entropy-stable positivity-preserving scheme (5.1).

5.2 High-Order Entropy-Stable Positivity-Preserving Scheme

In the previous section, we developed a scheme that is entropy-stable and positivity-preserving, however, it is only first-order accurate. In this section, inspiration is taken from the work of Upperman [62] to develop a scheme that is entropy-stable, positivity-preserving, and high-order.

The high-order entropy-stable positivity-preserving scheme is constructed by taking a convex combination of the first-order entropy-stable positivity-preserving scheme, (5.1), and a high-order entropy-conservative positivity-violating scheme (4.9). It is important to note that the first-order scheme is also used on elements where shocks are detected, therefore, the use of the high-order entropy-conservative scheme does not limit the shock capturing capabilities of the numerical scheme. Furthermore, using the first-order entropy-stable scheme on elements that contain discontinuities ensures that entropy is dissipated across shocks as required by the second law of thermodynamics. Thus, the high-order entropy-stable positivity-preserving scheme, if it converges, will converge to a physically relevant solution. Finally, since we mix the first-order entropy-stable positivity-preserving scheme and the high-order entropy-conservative scheme on an element-by-element basis, as detailed in this chapter, we drop the element subscript for the remainder of this section.

Assume that the time derivative is approximated with a first-order explicit forward Euler scheme, so that on any element we have the following approximations to the solution

at time t^{n+1}:

$$\boldsymbol{u}_p^{n+1} = \boldsymbol{u}^n + \Delta t \left(\frac{d\boldsymbol{u}}{dt}\right)_p,$$
$$\boldsymbol{u}_1^{n+1} = \boldsymbol{u}^n + \Delta t \left(\frac{d\boldsymbol{u}}{dt}\right)_1,$$

where $\boldsymbol{u}_p^{n+1}$ is the high-order numerical solution computed using (4.9) and $\boldsymbol{u}_1^{n+1}$ is the first-order numerical solution computed using (5.1). Furthermore, the second term on the right hand side of the above equations are the right hand side of the semi-discrete schemes, (4.9) and (5.1), if the temporal term is held on the left hand side and the spatial terms are moved to the right hand side. For example, in the high-order entropy-conservative single element scheme (4.8), we find that

$$\left(\frac{d\boldsymbol{u}}{dt}\right)_p = \boldsymbol{SATs} - 2\mathsf{D} \circ \boldsymbol{F}(\boldsymbol{u}, \boldsymbol{u})\mathbf{1}.$$

The first-order scheme has been proven to be positivity-preserving in the last section, but the high-order scheme has no positivity guarantees. We will combine the first-order and high-order schemes in troubled elements where the high-order scheme violates positivity or where a shock occurs in the solution. In these troubled elements the solution will be computed as follows

$$\begin{aligned} \boldsymbol{u}^{n+1}(\theta) &= \boldsymbol{u}^n + \Delta t \left[\theta \left(\frac{d\boldsymbol{u}}{dt}\right)_p + (1-\theta)\left(\frac{d\boldsymbol{u}}{dt}\right)_1\right], \\ &= \theta \boldsymbol{u}_p^{n+1} + (1-\theta)\boldsymbol{u}_1^{n+1}, \end{aligned} \tag{5.27}$$

where $\theta \in [0, 1]$. From theorem (5.1.5) and corollary (1) we immediately find that the mixing scheme (5.27) satisfies Abgrall's criterion.

Corollary 3. The high-order entropy-stable positivity-preserving scheme, (5.27), satisfies Abgrall's criterion as defined in theorem (5.1.5), for any $\theta \in [0, 1]$.

Proof: The proof follows from the fact that the mixing scheme, (5.27), is a convex combination of the high-order entropy-conservative scheme, (4.9), and the first-order entropy-stable scheme, (5.1), which both satisfy Abgrall's criterion as proved in theorem (5.1.5) and corollary (1). □

To step in time, we first compute the high-order scheme. Then, proceed element by element and use the shock sensor of Zhao *et al.* [71] to detect discontinuities in the solution.

The shock sensor uses the smoothness indicators for a weighted essentially non-oscillatory (WENO) scheme and measures the smoothness of the numerical solution by taking the ratio of the largest to the smallest smoothness indicators:

$$\delta = \frac{\beta_{max}}{\beta_{min} + \epsilon}. \tag{5.28}$$

The smoothness indicators that are used in this thesis are [71]:

$$\begin{aligned}
\beta_0 &= \frac{1}{36}\left(-2u_{j-3} + 9u_{j-2} - 18u_{j-1} + 11u_j\right)^2 + \frac{12}{13}\left(-u_{j-3} + 4u_{j-2} - 5u_{j-1} + 2u_j\right)^2 \\
&\quad + \frac{781}{720}\left(-u_{j-3} + 3u_{j-2} - 3u_{j-1} + u_j\right)^2, \\
\beta_1 &= \frac{1}{36}\left(u_{j-2} - 6u_{j-1} + 3u_j + 2u_{j+1}\right)^2 + \frac{12}{13}\left(u_{j-1} - 2u_j + u_{j+1}\right)^2 \\
&\quad + \frac{781}{720}\left(-u_{j-2} + 3u_{j-1} - 3u_j + u_{j+1}\right)^2, \\
\beta_2 &= \frac{1}{36}\left(-2u_{j-1} - 3u_j + 6u_{j+1} - u_{j+2}\right)^2 + \frac{12}{13}\left(u_{j-1} - 2u_j + u_{j+1}\right)^2 \\
&\quad + \frac{781}{720}\left(-u_{j-1} + 3u_j - 3u_{j+1} + u_{j+2}\right)^2, \\
\beta_3 &= \frac{1}{36}\left(-11u_j + 18u_{j+1} - 9u_{j+2} + 2u_{j+3}\right)^2 + \frac{12}{13}\left(2u_j - 5u_{j+1} + 4u_{j+2} - u_{j+3}\right)^2 \\
&\quad + \frac{781}{720}\left(-u_j + 3u_{j+1} - 3u_{j+2} + u_{j+3}\right)^2,
\end{aligned}$$

where u_j is the numerical solution for one of the five equations on the j^{th} node. We have dropped the element notation since the smoothness is determined on an element by element basis.

The ratio in (5.28) becomes large when at least one of the WENO sub-stencils contains a discontinuity. Note, ϵ is picked to be a small positive quantity to avoid division by zero, and here, we take $\epsilon = 10^{-6}$. Furthermore, the smoothness of each of the five equations in the isentropic Baer-Nunziato model are tested independently from each other. If a shock is found in any equation, then only the first-order scheme is run on that element, i.e., set $\theta = 0$ in (5.27) to find $\boldsymbol{u}^{n+1}(0) = \boldsymbol{u}_1^{n+1}$.

For elements where shocks are not present, we check whether or not the high-order scheme violates positivity. In the case of α_1, we also check if α_1 is greater than one, to ensure boundedness as required by the saturation condition (2.4). If the high-order scheme violates positivity or boundedness, then we mix the first-order scheme with the

high-order scheme to ensure positivity-preservation. To mix the schemes we first define local lower/upper limits per node for $u_i^{(a)}$, $a = \{1, 2, 4\}$ at the next time level, $n+1$. The lower limits are defined as

$$\epsilon_i^a = ((u_1)_i^{(a)})^{n+1} \, h^p,$$

and the upper limit for the first equation to ensure positivity of α_2 is defined as

$$\varepsilon_i^1 = \left[((u_1)_i^{(1)})^{n+1} \, h^p\right] + (1 - h^p).$$

This set up allows the high-order entropy-stable positivity-preserving scheme to get closer to zero (or one) than the first-order scheme, but, never cross zero (or one). Then, we can determine how much the scheme needs to be mixed in order to maintain the upper and lower limits ϵ_i^a and ε_i^1 through θ. We now consider quantities that are obtained at the time level $n+1$, thus, we drop the superscript "$n+1$". For every solution point, i, on an element where positivity has been violated, define the set

$$H_i^a = \{\theta_i \in [0, 1] | u_i^{(a)}(\theta_i) \geq \epsilon_i^a\}.$$

Recall from (5.27), that if θ_i is zero, only the first-order scheme is used to step in time. Similarly, if θ_i is taken to be one, then only the high-order scheme is used. The set H_i^a can be written as $H_i^a = [0, \theta_{i,max}]$, where, $\theta_{i,max} \in (0, 1]$ and if $0 \leq \theta_i < \theta_{i,max}$, then $u_i^{(a)}(\theta_i) > \epsilon_i^a$. Furthermore, by definition of $\theta_{i,max}$ we have $u_i^{(a)}(\theta_{i,max}) = \epsilon_i^a$. These relations follow immediately from the fact that $u_i^{(a)}(\theta)$, calculated using (5.27), is a linear combination of the first-order and high-order schemes. Similarly, define a set to ensure that the boundedness of α_1 is maintained

$$B^1 = \{\theta_i \in [0, 1] | u_i^{(1)}(\theta) \leq \varepsilon_i^1\}.$$

Again, if θ_i is taken to be zero we have that $(u_1)_i^{(1)} < \varepsilon_i^1$ by definition of ε_i^1, thus, there exits some $\theta_i = \theta_{i,max} > 0$ such that $u_i^{(1)}(\theta_{i,max}) = \varepsilon_i^1$. Therefore, to find the proper mixing coefficient, θ, for an element where the high-order scheme has violated positivity, first, go node by node in the troubled element and find $\theta_{i,max}$ on each node positivity was violated on, for equations 1, 2, and 4. Then, take the smallest value of $\theta_{i,max}$ and set it equal to θ_{max}. Finally, we set $\theta = 0.9 \times \theta_{max}$ so that $u_i^{(a)}(\theta) > \epsilon_i^a$ and $u_i^{(1)}(\theta) < \varepsilon_i^1$ for all $i = 1, 2, \ldots, N$. To maintain positivity in equations 1, 2, and 4, $\theta_{i,max}$ is calculated as

$$\begin{aligned}
(u_i^{(a)})^{n+1}(\theta_{i,max}) &= \theta_{i,max}((u_p)_i^{(a)})^{n+1} + (1 - \theta_{i,max})((u_1)_i^{(a)})^{n+1}, \\
\epsilon_i^a &= \theta_{i,max}((u_p)_i^{(a)})^{n+1} + (1 - \theta_{i,max})((u_1)_i^{(a)})^{n+1}, \\
\theta_{i,max} &= \frac{\epsilon_i^a - ((u_1)_i^{(a)})^{n+1}}{((u_p)_i^{(a)})^{n+1} - ((u_1)_i^{(a)})^{n+1}}.
\end{aligned} \tag{5.29}$$

Then, to maintain boundedness in equation 1, $\theta_{i,max}$ is calculated as

$$\begin{aligned}(u_i^{(a)}))^{n+1}(\theta_{i,max})} &= \theta_{i,max}((u_p)_i^{(a)})^{n+1} + (1-\theta_{i,max})((u_1)_i^{(a)})^{n+1},\\ \varepsilon_i^1 &= \theta_{i,max}((u_p)_i^{(a)})^{n+1} + (1-\theta_{i,max})((u_1)_i^{(a)})^{n+1},\\ \theta_{i,max} &= \frac{\varepsilon_i^1 - ((u_1)_i^{(a)})^{n+1}}{((u_p)_i^{(a)})^{n+1} - ((u_1)_i^{(a)})^{n+1}}.\end{aligned} \tag{5.30}$$

Once we find θ in a given element we update the numerical scheme according to (5.27). The advantage of this approach is that the first-order scheme is only used on troubled elements where there is either a discontinuity, or positivity is violated by the high-order scheme. This means that the scheme can capture shocks as well as maintain positivity of the densities and void fractions. In the case of smooth solutions, this further allows the overall scheme to maintain high-order accuracy which we will prove in the following theorem.

Theorem 5.2.1. The high-order positivity-preserving scheme, (5.27), achieves high-order accuracy through the use of high-order SBP operators, $\|\boldsymbol{u}_i^{n+1}(\theta) - \boldsymbol{u}_i^{ex}(t^{n+1})\| = \mathcal{O}(h^p)$, where $\boldsymbol{u}_i^{ex}(t^{n+1})$ denotes the exact solution at the i^{th} solution point at time $t = t^{n+1}$, and $\boldsymbol{u}_i^{n+1}(\theta)$ denotes the numerical solution computed using (5.27).

Proof: Here, we follow the steps taken by Upperman [62] closely and change notation to adapt to our schemes. In this proof $\|.\|$ denotes the Euclidean norm. We now assume that the solution is sufficiently smooth such that

$$\|(\boldsymbol{u}_1)_i^{n+1} - (\boldsymbol{u}_p)_i^{n+1}\| \leq \|(\boldsymbol{u}_1)_i^{n+1} - \boldsymbol{u}_i^{ex}(t^{n+1})\| + \|\boldsymbol{u}_i^{ex}(t^{n+1}) - (\boldsymbol{u}_p)_i^{n+1}\| = \mathcal{O}(h).$$

We wish to show that $\|\boldsymbol{u}_i^{n+1}(\theta) - \boldsymbol{u}_i^{ex}(t^{n+1})\| = \mathcal{O}(h^p)$ for all solution points, where $\boldsymbol{u}_i^{n+1}(\theta)$ is the numerical solution computed by (5.27). If $\theta = 1$, then $\boldsymbol{u}_i^{n+1}(1) = (\boldsymbol{u}_p)_i^{n+1}$ and the result follows immediately since $\boldsymbol{u}_p$ is the high-order accurate solution. All that remains to be shown is that $\|\boldsymbol{u}_i^{n+1}(\theta) - \boldsymbol{u}_i^{ex}(t^{n+1})\| = \mathcal{O}(h^p)$ for $\theta < 1$. In this case, it is sufficient to show that $1 - \theta = \mathcal{O}(h^{p-1})$ to prove the error properties of the mixing scheme. If $1 - \theta = \mathcal{O}(h^{p-1})$, then, for every solution point we have

$$\begin{aligned}\|\boldsymbol{u}_i^{n+1}(\theta) - \boldsymbol{u}_i^{ex}(t^{n+1})\| &\leq (1-\theta)\|(\boldsymbol{u}_1)_i^{n+1} - \boldsymbol{u}_i^{ex}(t^{n+1})\| + \theta\|(\boldsymbol{u}_p)_i^{n+1} - \boldsymbol{u}_i^{ex}(t^{n+1})\|,\\ &= (1-\theta)\mathcal{O}(h) + \theta\mathcal{O}(h^p),\\ &= \mathcal{O}(h^p).\end{aligned}$$

To show that $1 - \theta = 1 - \min(\theta_{i,max}) = \mathcal{O}(h^{p-1})$, we will show that $1 - \theta_{i,max} = \mathcal{O}(h^{p-1})$. We will break the discussion up into two cases: 1) computing $\theta_{i,max}$ to maintain positivity

in equations 1, 2, and 4 and 2) computing $\theta_{i,max}$ to maintain boundedness in equation 1. We begin with case 1. Since $\theta_{i,max} < 1$, the following inequality holds for equations 1, 2, and 4

$$(\boldsymbol{u}_p^{(a)})_i^{n+1} < \epsilon_i^{(a)} \leq (\boldsymbol{u}^{(a)})_i^{ex}(t^{n+1}), \quad a = \{1, 2, 4\}, \tag{5.31}$$

which leads to $(\boldsymbol{u}_p^{(a)})_i^{n+1} = \epsilon_i^{(a)} + \mathcal{O}(h^p)$. We have that $\theta_{i,max}$ satisfies

$$\begin{aligned}(\boldsymbol{u}^{(a)})_i^{n+1}(\theta_{i,max}) = \epsilon_i^{(a)} &= (1 - \theta_{i,max})(\boldsymbol{u}_1^{(a)})_i^{n+1} + \theta_{i,max}(\boldsymbol{u}_p^{(a)})_i^{n+1}, \\ \epsilon_i^{(a)} &= (\boldsymbol{u}_1^{(a)})_i^{n+1} + \theta_{i,max}[(\boldsymbol{u}_p^{(a)})_i^{n+1} - (\boldsymbol{u}_1^{(a)})_i^{n+1}].\end{aligned}$$

Thus,

$$1 - \theta_{i,max} = \frac{\epsilon_i^{(a)} - (\boldsymbol{u}_p^{(a)})_i^{n+1}}{(\boldsymbol{u}_1^{(a)})_i^{n+1} - (\boldsymbol{u}_p^{(a)})_i^{n+1}} = \frac{\mathcal{O}(h^p)}{\mathcal{O}(h)} = \mathcal{O}(h^{p-1}).$$

Case 2, has the exact same analysis as case 1, expect substitute $\epsilon_i^{(a)}$ with ε_i^1, so we omit the analysis here. Therefore, $1 - \theta_{i,max} = \mathcal{O}(h^{p-1})$ and it follows that $1 - \theta = \mathcal{O}(h^{p-1})$. Thus,

$$\begin{aligned}\|\boldsymbol{u}_i^{n+1}(\theta) - \boldsymbol{u}_i^{ex}(t^{n+1})\| &\leq (1 - \theta)\|(\boldsymbol{u}_1)_i^{n+1} - \boldsymbol{u}_i^{ex}(t^{n+1})\| + \theta\|(\boldsymbol{u}_p)_i^{n+1} - \boldsymbol{u}_i^{ex}(t^{n+1})\|, \\ &= (1 - \theta)\mathcal{O}(h) + \theta\mathcal{O}(h^p), \\ &= \mathcal{O}(h^p).\end{aligned}$$

Therefore, the high-order positivity-preserving scheme, (5.27), achieves high-order accuracy through the use of high-order SBP operators. □

The high-order mixing scheme, (5.27), is constructed by taking a convex combination of the first-order entropy-stable positivity-preserving scheme, (5.1), and the high-order entropy-conservative positivity-violating scheme (4.9). We will now show that this convex combination results in an entropy-stable scheme.

Theorem 5.2.2. The high-order positivity-preserving scheme defined in (5.27) is entropy-stable, that is, when left multiplied by the entropy variables $\boldsymbol{w}_i^{\mathrm{T}}$, the SBP norm matrix P, and summed over all elements $i = 1, 2, \ldots, n$,

$$\sum_{i=1}^{n} \overline{\mathbf{1}}^{\mathrm{T}} \overline{\mathsf{P}} \frac{d\boldsymbol{\eta}_i}{dt} \leq 0,$$

where $\mathsf{P} = \overline{\mathsf{P}} \otimes \mathsf{I}_5$ and $\boldsymbol{\eta}_i = \eta(\boldsymbol{u}_i)$.

Proof: To show that the scheme (5.27) is entropy-stable, we must show that when left multiplied by $\boldsymbol{w}^{\mathrm{T}}\mathsf{P}$ the contraction is less than or equal to zero.

$$\begin{aligned}\boldsymbol{w}^{\mathrm{T}}\mathsf{P}\frac{d\boldsymbol{u}}{dt} &= \boldsymbol{w}^{\mathrm{T}}\mathsf{P}\theta\left(\frac{d\boldsymbol{u}}{dt}\right)_p + \boldsymbol{w}^{\mathrm{T}}\mathsf{P}\left(1-\theta\right)\left(\frac{d\boldsymbol{u}}{dt}\right)_1, \\ &= \theta\boldsymbol{w}^{\mathrm{T}}\mathsf{P}\left(\frac{d\boldsymbol{u}}{dt}\right)_p + \left(1-\theta\right)\boldsymbol{w}^{\mathrm{T}}\mathsf{P}\left(\frac{d\boldsymbol{u}}{dt}\right)_1.\end{aligned}$$

From theorem (4.2.3), we have that $\boldsymbol{w}^{\mathrm{T}}\mathsf{P}\left(\frac{d\boldsymbol{u}}{dt}\right)_p = \sum_{i=1}^{n}\overline{\mathbf{1}}^{\mathrm{T}}\overline{\mathsf{P}}\frac{d\boldsymbol{\eta}_i}{dt} = 0$. Furthermore, from theorem (5.1.3), we have that $\boldsymbol{w}^{\mathrm{T}}\mathsf{P}\left(\frac{d\boldsymbol{u}}{dt}\right)_1 = \sum_{i=1}^{n}\overline{\mathbf{1}}^{\mathrm{T}}\overline{\mathsf{P}}\frac{d\boldsymbol{\eta}_i}{dt} \leq 0$. Therefore, the convex combination of the high-order and first-order schemes is entropy-stable. □

Furthermore, using theorem (5.1.6) and corollary (2), we find that, since the mixing scheme, (5.27), bounds the mathematical entropy of the system, there exists a bound on the norm of the solution itself.

Corollary 4. The discrete L_2 norm of the high-order entropy-stable positivity-preserving scheme, defined in (5.27), is bounded by the data of the problem as follows

$$\|\boldsymbol{u}\|_P^2 \leq 2\frac{C}{\eta''_{min}} + \|\boldsymbol{u}_0\|_P^2,$$

where η''_{min}, $\boldsymbol{u}_0$, and C are defined in theorem (5.1.6).

Proof: The proof follows immediately from theorem (5.1.6) and corollary (2). If the first-order entropy-stable positivity-preserving scheme satisfies

$$\|\boldsymbol{u}\|_P^2 \leq 2\frac{C}{\eta''_{min}} + \|\boldsymbol{u}_0\|_P^2,$$

and the entropy-conservative scheme satisfies

$$\|\boldsymbol{u}\|_P^2 = 2\frac{C}{\eta''_{min}} + \|\boldsymbol{u}_0\|_P^2,$$

then the mixing scheme, which is a convex combination of the first-order entropy-stable positivity-preserving scheme and the entropy-conservative scheme, satisfies

$$\|\boldsymbol{u}\|_P^2 \leq 2\frac{C}{\eta''_{min}} + \|\boldsymbol{u}_0\|_P^2. \square$$

All the schemes presented in this thesis have provable stability properties for the discretization of the spatial derivatives. The time integration technique that is used, SSP-RK3, is not guaranteed to be entropy-stable. This limitation can be addressed through the use of relaxation Runge-Kutta methods [37], which can be used to enforce conservation and stability in the time integration. However, this is not performed in this thesis and is a topic of future research. In the next section, we describe the implementation details of the high-order entropy-stable positivity-preserving scheme, and include the implementation details for the SSP-RK3 scheme, which we use to integrate in time.

5.3 Algorithm and Implementation Details

In the previous two sections we have proven that the first-order scheme, as well as the high-order scheme, preserve the positivity of densities and void fractions. However, the proofs in the previous section hold only when the explicit forward Euler method is used to discretize the time derivative. To extend the method to high-order temporal discretizations, we use SSP-RK schemes developed in [53], which can be represented as a convex combination of forward Euler schemes. Specifically, in this thesis, we use the third-order SSP-RK scheme with the form from [30]. Suppose the semi-discrete scheme reads $\boldsymbol{u}_t = \boldsymbol{RHS}(\boldsymbol{u})$, then the SSP-RK3 scheme reads:

$$\begin{aligned} \boldsymbol{u}^{(1)} &= \boldsymbol{u}^n + \Delta t \boldsymbol{RHS}(\boldsymbol{u}^{(n)}), \\ \boldsymbol{u}^{(2)} &= \frac{3}{4}\boldsymbol{u}^{(n)} + \frac{1}{4}\boldsymbol{u}^{(1)} + \frac{\Delta t}{4}\boldsymbol{RHS}(\boldsymbol{u}^{(1)}), \\ \boldsymbol{u}^{(n+1)} &= \frac{1}{3}\boldsymbol{u}^{(n)} + \frac{2}{3}\boldsymbol{u}^{(2)} + \frac{2\Delta t}{3}\boldsymbol{RHS}(\boldsymbol{u}^{(2)}). \end{aligned} \tag{5.32}$$

At each Runge-Kutta stage, the high-order positivity-preserving entropy-stable scheme is computed according to the following algorithm.

Algorithm

1. Before the start of the computation, the user sets the maximum allowable time step, and in this thesis, the maximum time step was set on and order between 10^{-5} and 10^{-6} depending on the simulation. The mixing scheme, (5.27), is then run using this maximum time step and the time step will only decrease as needed from the positivity-preserving algorithm. Furthermore, we require that $\Delta t^{(n+1)} \leq 1.01\Delta t^{(n)}$, where $\Delta t^{(n)}$ is the previous time step.

2. Compute $\left(\frac{d\boldsymbol{u}}{dt}\right)_p$ using (4.9).

3. Assuming n elements and N nodes per element, compute the shock sensor, (5.28), for each node $j = 4, 5, \ldots, N-4$. Do this calculation separately for each equation to determine if a shock occurs in any of the n elements, and any of the five equations.

4. On the elements where a shock has not been detected, check to see if positivity (or boundedness in the case of α_1) has been violated on any node.

5. On the elements where a shock has been detected or the high-order scheme has violated positivity, calculate $\left(\frac{d\boldsymbol{u}}{dt}\right)_1$ according to (5.1). Furthermore, if on the first Runge-Kutta stage and the time step restriction required for positivity is more stiff than the user defined maximum time step; change the time step.

6. Go element by element and mix the schemes together according to (5.27). If on an element with a shock, then, set $\theta = 0$. If on an element where positivity has been violated, then, compute θ according to (5.29) and (5.30). Finally, if not on a troubled element, set $\theta = 1$.

7. If on the second or later Runge-Kutta stage and (5.27) does not preserve positivity, set $\Delta t^{(n+1)} = 0.5\Delta t^{(n+1)}$ and restart from the first Runge-Kutta stage.

8. If positivity is not preserved on the second or later Runge-Kutta stage for three iterations of dividing the time step, as per step 7 in the algorithm, then, proceed to run a forward Euler scheme in time. Using a forward Euler scheme is guaranteed to preserve positivity.

9. Proceed to the next Runge-Kutta stage.

The scheme guarantees the positivity of densities and void fractions on the first Runge-Kutta stage by construction. For the subsequent Runge-Kutta stages, the scheme, which can be represented as a convex combination of forward Euler steps, will maintain positivity if the time step restriction that was chosen on the first stage also satisfies the time step restriction on the current stage. When the scheme fails to maintain positivity on a later stage of the Runge-Kutta scheme, simply update the time step to be half of the current time step and iterate until the constraint for positivity is satisfied for each stage, or you have run through 3 iterations. If, after 3 iterations, the scheme still does not maintain positivity on one of the later Runge-Kutta stages, march in time using a forward Euler scheme. This will guarantee that positivity is preserved. Note, however, that for all problems presented in this thesis, this condition was never met and we never needed to use a forward Euler update

in time. This potential issue in using a SSP-RK scheme to run the positivity-preserving algorithm can be avoided by using a SSP multi-time step discretization as detailed in [70], but we do not use this time discretization in this thesis.

Chapter 6

Results

We test the proposed high-order entropy-conservative, (4.9), first-order entropy-stable positivity-preserving, (5.1), and high-order entropy-stable positivity-preserving, (5.27), schemes numerically. For all three methods, we present convergence plots on smooth problems to demonstrate the convergence rates of each scheme. For these tests, we use the method of manufactured solutions (MMS). MMS is a technique that allows the user to select what they would like the exact solution of the PDE to be. This solution is then plugged into the equations and the result is added to the right hand side of the equations as a source term. Using the MMS technique, we created sinusoidal solutions to the isentropic Baer-Nunziato equations. Using these solutions, we numerically tested the convergence of the schemes presented in chapters 4 and 5, as we can compare the numerical solution against the exact solution. We also show numerical tests of entropy-conservation as well as entropy-stability for all schemes in sections 6.1, 6.2, and 6.3. Finally, in section 6.3, we demonstrate the shock capturing capabilities of the high-order entropy-stable positivity-preserving scheme on two Riemann problems.

In this chapter, all tests are run using the SSP-RK3 scheme, (5.32), to march in time. For any tests run using degree 1, 2, or 3 SBP operators, a maximum time step of 10^{-5} has been chosen, and for any test run using degree 4 operators, a maximum time step of 10^{-6} has been chosen since SSP-RK3 is third-order accurate in time. Furthermore, to obtain convergence rates using the log-log error plot, we take the slope of the line of best fit between the final three points on plot, unless otherwise noted. Finally, for all tests considered in this thesis, we set $k = 1$, $\gamma_1 = 3$, and $\gamma_2 = 1.5$ unless stated otherwise.

6.1 Results for the High-Order Entropy-Conservative Scheme

To study the high-order entropy-conservative scheme, (4.9), we consider a smooth, periodic problem that does not approach zero. It is important that the scheme does not approach zero since (4.9) has no positivity-preserving properties. We will refer to this problem as the easy problem which has an exact solution

$$\begin{aligned} \alpha_1 &= 0.25\sin(x+t)+0.5, \\ \rho_1 &= 0.25\sin(x+2t)+0.5, \\ v_1 &= 0.25\sin(x+t)+0.5, \\ \rho_2 &= 0.25\cos(x+2t)+0.5, \\ v_2 &= 0.25\cos(x+t)+0.5, \end{aligned} \tag{6.1}$$

where, the system is initialized following the exact solution at time $t = 0$. Figures (6.1), (6.2), (6.3), and (6.4), show the convergence plots for the entropy-conservative scheme, (4.9), using degree 1, 2, 3, and 4 SBP operators, respectively. Furthermore, each scheme was marched in time until $t = 0.1s$. We see that for degree 1 and 3, in figures (6.1) and (6.3), that the numerical scheme is converging at approximately $p + \frac{1}{2}$, where p is the degree of the SBP operators. Then, for degree 2, in figure (6.2), we see that the scheme is converging slightly over $p+1$, and degree 4, in figure (6.4), is converging between $p+\frac{1}{2}$ and $p+1$. We note that there is a phenomenon occurring here where the odd degree operators are slightly under-converging and the even degree operators are converging well. Although this is a well known phenomenon for linear problems and typically is corrected with an upwind numerical flux, for entropy-stable schemes, there appears, in general, to be some under convergence even with an upwind numerical flux [34].

Figure (6.5) shows the results of left multiplying all spatial terms in (4.9), by $\boldsymbol{w}^{\mathrm{T}}\mathsf{P}$, that is, we rearrange (4.9), abstractly as

$$\frac{d\boldsymbol{u}}{dt} = \boldsymbol{RHS}(\boldsymbol{u}),$$

and plot in figure (6.5), $\boldsymbol{w}^{\mathrm{T}}\mathsf{P}\boldsymbol{RHS}$, when the right hand side is discretized using degree 4 SBP operators. From theorem (4.2.3), we have that this contraction with the entropy variables should be equal to zero. While figure (6.5) may look like this sum is varying wildly, the scale is on the order of 10^{-16}, thus, the sum is always machine zero. We only show the result for degree 4 SBP operators since all other degrees return similar plots, thus, we omit them here. Therefore, we have numerically validated theorem (4.2.3) and the high-order entropy-conservative scheme, (4.9), does in fact, conserve entropy.

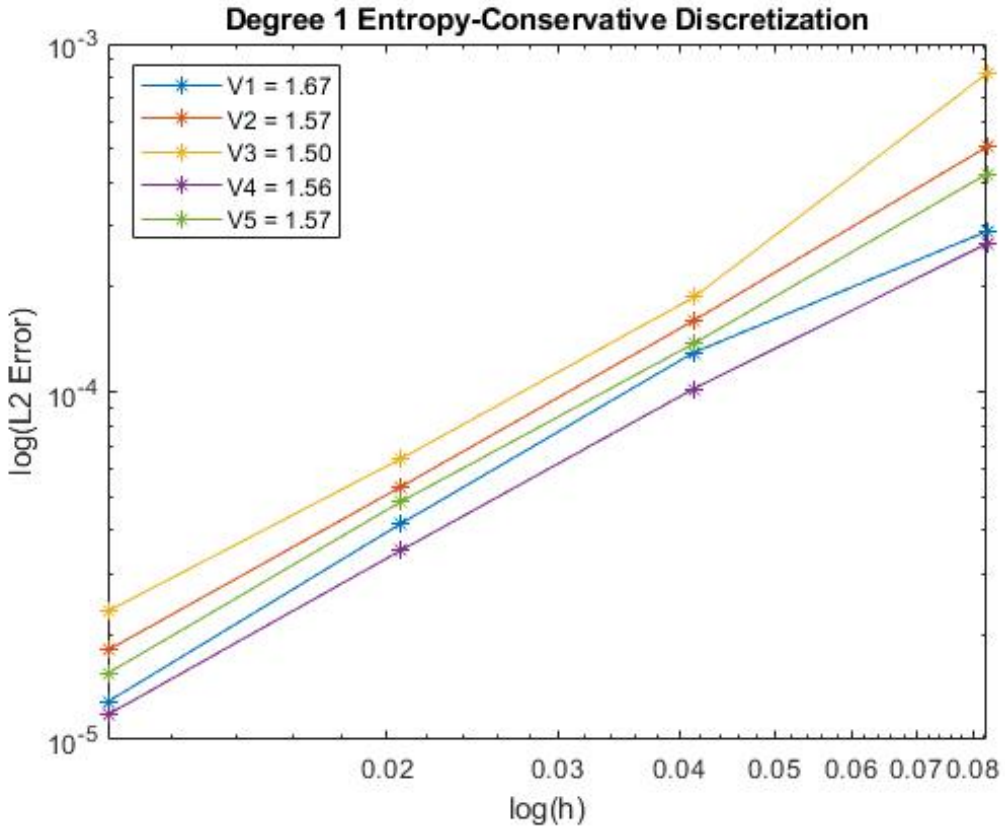

Figure 6.1: Convergence plot for the entropy-conservative discretization, (4.9), for degree 1 SBP operators using MMS solution (6.1). This is a log-log error plot of the grid spacing vs the approximate L_2 error computed using (3.16) in the numerical solution. For each grid level there were 20 nodes per element and then the number of elements was set to 4, 8, 16, and 32.

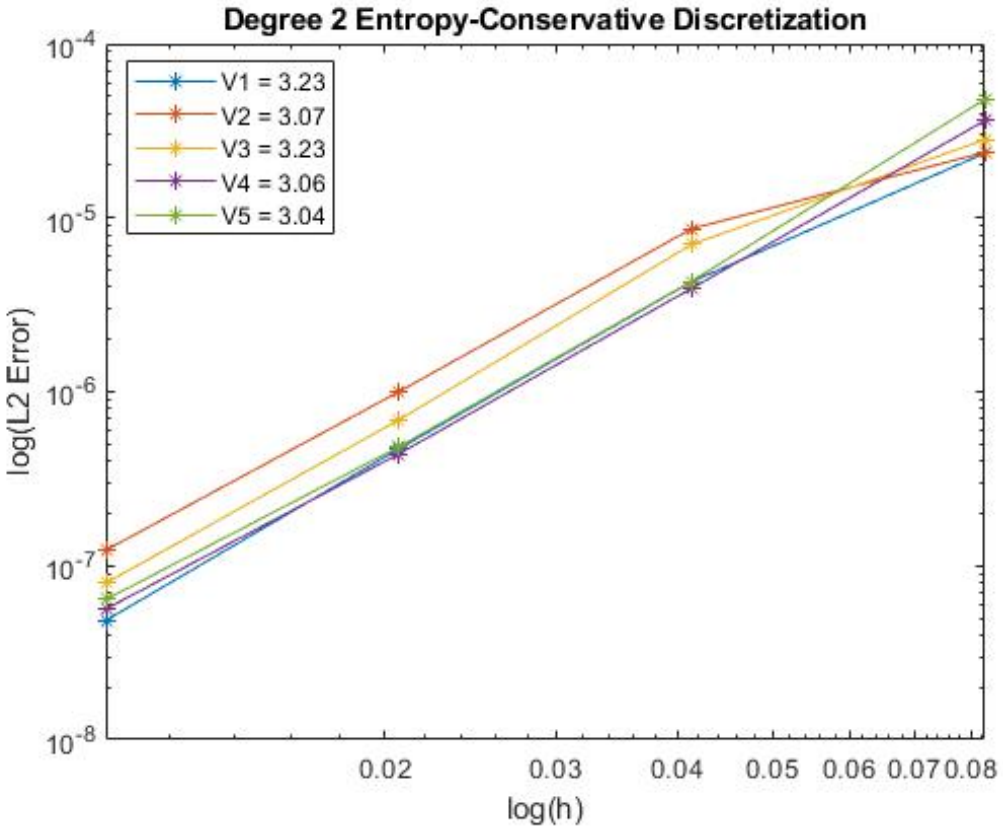

Figure 6.2: Convergence plot for the entropy-conservative discretization, (4.9), for degree 2 SBP operators using MMS solution (6.1). This is a log-log error plot of the grid spacing vs the approximate L_2 error computed using (3.16) in the numerical solution. For each grid level there were 20 nodes per element and then the number of elements was set to 4, 8, 16, and 32.

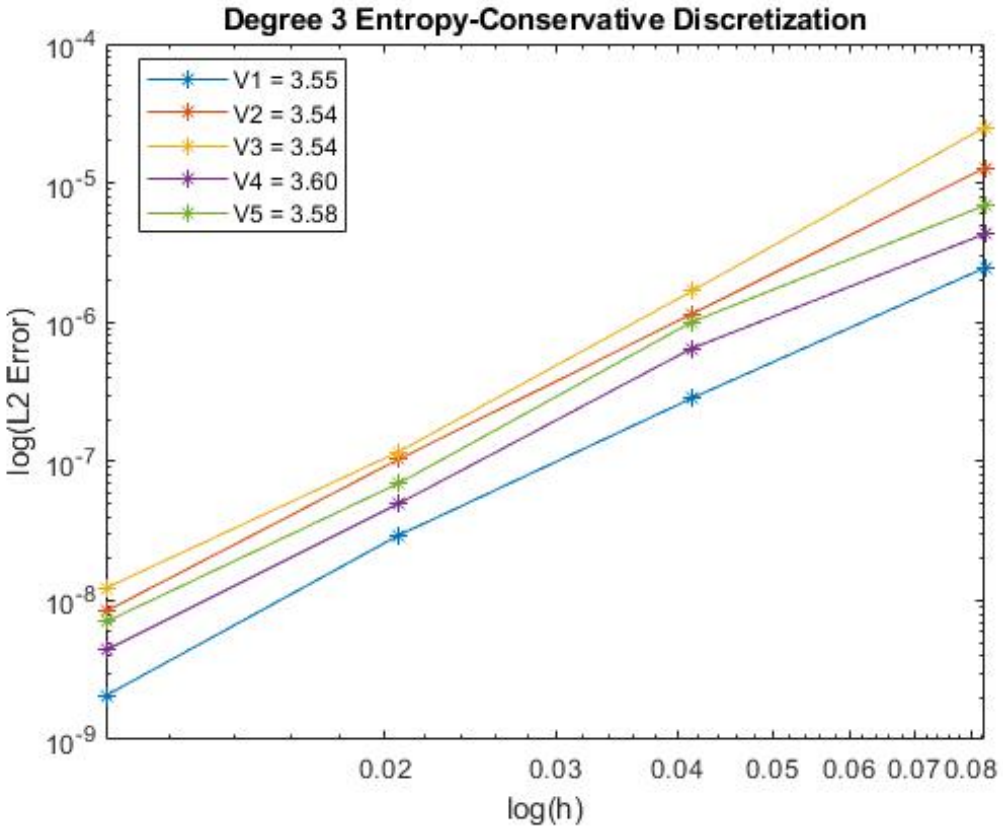

Figure 6.3: Convergence plot for the entropy-conservative discretization, (4.9), for degree 3 SBP operators using MMS solution (6.1). This is a log-log error plot of the grid spacing vs the approximate L_2 error computed using (3.16) in the numerical solution. For each grid level there were 20 nodes per element and then the number of elements was set to 4, 8, 16, and 32.

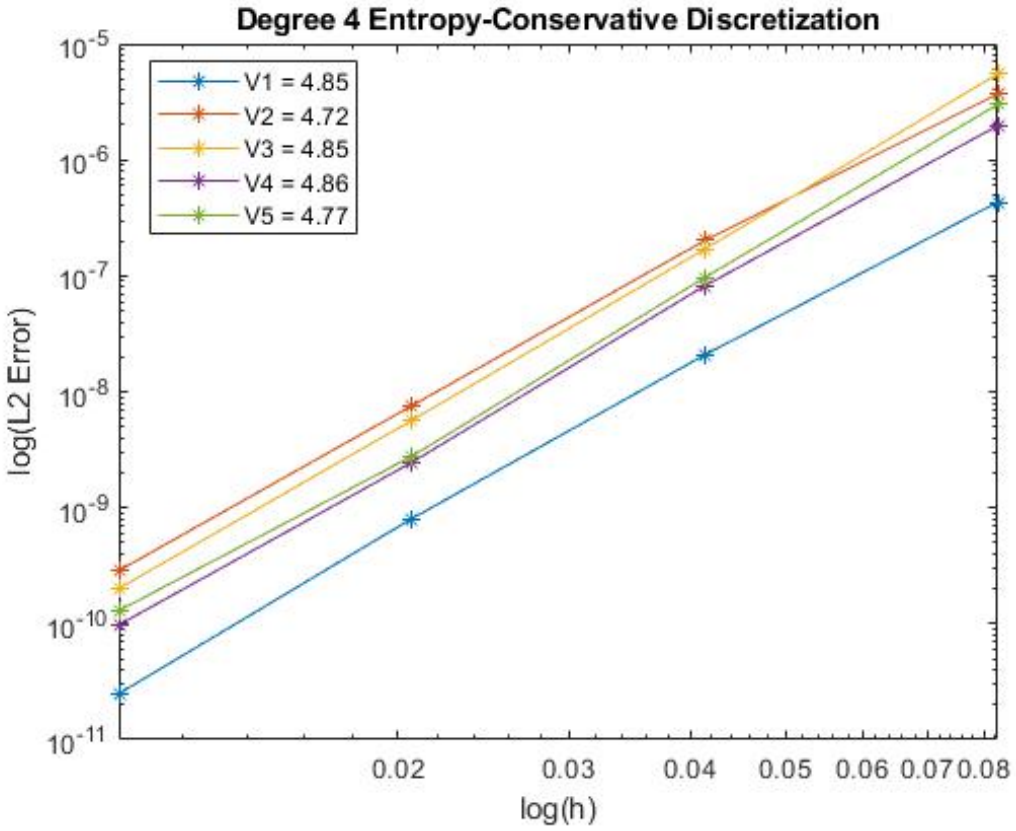

Figure 6.4: Convergence plot for the entropy-conservative discretization, (4.9), for degree 4 SBP operators using MMS solution (6.1). This is a log-log error plot of the grid spacing vs the approximate L_2 error computed using (3.16) in the numerical solution. For each grid level there were 20 nodes per element and then the number of elements was set to 4, 8, 16, and 32.

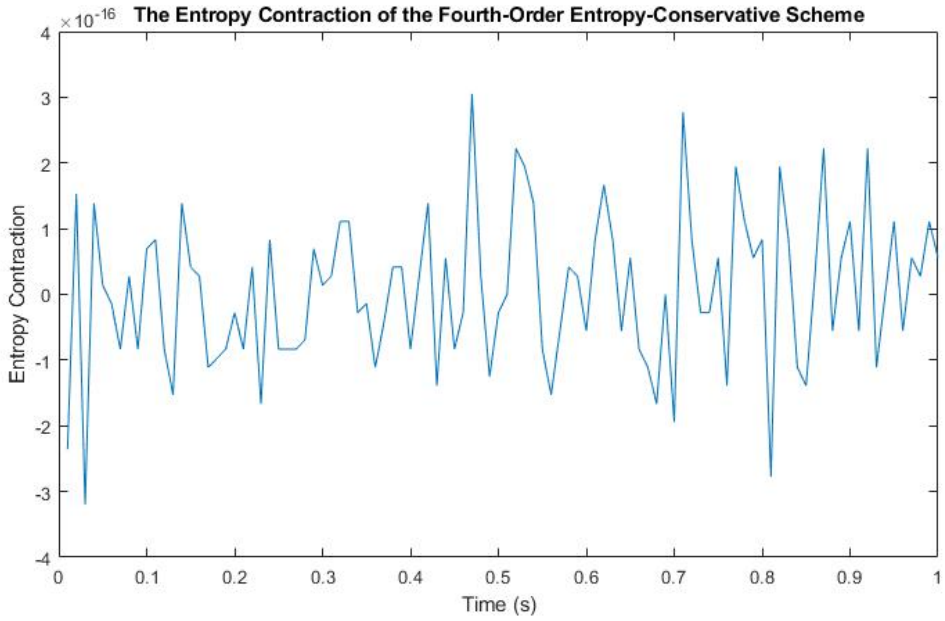

Figure 6.5: The entropy contraction is the result of left multiplying the entropy-conservative scheme, (4.9), for degree 4 SBP operators, by $\boldsymbol{w}_i^{\mathrm{T}}\mathsf{P}$ and summing over all elements $i = 1, 2, \ldots, n$. Notice that the scale on the contraction is on the order of 10^{-16}.

6.2 Results for the First-Order Entropy-Stable Positivity-Preserving Scheme

To test both the first-order and high-order entropy-stable positivity-preserving schemes, we will consider another problem that approaches zero, since now, we also want to test the positivity-preserving properties of the schemes. We will refer to this problem as the hard problem which has an exact solution

$$\begin{aligned}
\alpha_1 &= 0.4999 \sin(x + t - 0.05) + 0.5, \\
\rho_1 &= 0.25 \sin(x + 2t - 0.1) + 0.5, \\
v_1 &= 0.25 \sin(x + t - 0.05) + 0.5, \\
\rho_2 &= 0.25 \cos(x + 2t - 0.1) + 0.5, \\
v_2 &= 0.25 \cos(x + t - 0.05) + 0.5,
\end{aligned} \tag{6.2}$$

where, the system is initialized following the exact solution at time $t = 0$. At the current time of writing this thesis, simulating problems that get close to zero become ill-conditioned as we march in time due to the need to convert from conserved variables to primitive variables. For example, when computing the velocity of the second phase, we compute this as

$$v_2 = \frac{u_5}{u_4} = \frac{\alpha_2 \rho_2 v_2}{\alpha_2 \rho_2},$$

where u_4 is the fourth conserved variable and u_5 is the fifth conserved variable. This becomes ill-conditioned for two reasons, the first being that dividing two small numbers can lead to rounding error in the computation. The second reason is that, as the error builds in the numerical scheme, this can lead to a disproportionately large error in the computation of the primitive variables. Take our example of computing the velocity of the second phase again, but, this time consider the the error in computing v_2. We assume that the numerical solution $(u_4)_{num} = (u_4)_{exact} + \text{Error}_1$, and likewise $(u_5)_{num} = (u_5)_{exact} + \text{Error}_2$. Therefore, to compute v_2 we have that

$$v_2 = \frac{(u_5)_{num}}{(u_4)_{num}} = \frac{(u_5)_{exact} + \text{Error}_2}{(u_4)_{exact} + \text{Error}_1},$$

where it is clear that as the error in the fourth and fifth conserved variables grow to be about the order of magnitude of the exact solution, there will be large error in computing the value of v_2. This error causes instabilities to grow in the numerical solution and prevents us from marching indefinitely in time as, even though the error in the conserved variables may be small, the error when converting to primitive variables is large. For this reason, the

first-order entropy-stable positivity-preserving scheme, (5.1), as well as the mixing scheme, (5.27), discretized using degree 2 and 3 SBP operators, shown in figures (6.6), (6.10), and (6.11) were marched until $t = 0.055s$, as this time was able to be reached for all mesh levels. However, since degree 4 operators result in a discretization that is significantly more accurate than degree 1, 2, and 3 operators, the mixing scheme, (5.27), discretized using degree 4 SBP operators, was marched until t=0.5s. We believe that the velocity limiters of Upperman and Yamaleev [63], which were implemented for the Navier-Stokes equations, can rectify this problem. This will be discussed in the future work section of chapter 7. Here, we also emphasize that our stability proofs are at the semi-discrete level, and we have no guarantees on stability once we discretize in time using SSP-RK3. However, this has a known solution, namely one can use relaxation Runge-Kutta methods [37, 49] to extend the semi-discrete stability properties to the fully discrete case and this is an area of future research.

Figure (6.6) shows the convergence test of the first-order entropy-stable positivity-preserving scheme, (5.1), run on the hard problem. Note that, when the first-order entropy conservative scheme was used to try and run the hard problem, the scheme crashed between 6×10^{-3}s and 9×10^{-2}s, depending on the mesh level, due to positivity being violated. Thus, (5.1) is ensuring that positivity of the void fractions and densities are maintained whereas the entropy-conservative scheme, (4.9), does not. From figure (6.6), we see that the first-order entropy-stable positivity-preserving scheme is converging at first-order as stated in section 5.1. Then, we also test the entropy-dissipative properties of the artificial dissipation operator, (5.2), and the element interface dissipation, (5.7), as proved in theorem (5.1.3). Figure (6.7) shows the result obtained when left multiplying the artificial dissipation operator and element interface dissipation by $\boldsymbol{w}_i^{\mathrm{T}}\mathsf{P}$ and summing over all elements $i = 1, 2, \ldots, n$. As shown in theorem (5.1.3), these contractions with the entropy variables should be less than or equal to zero for finite time, and as seen in figure (6.7), this contraction is numerically less than or equal to zero between $t = 0$ and $t = 1s$. Thus, we have validated numerically that the artificial dissipation operator, (5.2), and the element interface dissipation, (5.7), are entropy-dissipative terms. Note that this test was run on the easy problem so that we could march in time until $1s$.

Similarly, we have shown that the remainder of theorem (5.1.3) holds numerically. That is, the first-order entropy-stable positivity-preserving scheme is entropy-stable. As done before to prove entropy-conservation of the entropy-conservative scheme, (4.9), we move all of the spatial terms to the right hand side of (5.1), such that only the time derivative term remains on the left hand side. Then, left multiply the right hand side by $\boldsymbol{w}_i^{\mathrm{T}}\mathsf{P}$ and sum over all elements $i = 1, 2, \ldots, n$. For this test, we ran (5.1) on the easy problem so that we could step all the way to one second and the result is seen in figure (6.8). From

the figure we have that the contraction with the entropy variables is less than zero for all time between $t = 0$ and $t = 1s$. Thus, we have numerically validated that the first-order entropy-stable positivity-preserving scheme, (5.1), is in fact entropy-stable.

The last property we wish to show for the first-order entropy-stable positivity-preserving scheme, (5.1), is that the artificial dissipation operator, (5.2), converges to zero at first-order. Figure (6.9), shows the convergence plot of the maximum absolute value in the artificial dissipation operator when given the initial condition of the hard problem. After a single instance of calling the operator, the maximum absolute value is found. Theorem (5.1.1) proves that the artificial dissipation operator vanishes for a constant solution, thus, for smooth problems, as the grid is refined, the artificial dissipation operator should converge to zero. In chapter 5, we argue that the artificial dissipation operator should converge to zero at first-order. Figure (6.9) numerically demonstrates that the artificial dissipation operator converges to zero at first-order.

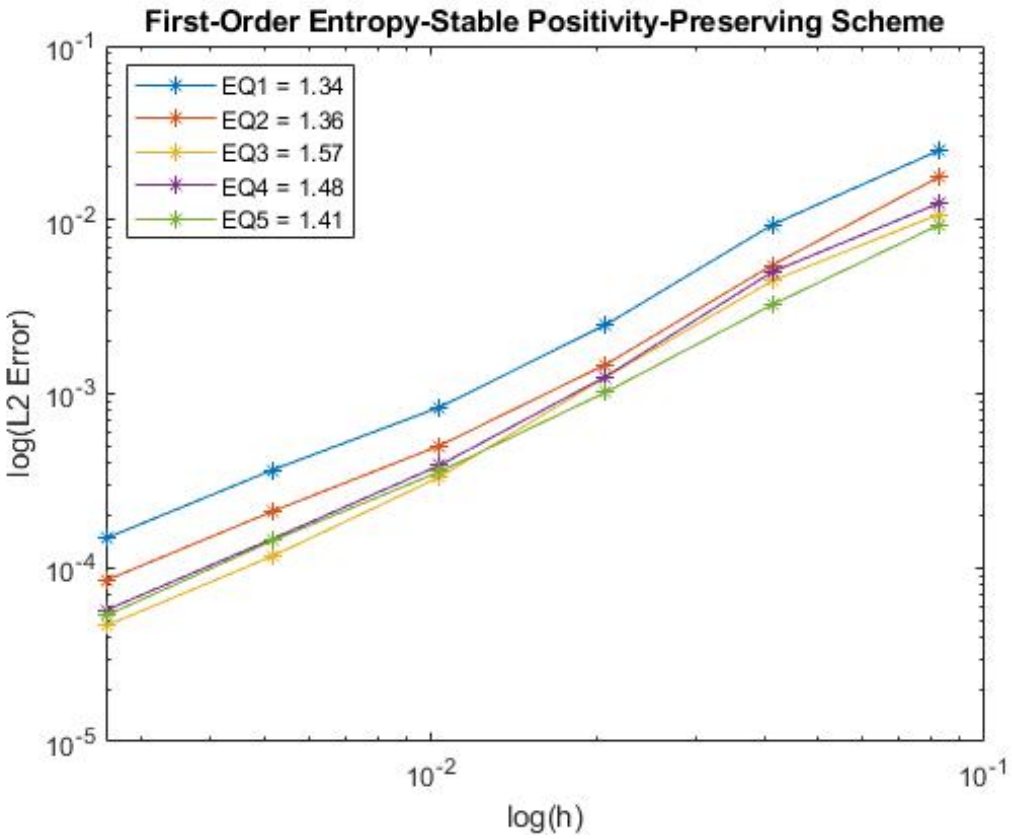

Figure 6.6: Convergence plot for the first-order entropy-stable positivity-preserving scheme, (5.1). This is a log-log error plot of the grid spacing vs the approximate L_2 error computed using (3.16) in the numerical solution. For each grid level there were 20 nodes per element and then the number of elements was set to 4, 8, 16, 32, 64, and 128.

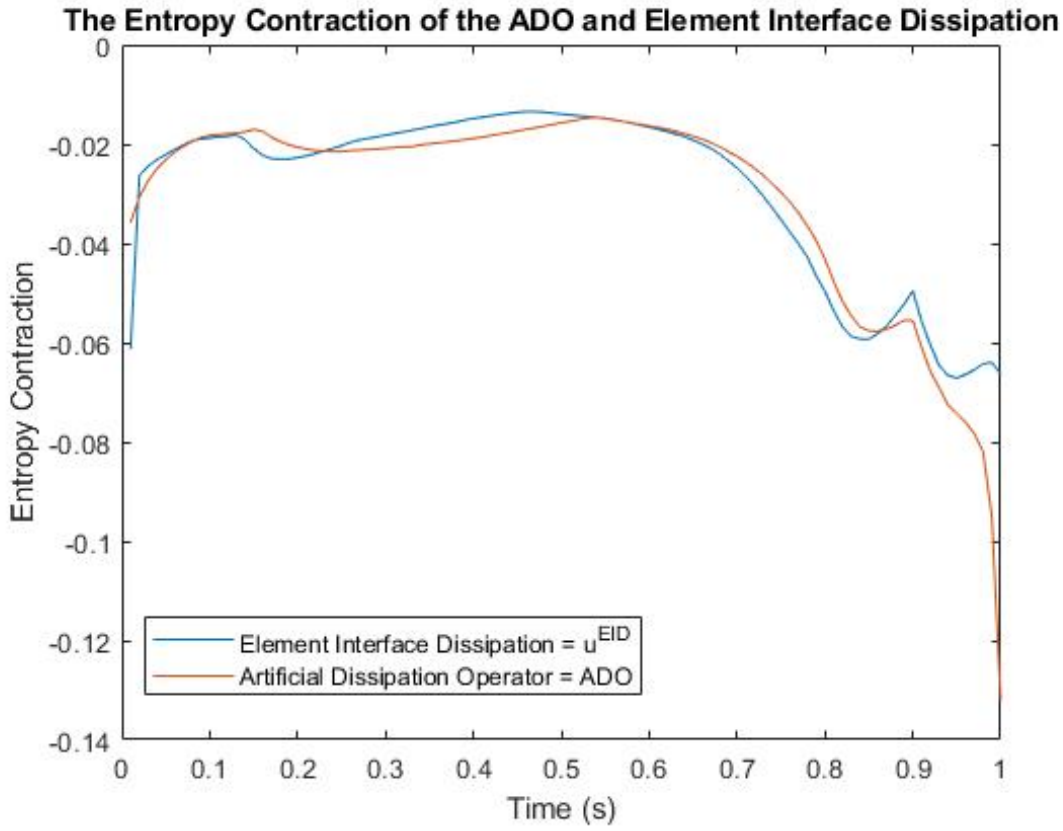

Figure 6.7: The entropy contraction is the result of left multiplying the artificial dissipation operator, (5.2), and the element interface dissipation, (5.7), by $\boldsymbol{w}_i^{\mathrm{T}}\mathsf{P}$ and summing over all elements $i = 1, 2, \ldots, n$.

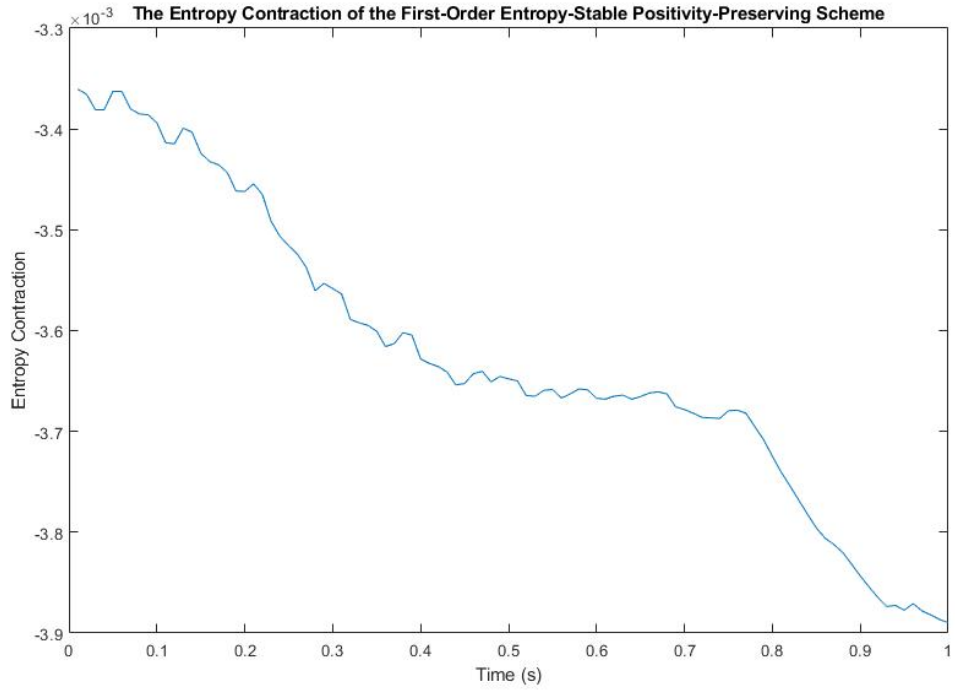

Figure 6.8: The entropy contraction is the result of left multiplying the first-order entropy-stable positivity-preserving scheme, (5.1), by $\boldsymbol{w}_i^{\mathrm{T}}\mathsf{P}$ and summing over all elements $i = 1, 2, \ldots, n$.

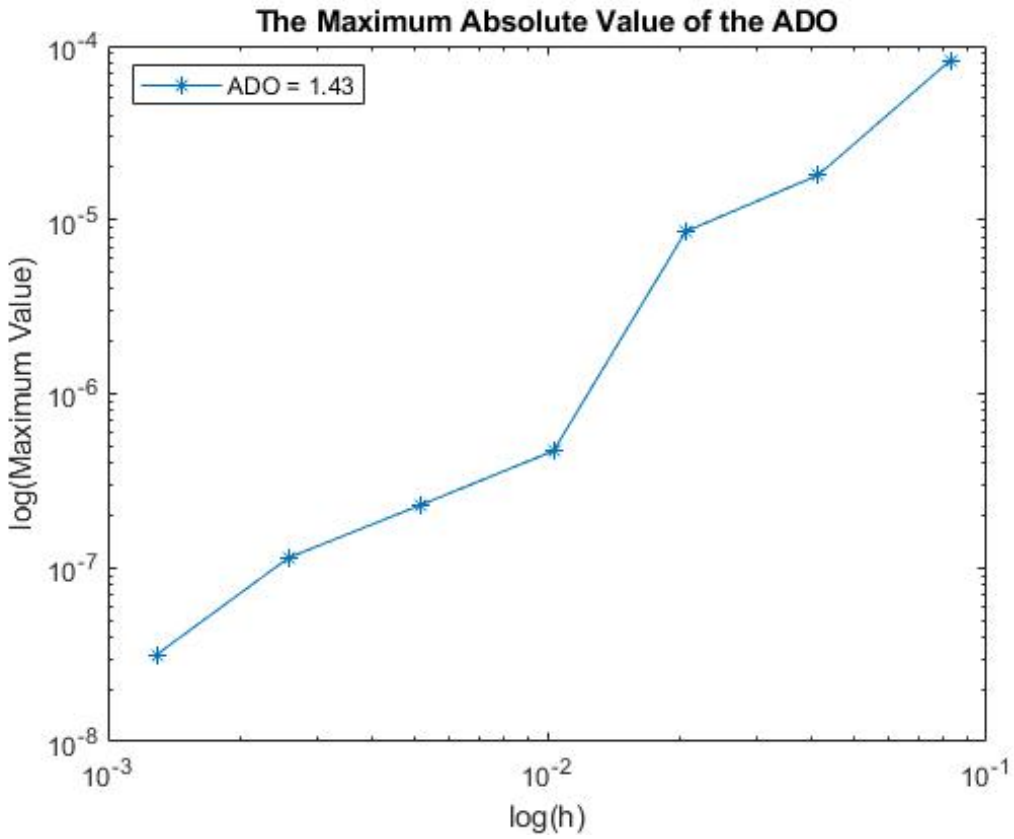

Figure 6.9: The convergence plot for the artificial dissipation operator, (5.2). This is a log-log plot of the grid spacing vs the maximum absolute value of the operator. For each grid level, there were 20 nodes per element and the number of elements was set to 4, 8, 16, and 32.

6.3 Results for the High-Order Entropy-Stable Positivity-Preserving Scheme

In this section, we first test the convergence properties of the high-order entropy-stable positivity-preserving scheme, (5.27), on the hard problem detailed in section 6.2. Since the base entropy-stable positivity-preserving scheme, (5.1), is already first-order, we test the convergence properties of (5.27) using degree 2, 3, and 4 SBP operators. Furthermore, due to the current limitations of the numerical algorithm on handling the division between small numbers as discussed in section 6.2, it is not possible to run smooth solutions that would become negative for degree 2 through 4 SBP operators. This is because the degree 2 through 4 SBP operators are accurate enough that, for a smooth problem to become negative due to error build-up, would require problems that are very close to zero, thus exacerbating the numerical instability. Instead, the schemes are mixed when they cross a threshold slightly above 0 and below 1. For the degree 2 mixing scheme, this threshold was taken as 2.49×10^{-5}, for the degree 3 mixing scheme, this threshold was taken as 2.4999×10^{-5}, and for the degree 4 mixing scheme, this threshold was taken as 2.499999×10^{-5}. These thresholds were picked because the minimum value of the exact solution in the hard problem is 2.5×10^{-5}, thus, when the high-order numerical solution crosses slightly below this minimum value, we used the mixing scheme to update the numerical solution. Notice that the threshold gets closer to 2.5×10^{-5} as the degree of the operator increases. This is because, the error decreases very rapidly as the degree of the SBP operators are increased for a fixed mesh size and we wanted the mixing scheme to be required at least once on every mesh level. Thus, the degree 4 operators require a threshold closer to the minimum value of the exact solution than the degree 2 and 3 operators, such that enough error is built up in the simulation that the entropy-conservative scheme needs to be mixed with the entropy-stable scheme at each mesh level.

Figures (6.10), (6.11), and (6.12) show the convergence plots for the degree 2, 3, and 4 mixing schemes, respectively. Each figure also contains a bar chart to show the total number of times the high-order entropy-conservative scheme needed to be mixed with the first-order entropy-stable positivity-preserving scheme to maintain positivity of the scheme (when the high-order scheme violated the threshold for positivity or boundedness). It is clear from these figures that the high-order entropy-stable positivity-preserving scheme is converging between $p + \frac{1}{2}$ and $p + 1$, thus, the scheme (5.27) achieves high-order accuracy for smooth solutions as proved in theorem (5.2.1). Furthermore, as can be seen in the bar charts of the figures, as the mesh is refined, the amount of mixing that is required between the schemes (4.9) and (5.1) goes down, as is expected, since a finer mesh means a more accurate solution.

Note that figure (6.11), includes guiding lines that show each slope is bound between 3 and 4 since there was a large drop in the error in equation 1 going from 8 to 16 elements. For this reason, in this figure, the slope of the line for equation 1 is taken from only the last two nodes, as the large decrease in error from 8 elements to 16 elements skews the results. Ideally, this plot would be pushed further to show that the trend we observe in the last two data points continues, however, mixing was only required on a single element in the 32 element case. Thus, if we continued to refine the mesh, we would simply be running the entropy-conservative scheme with degree 3 SBP operators, and the convergence properties of this scheme have already been studied in section 6.1.

Finally, we consider two Riemann problems that were studied in [50]. Both problems are associated with initial conditions of the form

$$\boldsymbol{u}_0 = \begin{cases} \boldsymbol{u}_L, & x < 0, \\ \boldsymbol{u}_R, & x > 0, \end{cases}$$

where $x \in [-0.5, 0.5]$. The first problem we study is denoted as RP1 and takes the initial condition

$$\begin{aligned} \boldsymbol{u}_L &= (0.1, 0.85, 0.4609513139, 0.96, 0.0839315299)^{\mathrm{T}}, \\ \boldsymbol{u}_R &= (0.6, 1.2520240113, 0.7170741165, 0.2505659851, -0.3764790609)^{\mathrm{T}}, \end{aligned} \tag{6.3}$$

and the problem is evolved in time until $t = 0.14s$. Then, the second problem we study is denoted RP2 and takes a constant solution, except for a shock in α_1. This problem was chosen to validate that the high-order entropy-stable positivity-preserving scheme, (5.27), satisfies Abgrall's criterion. This problem is denoted RP2 and takes the initial condition

$$\begin{aligned} \boldsymbol{u}_L &= (0.6, 0.5, 1.0, 0.5, 1.0)^{\mathrm{T}}, \\ \boldsymbol{u}_R &= (0.4, 0.5, 1.0, 0.5, 1.0)^{\mathrm{T}}, \end{aligned} \tag{6.4}$$

and the problem is evolved in time until $t = 0.1s$. Furthermore, for RP2 we set $k = 1$, $\gamma_1 = 3$, and $\gamma_2 = 3$ such that the velocities and pressures are equal for both phases, as is required for Abgrall's criterion.

Figures (6.13), (6.14), and (6.15) show the convergence of the entropy-stable positivity-preserving scheme, (5.27), discretized using degree 4 SBP operators, on RP1. It can be seen that as the number of elements increases, the discontinuities are more accurately captured, but, even in the 128 element case, there are still large oscillations that occur at the shock. This tells us that, while the entropy-stable positivity-preserving scheme, (5.27), can capture shocks, more dissipation is required to damp these oscillations. How this limitation will

be addressed is contained in the future work section of chapter 7. Then, figure (6.16) shows that the high-order positivity-preserving scheme, (5.27), is in fact entropy-stable. These results were obtained using degree 4 SBP operators, on RP1, but similar results hold for all other degrees, thus, they are omitted here. From the figure, we have that the contraction is less than zero for all time, thus, the we have validated theorem (5.2.2), as we have numerically shown that the scheme (5.27) is entropy-stable.

Finally, figure (6.17) shows the results of RP2 discretized using the entropy-stable positivity-preserving scheme, (5.27), and degree 4 SBP operators. RP2, was the test to ensure the numerical scheme satisfies Abgrall's criterion. The velocities and pressure remain uniform as required by corollary (3), thus, the numerical scheme (5.27) satisfies Abgrall's criterion.

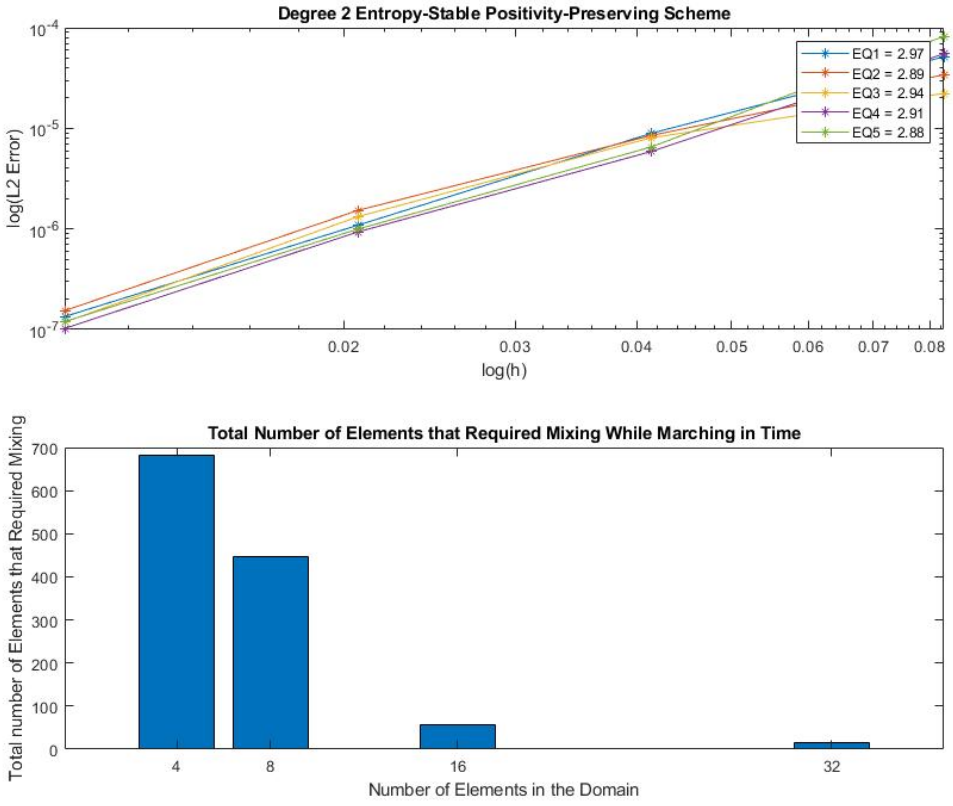

Figure 6.10: The convergence plot for the entropy-stable positivity-preserving mixing scheme, (5.27), for degree 2 SBP operators. This is a log-log error plot of the grid spacing vs the approximate L_2 error computed using (3.16) in the numerical solution. For each grid level there were 20 nodes per element and then the number of elements was set to 4, 8, 16, and 32. Then, the bar chart below shows the total number of elements that required the entropy-conservative scheme to be mixed with the first-order entropy-stable positivity-preserving scheme during the simulation for each mesh level. The number of elements that required mixing were 681, 447, 57, and 15 for the mesh levels with 4, 8, 16, and 32 elements, respectively.

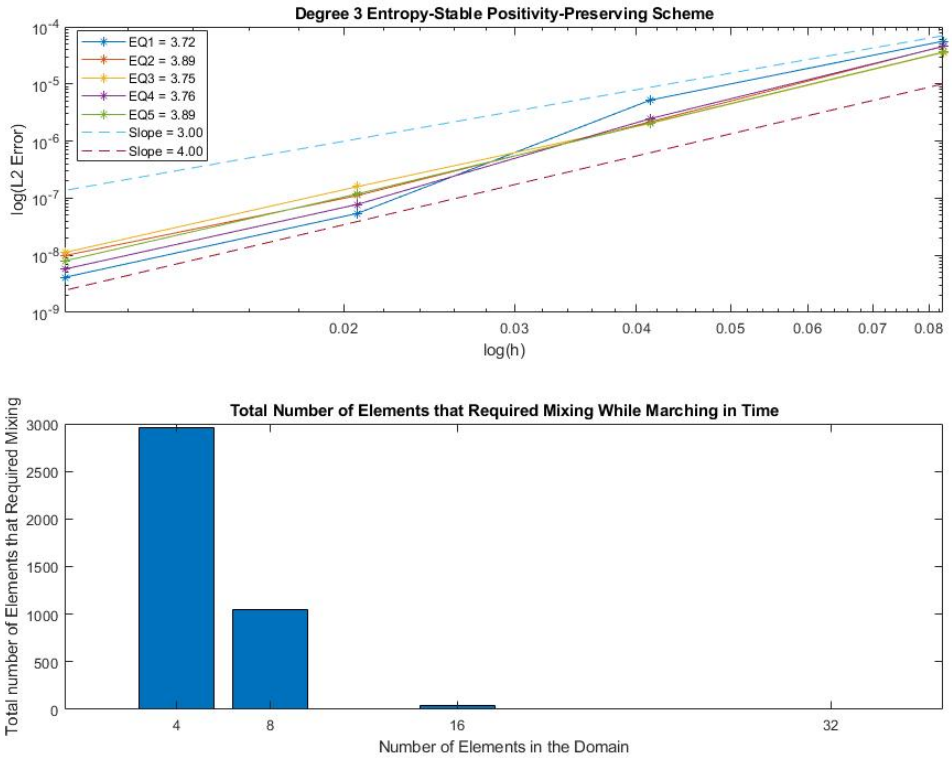

Figure 6.11: The convergence plot for the entropy-stable positivity-preserving mixing scheme, (5.27), for degree 3 SBP operators. This is a log-log error plot of the grid spacing vs the approximate L_2 error computed using (3.16) in the numerical solution. For each grid level there were 20 nodes per element and then the number of elements was set to 4, 8, 16, and 32. Then, the bar chart below shows the total number of elements that required the entropy-conservative scheme to be mixed with the first-order entropy-stable positivity-preserving scheme during the simulation for each mesh level. The number of elements that required mixing were 2959, 1044, 39, and 1 for the mesh levels with 4, 8, 16, and 32 elements, respectively.

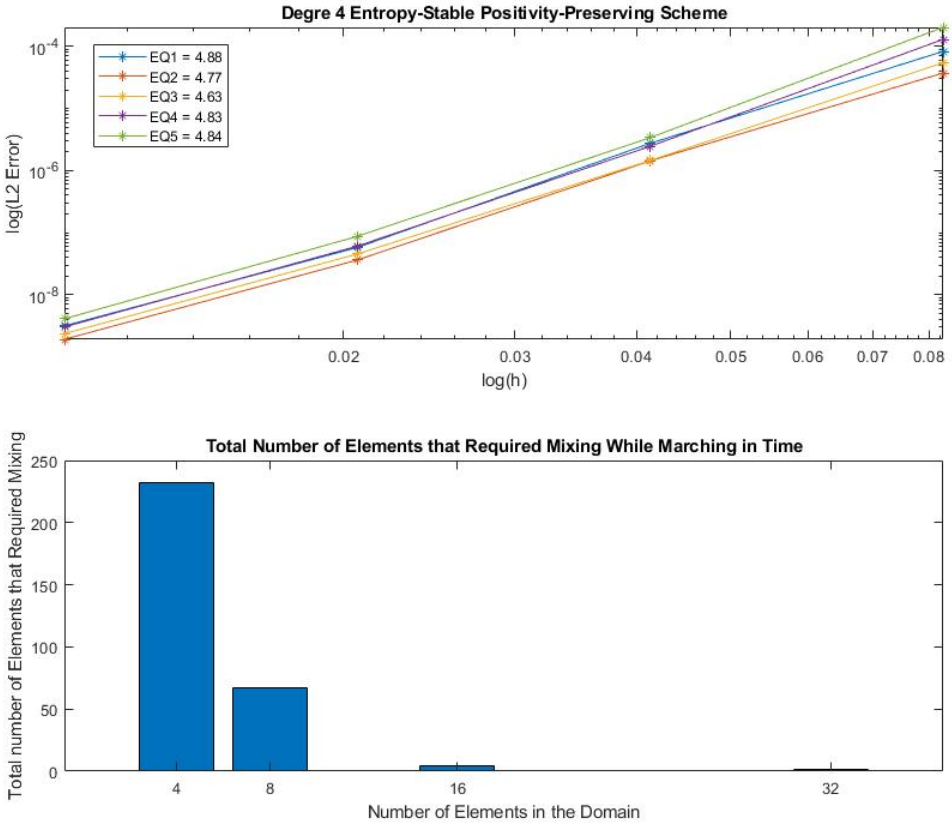

Figure 6.12: The convergence plot for the entropy-stable positivity-preserving mixing scheme, (5.27), for degree 4 SBP operators. This is a log-log error plot of the grid spacing vs the approximate L_2 error computed using (3.16) in the numerical solution. For each grid level there were 20 nodes per element and then the number of elements was set to 4, 8, 16, and 32. Then, the bar chart below shows the total number of elements that required the entropy-conservative scheme to be mixed with the first-order entropy-stable positivity-preserving scheme during the simulation for each mesh level. The number of elements that required mixing were 232, 67, 4, and 1 for the mesh levels with 4, 8, 16, and 32 elements, respectively.

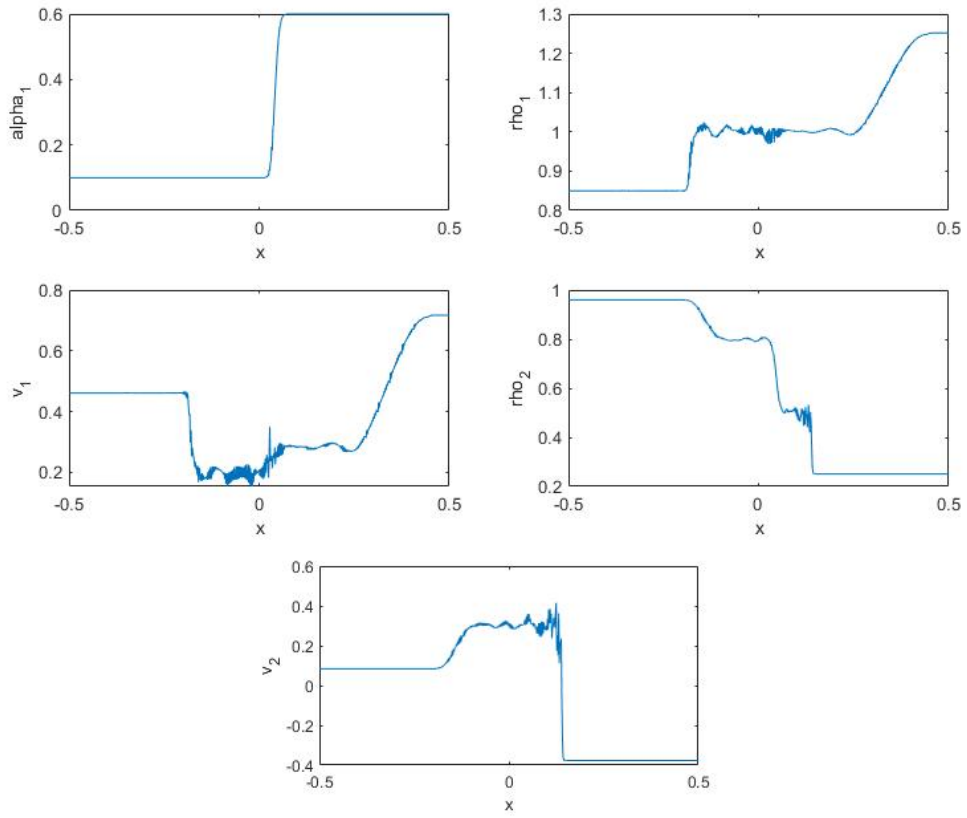

Figure 6.13: RP1 discretized using the entropy-stable positivity-preserving scheme, (5.27), for degree 4 SBP operators, with 20 nodes per element and 32 elements.

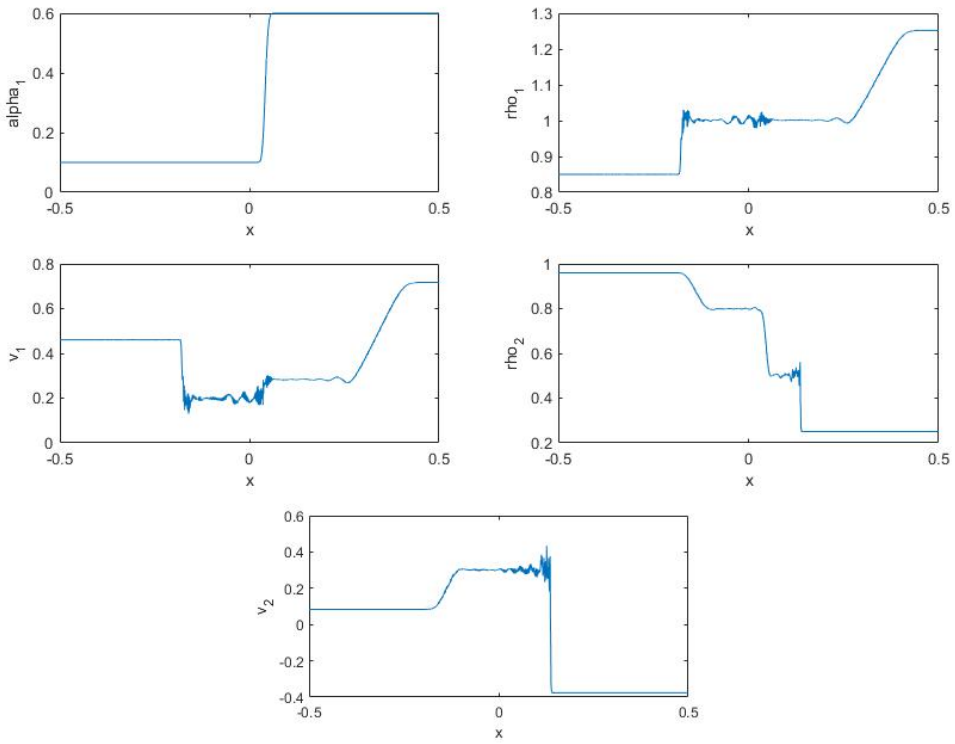

Figure 6.14: RP1 discretized using the entropy-stable positivity-preserving scheme, (5.27), for degree 4 SBP operators, with 20 nodes per element and 64 elements.

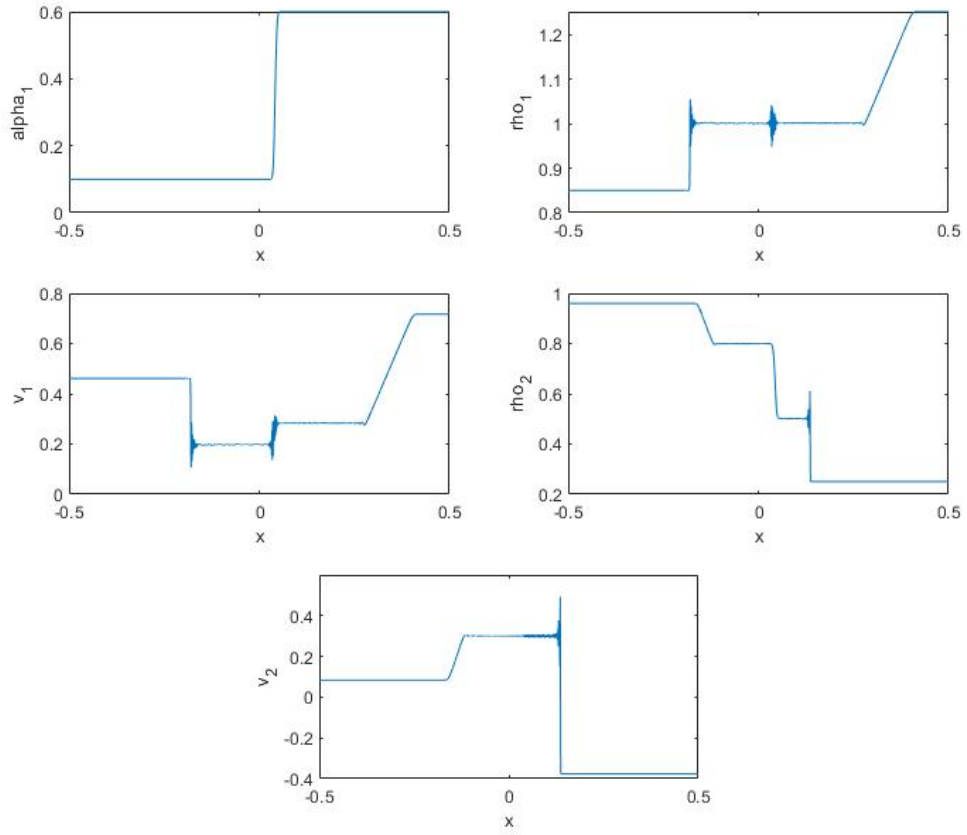

Figure 6.15: RP1 discretized using the entropy-stable positivity-preserving scheme, (5.27), for degree 4 SBP operators, with 20 nodes per element and 128 elements.

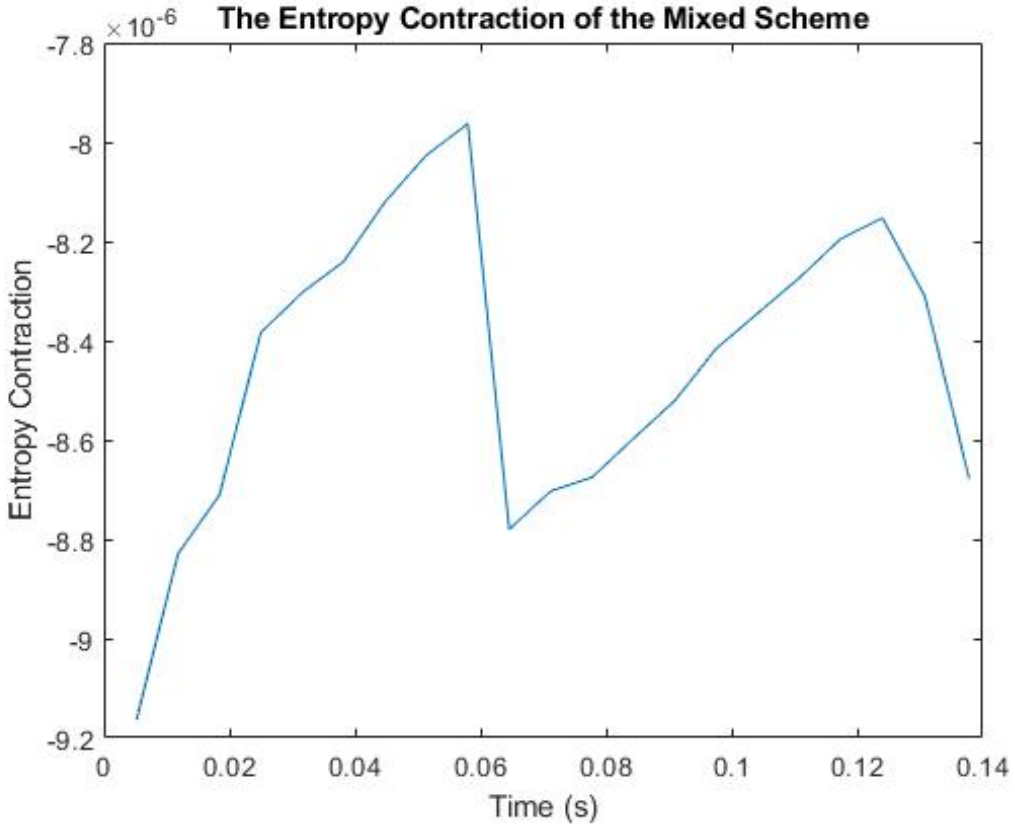

Figure 6.16: The entropy contraction is the result of left multiplying the entropy-stable positivity-preserving mixing scheme, (5.27), using degree 4 SBP operators, by $\boldsymbol{w}_i^{\mathrm{T}}\mathsf{P}$ and summing over all elements $i = 1, 2, \ldots, n$.

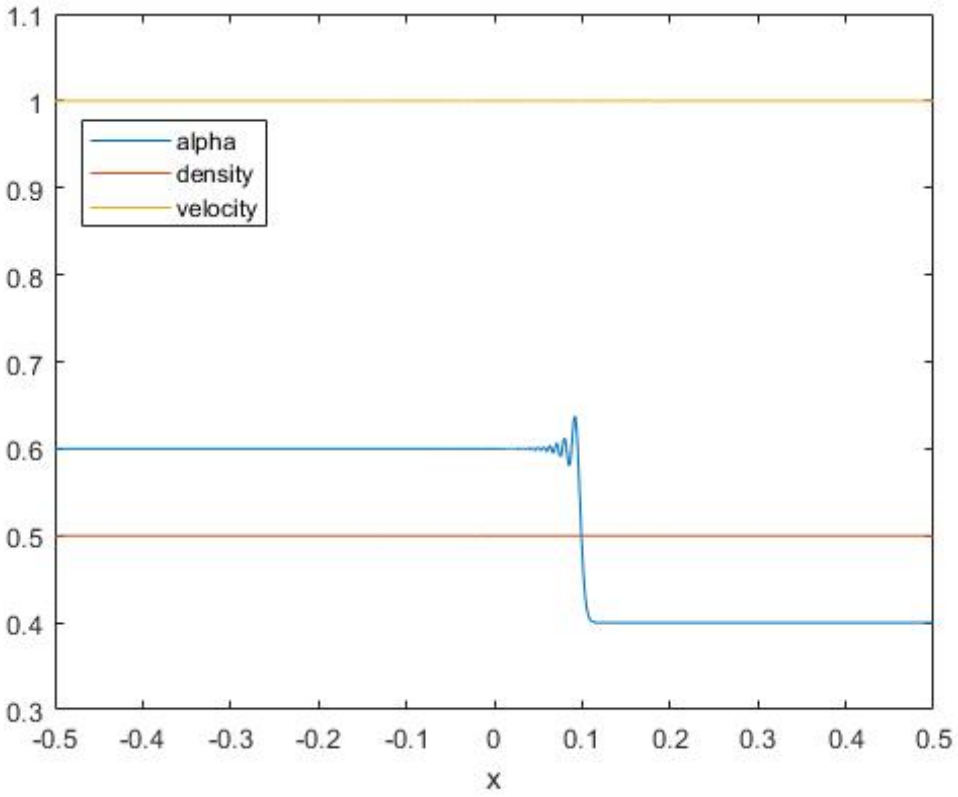

Figure 6.17: RP2 discretized using the entropy-stable positivity-preserving scheme, (5.27), for degree 4 SBP operators, with 50 nodes per element and 20 elements. While there only appears to be three lines on the plot, the density line contains both ρ_1 and ρ_2. Furthermore, the velocity line contains both v_1 and v_2.

Chapter 7

Conclusion

7.1 Summary of Work

We have presented a new high-order entropy-stable positivity-preserving scheme for the 1-D isentropic Baer-Nunziato equations. We began by developing an entropy-conservative scheme, which is capable of attaining high-order accuracy for smooth solutions. However, this entropy-conservative scheme is not capable of handling discontinuous solutions as it is prone to Gibbs oscillations around discontinuities, and will not converge to a physically relevant weak solution. Our targeted scheme needed to be able to handle discontinuous solutions to the isentropic Baer-Nunziato model, as our goal is the simulation of the bubble collapse problem in relation to HIFU. The collapse of the bubble introduces a shock into the system and therefore, we need a scheme which can capture shocks. Therefore, we sought a scheme which is entropy-stable, ensuring that the mathematical entropy across a shock is dissipated, as is required by the second law of thermodynamics. Furthermore, as shown in chapter 5, bounding the entropy of the solution implies a bound on the norm of the solution itself, thus, for finite time, the norm of the solution will not diverge to infinity and cause the simulation to crash. Another desirable property we wish for our scheme to have is positivity-preservation. The set of admissible states requires the densities and void fractions to be strictly positive, yet, we wish to simulate problems where the densities and void fractions can get arbitrarily close to zero. Furthermore, positivity-preservation is needed to ensure code stability as there are several computations that are not defined for negative densities and void fractions. Additionally, the entropy-stability proofs presented in this thesis, depend on keeping the solution within the set of admissible states, therefore, if a negative void fraction were to occur, then the entropy-stability proofs no longer hold.

To develop an entropy-stable positivity-preserving scheme we began by developing a first-order entropy-stable positivity-preserving scheme in section 5.1, where we used the entropy-conservative scheme developed in chapter 4 as a base to which entropy-dissipative terms were introduced to add entropy-stability and positivity-preserving properties. First, we added element interface dissipation, which couples adjacent elements and results in entropy-dissipation at these interfaces. Then, we present the key development in this thesis, namely, the novel artificial dissipation operator, which adds volume dissipation to the scheme. The artificial dissipation operator was designed in such a way that, it is not only an entropy-dissipative term, but, it also can be used to add provable positivity-preservation to the scheme. The dissipation operator has tuneable dissipation coefficients that can be selected to provably maintain positivity of the densities and void fractions node-wise, in conjunction with a time step restriction. Furthermore, in section 5.1, it was shown that the dissipation coefficients will not diverge to infinity no matter how close the primitive variables get to zero. Consequently, the time step restriction required to maintain positivity will not become arbitrarily small, which is of practical importance in running simulations. Finally, the derivative operator used in the first-order entropy-stable positivity-preserving scheme is a special derivative operator which is composed of high-order P, and first-order Q. In chapter 3, we proved that discretizing in space using this special derivative operator results in a scheme that has first-order truncation error and we demonstrated numerically that it converges at first-order.

This special operator was used in the first-order scheme so that we could mix the high-order entropy-conservative scheme, with the first-order entropy-stable positivity-preserving scheme, to create a high-order entropy-stable positivity-preserving scheme. When the norm matrix used to create the special derivative operator is selected such that it matches the order of the entropy-conservative scheme, it was proved in section 5.2, that the high-order positivity-preserving scheme, which mixes the entropy-conservative scheme with the first-order entropy-stable positivity-preserving scheme, is entropy-stable. To create the high-order entropy-stable positivity-preserving scheme we march in time using the high-order entropy-conservative scheme and, at each time step, check for two conditions on each element. First, we check if a discontinuity is present on an element by using WENO smoothness indicators. If a discontinuity is detected in an element, then only the first-order entropy-stable positivity-preserving scheme is used to evolve that element. The second condition that is checked at each time level is if positivity is violated by the high-order entropy-conservative scheme. If positivity is violated, then the high-order entropy-conservative scheme is mixed with the first-order positivity-preserving scheme, as detailed in section 5.2. This mixing scheme results in a novel high-order entropy-stable positivity-preserving scheme which solves the 1-D isentropic Baer-Nunziato equations.

In chapter 6, all three schemes developed in this thesis were tested on several different problems. First, we demonstrated the convergence properties of the high-order entropy-conservative numerical scheme, where, we observed convergence rates between $p+\frac{1}{2}$ and $p+1$ for all SBP operators of degree $p = \{1, 2, 3, 4\}$. Then, we tested the entropy-conservative properties of the scheme and observe that at each time level, entropy is conserved down to machine accuracy.

Next, we test the first-order entropy-stable positivity-preserving scheme on a problem that gets close to zero. This is a problem which the entropy-conservative scheme cannot run using degree 1 SBP operators, due to positivity being violated as the scheme is marched in time. Not only do we observe that the scheme preserves positivity of the densities and void fractions, but, we see that the scheme converges at first-order as claimed in section 5.1. Furthermore, we test that the element interface dissipation and novel artificial dissipation operator are entropy-dissipative terms and we find that, numerically, they are entropy-dissipating for all time. To show that the addition of these two terms to the entropy-conservative scheme leads to an entropy-stable scheme, we also numerically test for entropy-stability of the first-order entropy-stable positivity-preserving scheme. Finally, we run a test on the convergence of the novel artificial dissipation operator, to validate our claim that it should converge to 0 at first-order. We observe that the artificial dissipation operator, does converge to zero at first-order.

Finally, we tested the mixed high-order entropy-stable positivity-preserving scheme. First, we demonstrated the convergence properties of the scheme by running the scheme using degree 2, 3, and 4 SBP operators, where we observed convergence rates between $p + \frac{1}{2}$ and $p + 1$ for all degrees tested. We also observed that the number of elements that required mixing due to positivity being violated decreased as the mesh was refined. This is exactly the property that was desired, since, a finer mesh, equates to a more accurate numerical solution, which should require less mixing to maintain positivity. Then, we demonstrate the shock capturing capabilities of the high-order entropy-stable positivity-preserving scheme by running two Riemann problems. For the first Riemann problem, we demonstrate how refining the mesh leads to a more accurate capturing of the shocks by displaying the numerical solution on three different mesh levels. The final Riemann problem that is shown, numerically validates that the high-order entropy-stable positivity-preserving scheme satisfies Abgrall's criterion. We demonstrated that, given uniform and equal velocities and pressures at time $t = 0$, they remain uniform and equal as proved in corollary (3). Satisfying Abgrall's criterion is not straightforward, but highly necessary to discretize the non-conservative term in the Baer-Nunziato equations, especially given the context of bubble collapse. Therefore, theorem (5.1.5), corollary (1), and corollary (3) is a significant contribution of this work. Finally, we showed the entropy-stability properties

of the high-order entropy-stable positivity-preserving scheme.

7.2 Future Work

In this thesis, we presented numerical schemes that solve the 1-D isentropic Baer-Nunziato model. We have developed a scheme which is positivity-preserving and capable of capturing shocks. In the short term, the numerical instability that occurs when the values of the conservative variables get close to zero needs to be addressed. To do so, we plan to use a similar technique to the velocity limiters presented by Upperman and Yamaleev [63]. In their work on entropy-stable positivity-preserving schemes for the Navier-Stokes equations, they introduce entropy-stable velocity limiters which keeps the time step restriction of their scheme from becoming too stiff. The general idea is to bound the deviation from the average velocity by an upper limit, and if the velocity at any node falls outside of this limit, then the entropy-stable velocity limiter is applied iteratively until the velocity at all nodes satisfy the upper limit. In our work, we are seeing spikes occur in the velocities and densities as the values in the conserved variables become close to zero, thus, we believe that taking inspiration from the work of Upperman and Yamaleev, to create our own entropy-stable velocity and density limiters, will solve this numerical instability.

Then, as demonstrated in section 6.3, our entropy-stable positivity-preserving scheme, (5.27), is capable of capturing shocks, and as we mesh refine, the solution is more resolved. However, more dissipation is needed to damp oscillations occurring at the discontinuity. This is typical for this class of schemes, for example, Upperman and Yamaleev add more operators and limiting to their entropy-stable positivity-preserving scheme for the Navier-Stokes equations to ensure sufficient dissipation is being added to the scheme around shocks; such as artificial viscosity and velocity limiting [63, 62]. First, we plan to add dissipation to the high-order entropy-conservative scheme, (4.9), using the dissipation operators constructed by Mattsson *et al.* [43]. This will immediately add more dissipation to the numerical scheme since, currently, the high-order scheme has no dissipation. Furthermore, we will add more artificial dissipation to our first-order entropy-stable positivity-preserving scheme. The key will be to add a shock sensor that will not only inform where the shocks in the numerical solution are occurring, but also, inform how much dissipation needs to be added to the scheme. For this, we look to the work of Upperman [62], who has developed an entropy residual-based sensor for the Navier-Stokes equations. Finally, we believe that the velocity and density limiters we will add to our scheme to address the numerical instability, will also damp oscillations that occur around a shock.

The approach for stability taken in this thesis, only gives semi-discrete stability proofs

and the fully discrete scheme presented in this thesis, does not inherit these stability properties, though in practice, we see that such schemes are more robust. However, by using the relaxation Runge-Kutta approach [37, 49], one can extend the semi-discrete stability proofs to the fully discrete case.

With these changes to our entropy-stable positivity-preserving scheme, (5.27), we will have developed a strong building block to be able to simulate a bubble collapse problem in the context of HIFU. However, such a problem would need to be simulated in at least 2-D, and as such, upgrading the scheme to be able to handle multi-dimensional problems is a necessary point to be addressed in future work. The work in 1-D could be extended to multi-D through the use of tensor products and the author does not foresee any complications in upgrading the scheme to be able to handle multi-dimensional problems. Furthermore, to serve clinical applications, the bubble collapse problem needs to be studied in relation to how it interacts with soft tissues. Such knowledge would support the development of revolutionary applications of HIFU and improve upon existing techniques such as tumor ablation, thus improving patient outcomes.

References

[1] R. Abgrall. How to prevent pressure oscillations in multicomponent flow calculations. *Journal of Computational Physics*, 125:150–160, 1996.

[2] R. Abgrall and S. Karni. A comment on the computation of non-conservative products. *Journal of Computational Physics*, 229:2759–2763, 2015.

[3] A. Ambroso, C. Chalons, F. Coquel, T. Galié, E. Godlewski, P.A. Raviart, and N. Seguin. The drift-flux asymptotic limit of barotropic two-phase two-pressure models. *Communications in Mathematical Sciences*, 6:521–529, 2008.

[4] M.R. Baer and J.W. Nunziato. A two-phase mixture theory for the deflagration-to-detonation transition (DDT) in reactive granular materials. *International Journal of Multiphase Flow*, 12:861–889, 1986.

[5] G.E. Barter and D.L. Darmofal. Shock capturing with PDE-based artificial viscosity for DGFEM: Part i. formulation. *Journal of Computational Physics*, 229:1810–1827, 2010.

[6] C. Berthon, F. Coquel, and P. LeFloch. Why many theories of shock waves are necessary: kinetic relations for non-conservative systems. *Proceedings of the Royal Society of Edinburgh Section A: Mathematics*, 142:1–37, 2012.

[7] B. Boyd and S. Becker. Numerical modeling of the acoustically driven growth and collapse of a cavitation bubble near a wall. *Physics of Fluids*, 31:032102, 2019.

[8] M. Carpenter, T. Fisher, E. Nielsen, M. Parsani, M. Svärd, and N. Yamaleev. Entropy stable summation-by-parts formulations for compressible computational fluid dynamics. *Handbook of Numerical Analysis*, 17:495–524, 2016.

[9] M.H. Carpenter, D. Gottlieb, and S. Abarbanel. Time-stable boundary conditions for finite-difference schemes solving hyperbolic systems: Methodology and application to high-order compact schemes. *Journal of Computational Physics*, 111:220–236, 1994.

[10] M.J. Castro, U.S. Fjordholm, S Mishra, and C. Parés. Entropy conservative and entropy stable schemes for nonconservative hyperbolic systems. *SIAM Journal on Numerical Analysis*, 51:1371–1391, 2013.

[11] F. Coquel, T. Gallouët, J.M. Hérard, and N. Seguin. Closure laws for a two-fluid two-pressure model. *Comptes Rendus Mathematique*, 334:927–932, 2002.

[12] F. Coquel, J.M. Hérard, and K. Saleh. A positive and entropy-satisfying finite volume scheme for the Baer–Nunziato model. *Journal of Computational Physics*, 330:401–435, 2017.

[13] F. Coquel, J.M. Hérard, K. Saleh, and N. Seguin. A robust entropy-satisfying finite-volume scheme for the isentropic Baer-Nunziato model. *ESAIM: Mathematical Modelling and Numerical Analysis*, 48:165–206, 2014.

[14] F. Coquel, P. Rai, C Marmignon, and F. Renac. An entropy stable high-order discontinuous Galerkin spectral element method for the Baer-Nunziato two-phase flow model. *Journal of Computational Physics*, 431, 2021.

[15] C.C. Coussios, C.H. Farny, G. Ter Haar, and R.A. Roy. Role of acoustic cavitation in the delivery and monitoring of cancer treatment by high-intensity focused ultrasound (hifu). *International Journal of Hyperthermia*, 23, 2013.

[16] C.M. Dafermos. *Hyperbolic Conservation Laws in Continuum Physics*, volume 3. Berlin: Springer, 2005.

[17] G. Dal Maso, P. LeFloch, and F. Murat. Definition and weak stability of nonconservative products. *Journal de Mathématiques Pures et Appliquées*, 74:483–548, 1995.

[18] D.C. Del Rey Fernández, J.E. Hicken, and D.W. Zingg. Review of summation-by-parts operators with simultaneous approximation terms for the numerical solution of partial differential equations. *Computers Fluids*, 95:171–196, 2014.

[19] D.C. Del Rey Fernández, J.E. Hicken, and D.W. Zingg. Simultaneous approximation terms for multi-dimensional summation-by-parts operators. *Journal of Scientific Computing*, 75:83–110, 2018.

[20] P. Diener, E. Dorband, E.N. Schnetter, and M. Tiglio. Optimized high-order derivative and dissipation operators satisfying summation by parts, and applications in three-dimensional multi-block evolutions. *Journal of Scientific Computing*, 32:109–145, 2007.

[21] D.A. Drew and S.L. Passman. Theory of multicomponent fluids. *Springer Science Business Media*, 135, 2006.

[22] L.C. Evans. *Partial Differential Equations*. American Mathematical Society, 2010.

[23] P. Fernandez, N.-C. Nguyen, and J. Peraire. A physics-based shock capturing method for large-eddy simulation. *arXiv:1806.06449 [physics.comp-ph]*, 2018.

[24] T. Fisher, M.H. Carpenter, J. Nordström, N.K. Yamaleev, and C. Swanson. Discretely conservative finite-difference formulations for nonlinear conservation laws in split form: Theory and boundary conditions. *Journal of Computational Physics*, 23:353–375, 2013.

[25] T.C. Fisher and M.H. Carpenter. High-order entropy stable finite difference schemes for nonlinear conservation laws: Finite domains. *Journal of Conputational Physics*, 252:518–557, 2013.

[26] D. Funaro and D. Gottlieb. A new method of imposing boundary conditions in pseudospectral approximations of hyperbolic equations. *Mathematics and Computation*, 51:599–613, 1988.

[27] T. Gallouët, J.M. Hérard, and N. Seguin. Numerical modeling of two-phase flows using the two-fluid two-pressure approach. *Mathematical Models and Methods in Applied Sciences*, 14:663–700, 2004.

[28] B. Gustafsson. *High Order Difference Methods for Time Dependent PDE*. Springer Series in Computational Mathematics, 2008.

[29] J Hadamard. *Lectures on Cauchy's Problem in Linear Partial Differential Equations*. Yale University Press, 1923.

[30] Jan S. Hesthaven. *Numerical Methods for Conservation Laws - From Analysis to algorithms*. SIAM Computational Science and Engineering, 2018.

[31] J.S. Hesthaven and T. Warburton. *Nodal discontinuous Galerkin methods: algorithms, analysis, and applications*. Springer Science Business Media, 2007.

[32] J.E. Hicken, D.C. Del Rey Fernández, and D.W. Zingg. Multi-dimensional summation-by-parts operators: General theory and application to simplex elements. *SIAM Journal on Scientific Computing*, 38:A1935–A1958, 2016.

[33] D.J. Hill and D.I. Pullin. Hybrid tuned center-difference-weno method for large eddy simulations in the presence of strong shocks. *Journal of Computational Physics*, 194:435–450, 2004.

[34] F.J. Hindenlang and G.J. Gassner. On the order reduction of entropy stable DGSEM for the compressible Euler equations. *ICOSAHOM 2018 conference proceedings*, pages 21–44, 2018.

[35] F. Ismael and P.L. Roe. Affordable, entropy-consistent euler flux functions ii: entropy production at shocks. *Journal of Conputational Physics*, 228:5410–5436, 2009.

[36] Zarah. Izadifar, Zohreh. Izadifar, D. Chapman, and P. Babyn. An introduction to high intensity focused ultrasound: Systematic review on principles, devices, and clinical applications. *Journal of Clinical Medicine*, 9, 2020.

[37] D.I. Ketcheson. Relaxation Runge–Kutta methods: Conservation and stability for inner-product norms. *SIAM Journal on Numerical Analysis*, 57:10.1137/19M1263662, 2019.

[38] H.O. Kreiss and J Oliger. Comparison of accurate methods for the integration of hyperbolic equations. *Tellus*, 24:199–215, 1972.

[39] C. Lafon, D. Melodelima, R. Salomir, and J.Y. Chapelon. Interstitial devices for minimally invasive thermal ablation by high-intensity ultrasound. *International Journal of Hyperthermia*, 23:153–163, 2007.

[40] P. Lax and B. Wendroff. Systems of conservation laws. *Communications on Pure and Applied Mathematics*, 13:217–237, 1960.

[41] P.G. LeFloch, J.M. Mercier, and C. Rohde. Entropy conservative and entropy stable schemes for nonconservative hyperbolic systems. *SIAM Journal on Numerical Analysis*, 40:1968–1992, 2003.

[42] S. Majidi and A. Afshari. A ghost fluid method for sharp interface simulations of compressible multiphase flows. *Journal of Mechanical Science and Technology*, 30:1581–1593, 2016.

[43] K. Mattsson, M. Svärd, and Nordström. J. Stable and accurate artificial dissipation. *Journal of Scientific Computing*, 21:57–79, 2004.

[44] J. Mondal, R. Lakkaraju, P. Ghosh, and M. Ashokkumar. Acoustic cavitation-induced shear: a mini-review. *Biophysical Reviews*, 13:1229–1243, 2021.

[45] D. Moro, C. Nguyen, and J. Peraire. Dilation-based shock capturing for high-order methods. *International Journal for Numerical Methods in Fluids*, 82:398–416, 2016.

[46] A. Murrone and P. Villedieu. Numerical modeling of dispersed two-phase flows. *Aerospace Lab*, 2:1–12, 2011.

[47] C. Nguyen and J. Peraire. An adaptive shock-capturing HDG method for compressible flows. *20th AIAA Computational Fluid Dynamics Conference*, page 3060, 2011.

[48] C. Parés. Numerical methods for nonconservative hyperbolic systems: a theoretical framework. *SIAM Journal on Numerical Analysis*, 44:300–321, 2006.

[49] H. Ranocha, M. Sayyari, L. Dalcin, M. Parsani, and D.I. Ketcheson. Relaxation Runge–Kutta methods: Fully discrete explicit entropy-stable schemes for the compressible Euler and Navier–Stokes equations. *SIAM Journal on Scientific Computing*, 42(2):A612–A638, January 2020.

[50] F. Renac. Entropy stable DGSEM for nonlinear hyperbolic systems in nonconservative form with applications to two-phase flows. *Journal of Computational Physics*, 382:1–26, 2019.

[51] A.M. Rueda-Ramírez and Gassner. G.J. A flux-differencing formula for split-form summation by parts discretizations of non-conservative systems: Applications to subcell limiting for magneto-hydrodynamics. *Journal of Computational Physics*, 496:112607, 2022.

[52] R. Saurel and R. Abgrall. A multiphase godunov method for compressible multifluid and multiphase flows. *Journal of Computational Physics*, 150:425–467, 1999.

[53] C-W. Shu. Total-variation-diminishing time discretizations. *SIAM journal on Scientific and Statistical Computing*, 9:1073–1084, 1988.

[54] C-W. Shu. High-order finite difference and finite volume weno schemes and discontinuous Galerkin methods for cfd. *International Journal of Compuational Fluid Dynamics*, 17:107–118, 2003.

[55] M. Sonntag and C.-D. Munz. Efficient parallelization of a shock capturing for discontinuous Galerkin methods using finite volume sub-cells. *Journal of Scientific Computing*, 70:1262–1289, 2017.

[56] B. Strand. Summation by parts for finite difference approximations for d/dx. *Journal of Computational Physics*, 110:47–67, 1994.

[57] M. Svärd. Weak solutions and convergent numerical schemes of modified compressible Navier–Stokes equations. *Journal of Computational Physics*, 228:19–51, 2015.

[58] M. Svärd and J. Nordström. Review of summation-by-parts schemes for initial–boundary-value problems. *Journal of Computational Physics*, 268:17–38, 2014.

[59] B. Swartz and B Wendroff. The relative efficiency of finite difference and finite element methods. i: Hyperbolic problems and splines. *SIAM Journal on Numerical Analysis*, 1:979–993, 1974.

[60] E. Tadmor. The numerical viscosity of entropy stable schemes for systems of conservation laws. *Mathematics of Computation*, 49:91–103, 1987.

[61] W. Trojak and T. Dzanic. Positivity-preserving discontinuous spectral element methods for compressible multi-species flows. *arXiv:2308.02426 [physics.flu-dyn]*, 2023.

[62] J. Upperman. *High-Order Positivity-Preserving L2-Stable Spectral Collocation Schemes for the 3-D Compressible Navier-Stokes Equations*. PhD thesis, Old Dominion university, 2021.

[63] J. Upperman and N.K. Yamaleev. Positivity-preserving entropy stable schemes for the 1-d compressible Navier-Stokes equations: First-order approximation. *Journal of Computational Physics*, 466:111355, 2022.

[64] J. VonNeumann and R.D. Richtmyer. A method for the numerical calculation of hydrodynamic shocks. *Journal of Applied Physics*, 21:232–237, 1950.

[65] M. Wang, Y. Lei, and Y. Zhou. High-intensity focused ultrasound (hifu) ablation by the frequency chirps: Enhanced thermal field and cavitation at the focus. *Ultrasonics*, 91:134–149, 2019.

[66] F.D. Witherden and A. Jameson. Future directions in computational fluid dynamics. *AIAA Computational Fluid Dynamics Conference*, 3791, 2017.

[67] T. Ye, W. Shyy, and J.N. Chung. A fixed-grid, sharp-interface method for bubble dynamics and phase change. *Journal of Computational Physics*, 174:781–815, 2001.

[68] F.R. Young. *Cavitation*. World Scientific, 1999.

[69] M.H. Yu, J.Y. Lee, H.R. Kim, B.R. Kim, Park E-J., H.S. Kim, J.K. Han, and B.I. Choi. Therapeutic effects of microbubbles added to combined high-intensity focused ultrasound and chemotherapy in a pancreatic cancer xenograft model. *Korean Journal of Radiology*, 17:779–788, 2016.

[70] X. Zhang and C.W. Shu. On positivity-preserving high order discontinuous Galerkin schemes for compressible euler equations on rectangular meshes. *Journal of Computational Physics*, 229:8918–8934, 2010.

[71] GY. Zhao, MB. Sun, and S. Pirozzoli. On shock sensors for hybrid compact/weno schemes. *Computers and Fluids*, 199, 2020.

APPENDICES

Appendix A

The Eigenvalues of the Flux Jacobian for the Isentropic Baer-Nunziato Model

In section (5.1), we introduced the element interface dissipation

$$\boldsymbol{u}^{EID} = \tilde{\mathsf{P}}^{-1}[-\mathsf{M}^{i}_{N1}\Delta^{i}\boldsymbol{v}, 0, \ldots, 0, \mathsf{M}^{(\mathsf{i+1})}_{\mathsf{N1}}\Delta^{(i+1)}\boldsymbol{v}]^{\mathrm{T}},$$

where the dissipation coefficients, σ_a, $a \in [1, 2, 4]$, are calculated by scaling the maximum absolute value of the eigenvalues of the flux Jacobian. To find the flux Jacobian, consider the isentropic Baer-Nunziato equations

$$\frac{\partial \boldsymbol{u}}{\partial t} + \frac{\partial \boldsymbol{f}(\boldsymbol{u})}{\partial x} + \mathsf{c}(\boldsymbol{u})\frac{\partial \boldsymbol{u}}{\partial x} = 0.$$

Now, rewrite the spatial terms in the equations in terms of the primitive variables, $\boldsymbol{v}$, as follows

$$\frac{\partial \boldsymbol{u}}{\partial t} + \left(\frac{\partial \boldsymbol{f}}{\partial \boldsymbol{v}}\frac{\partial \boldsymbol{v}}{\partial x} + \mathsf{c}\frac{\partial \boldsymbol{u}}{\partial \boldsymbol{v}}\frac{\partial \boldsymbol{v}}{\partial x}\right) = 0,$$
$$\frac{\partial \boldsymbol{u}}{\partial t} + \left(\frac{\partial \boldsymbol{f}}{\partial \boldsymbol{v}} + \mathsf{c}\frac{\partial \boldsymbol{u}}{\partial \boldsymbol{v}}\right)\frac{\partial \boldsymbol{v}}{\partial x} = 0.$$

We seek the maximum absolute absolute eigenvalue of

$$\text{Flux Jacobian} = \frac{\partial \boldsymbol{f}}{\partial \boldsymbol{v}} + \mathsf{c}\frac{\partial \boldsymbol{u}}{\partial \boldsymbol{v}},$$

using both of the values on either side of the element interface. The element interface dissipation coefficients are then set to the maximum absolute eigenvalue, e_{max}, i.e.,

$$\sigma_a = e_{max},\ a = [1, 2, 4].$$

The eigenvalues are defined as

$$\begin{aligned}
e_1 &= v_2, \\
e_2 &= \frac{\alpha_2 v_2}{2} + \alpha_2\rho_2 v_2 + \frac{\sqrt{4\alpha_2(v_2^2 + p_2')\alpha_2\rho_2 + \alpha_2 v_2^2 - 4\alpha_2^2\rho_2 v_2^2 + 4\alpha_2\rho_2 v_2^2}}{2}, \\
e_3 &= \frac{\alpha_2 v_2}{2} + \alpha_2\rho_2 v_2 - \frac{\sqrt{4\alpha_2(v_2^2 + p_2')\alpha_2\rho_2 + \alpha_2 v_2^2 - 4\alpha_2^2\rho_2 v_2^2 + 4\alpha_2\rho_2 v_2^2}}{2}, \\
e_4 &= \frac{\alpha_1 v_1}{2} + \alpha_1\rho_1 v_1 + \frac{\sqrt{4\alpha_1(v_1^2 + p_1')\alpha_1\rho_1 + \alpha_1 v_1^2 - 4\alpha_1^2\rho_1 v_1^2 + 4\alpha_1\rho_1 v_1^2}}{2}, \\
e_5 &= \frac{\alpha_1 v_1}{2} + \alpha_1\rho_1 v_1 - \frac{\sqrt{4\alpha_1(v_1^2 + p_1')\alpha_1\rho_1 + \alpha_1 v_1^2 - 4\alpha_1^2\rho_1 v_1^2 + 4\alpha_1\rho_1 v_1^2}}{2},
\end{aligned}$$

where $p_a' = \frac{dp_a}{d\rho_a}$, $a = \{1, 2\}$.

Glossary

Entropy inequality A condition which weak solutions to the isentropic Baer-Nunziato model must satisfy, in a weak sense.

Entropy-conservative scheme A semi-discrete scheme which conserves the mathematical entropy of the numerical solution.

Entropy-dissipative term A term which dissipates (or decreases) the mathematical entropy of the numerical solution.

Entropy-stable scheme A semi-discrete scheme which decreases the mathematical entropy of the numerical solution.

High-order scheme A semi-discrete scheme that has an order of accuracy greater than 1.

Mixed scheme A semi-discrete scheme that mixes the high-order entropy-conservative scheme with the first-order entropy-stable positivity-preserving scheme.

Positivity-preserving scheme A semi-discrete scheme which maintains the positivity of the densities and void fractions in the isentropic Baer-Nunziato model.

Void fractions Describes the fraction of space which is occupied by a phase in the isentropic Baer-Nunziato model.